UNDERSTANDING THE FUNCTION OF GENES INVOLVED IN INHERITED RETINAL DEGENERATION-INSIGHTS INTO THE PATHOGENESIS AND FUNCTION OF C8ORF37

by

Ali Sakawa Sharif

A dissertation submitted to the faculty of
The University of Utah
in partial fulfillment of the requirements for the degree of

Doctor of Philosophy

Department of Neurobiology and Anatomy

The University of Utah

May 2017

The University of Utah Graduate School

STATEMENT OF DISSERTATION APPROVAL

The dissertation of **Ali Sakawa Sharif**

has been approved by the following supervisory committee members:

Jun Yang	, Chair	**1/9/2017** Date Approved
Monica L. Vetter	, Member	**1/12/2017** Date Approved
Wolfgang Baehr	, Member	**1/9/2017** Date Approved
Yukio Saijoh	, Member	**1/12/2017** Date Approved
Michael Robert Deans	, Member	**1/11/2017** Date Approved

and by **Monica L. Vetter** , Chair/Dean of

the Department/College/School of **Neurobiology and Anatomy**

and by David B. Kieda, Dean of The Graduate School.

ABSTRACT

Inherited retinal degenerative diseases (IRD) are a group of disorders that lead to progressive deterioration of mainly the photoreceptors. Retinitis pigmentosa (RP) and cone-rod dystrophy (CRD) are two forms of IRDs. RP is the most common form of IRD and is due to rod photoreceptor degeneration followed by cone photoreceptor loss. CRD, on the other hand, is characterized by the loss of cones or the concurrent degeneration of both cones and rods. Both RP and CRD are presently incurable. More than 200 genes have been identified to cause IRDs and the functions of many of these genes remain unclear. Mutations in a novel gene, *C8ORF37*, were identified to cause recessive, severe, and early-onset RP and CRD. I, therefore, pioneered in characterizing the role of C8ORF37 in the retina.

This dissertation is comprised of four chapters that is organized as follows: (1) summary of an ocular disorder (2) a genetic model of a retinal disorder (3) biochemical/proteomic analysis of C8ORF37 (4) potential clinical applications. A summary of ocular disorders is discussed in Chapter 1, with an emphasis on CRD. Chapter 2 focuses on the generation and characterization of *C8orf37* mutant mouse models that recapitulate the retinal pathologies observed in human patients. In *C8orf37* knockout retinas, the outer segment (OS) was nonuniform, swollen, and wider in width when compared to the controls. Moreover, many OS membrane proteins were reduced in the retina of *C8orf37* knockout, including CNGB1 and RDS, proteins essential for OS disc

morphogenesis and alignment. Our findings shed new light on the pathogenesis underlying retinal dysfunction and degeneration in *C8ORF37*-deficient patients.

To determine the function of a novel protein, a powerful approach is by identifying its binding partners. In Chapter 3, I discuss GST pull-down using bovine retinal lysates, yeast-two-hybrid, and immunoprecipitation with mouse retinal lysate in order to identify C8ORF37-interacting proteins. Our pull-downs identified KTN1, RAB28, UCHL1, and PSMD14 suggesting that C8ORF37 may have a role in protein homeostasis.

Chapter 4 concludes and discusses the impact of generating and characterizing *C8orf37* animal models for future studies in understanding photoreceptor function and in the development of therapeutics against retinal degeneration.

I dedicate this work to my parents, Sakawa and Safia.

TABLE OF CONTENTS

ACKNOWLEDGEMENTS

Indeed, it is very difficult to adequately acknowledge all of the people that have been immensely generous to me. I wholeheartedly express my gratitude to my graduate advisor Dr. Jun Yang for training me. I have immeasurably benefited from her encyclopedic knowledge of the retina, her dedication towards meticulous experimental designs, and her consistency and passion for success. I sincerely thank her for her wisdom, tolerance, and most importantly, her generosity towards helping me reach my greatest potentials. Working in her lab has been exciting and a lifelong experience that I will never forget.

I would like to thank Dr. Carol Lim for opening the elegant door of empirical knowledge to me. Dr. Lim embraced and instilled confidence in me when I lacked laboratory experience. Dr. Lim's altruistic nature and unflinching efforts for an auspicious planet has made it compulsory for me to follow in her footsteps. I hope to pass on what she has given to me.

I would also like to express my gratitude to my committee members Dr. Wolfgang Baehr, Dr. Monica Vetter, Dr. Yukio Saijoh, and Dr. Michael Deans. Their mentorship has sharpened my focus and their expertise has broadened my knowledge and ambition for science. I would like to sincerely express my gratitude to Dr. Wolfgang Baehr for encouraging me, giving me priceless ideas, teaching me without any restrictions, giving me his time, and most importantly desiring for me to succeed in every aspect.

I also thank all of the members in the Yang lab for the interesting discussions, experimental troubleshootings, and friendships over the years. My lab members, specifically Junhuang Zou, Dongmei Yu, Anna Clark, and Pranav Mathur have been awesome to work with. I would like to thank Stuart Loertscher and Kevin Nguyen for giving me the opportunity to mentor them for their undergraduate projects. I would also like to thank Jiahui Yang and Kevin Rapp for helping me process tissues and letting me use the Moran Electron Microscopy Core. I would like to thank Timothy Dahlem and Susan Tamowski for helping me generate the *C8orf37* mutant mice.

Lastly, I would like to express a special gratitude to my family. I will forever be indebted to my parents, Sakawa Sharif Noor and Safia Sharif Ahmed for their lifelong commitment in assuring my success. In their faces, I always find hope. I would also like to express my heartfelt gratitude to my siblings, my wife, and my two daughters for their constant love and support.

CHAPTER 1

AN INTRODUCTION TO CONE-ROD DYSTROPHY AND THE BASIC FUNCTIONS OF ASSOCIATED GENES

1.1 Introduction

Rod and cone photoreceptors are the light-sensitive neurons in the retina. In primates, approximately 95-97% (~120 million) of photoreceptor cells are rods whereas 3-5% (3-6 million) are cones (Mustafi, Engel, & Palczewski, 2009; Packer, Hendrickson, & Curcio, 1989). The rods and cones are highly compartmentalized with an outer segment (OS, a modified primary cilium), a connecting cilium (CC), an inner segment (IS), a cell body, and a synaptic terminus (R. S. Molday & Moritz, 2015) (Figure 1.1A). The OS holds many tightly stacked membrane disks. The OS disks carry the opsin molecule, a G-protein coupled receptor, responsible for light detection. The CC is a narrow passageway that enables protein transfer from the IS to the OS. The CC consists of a microtubule axoneme that is anchored to the basal body (Figure 1.1B). The IS of the photoreceptors contains several organelles including the endoplasmic reticulum (ER), Golgi apparatus, and the mitochondria (Figure 1.1B). The synaptic terminal is a specialized compartment responsible for mediating signal transmission via glutamate to horizontal and bipolar cells (Figure 1.1C).

Rod photoreceptors are specialized for dim-light conditions, provide achromatic vision, and outnumber cones by 20 times (Curcio et al., 1991; Ingram, Sampath, & Fain, 2016; Mustafi et al., 2009). In the primate retina, rod photoreceptors are absent at the fovea and abundant at the peripheral retina (Wensel et al., 2016). Cones, however, function optimally under bright light conditions and provide color discrimination. In the primate retina, there are three types of cones (L-cones, M-cones, and S-cones) based on their sensitivity to a specific wavelength of light (Curcio et al., 1991; Mustafi et al., 2009). The L-cones sense red light (555-537nm), the M-cones sense green light (530-537nm), and the

S-cones sense blue light (417-430nm) (Imamoto & Shichida, 2014; Mustafi et al., 2009). Cone photoreceptors also provide high visual acuity and spatial resolution (R. S. Molday & Moritz, 2015; Shichida & Matsuyama, 2009) (Table 1.1).

Cone-rod dystrophy (CRD) is a form of an inherited retinal degenerative disease (IRD) that affects 1 in 40,000 people worldwide (Hamel, 2007). CRD is due to cone photoreceptor degeneration followed by rod photoreceptor loss (Thiadens et al., 2012). In some cases, concurrent loss of both cones and rods is observed (Thiadens et al., 2012). The genetic etiology of CRD is heterogeneous with autosomal recessive, autosomal dominant, and X-linked patterns of inheritance. To date, there are at least 29 known CRD-causing genes (Table 1.2). The most common form of inheritance is autosomal recessive mutations and approximately fifteen genes have been identified (Table 1.2**)**. Autosomal dominant mutations have been identified in eleven genes and mutations in three genes have been identified in patients with X-linked forms of CRD (Table 1.2). Understanding the pathogenesis of CRD will accelerate the diagnoses, prognoses, and most importantly, the treatment of IRDs. The purpose of this introduction is to provide an overview of the retinal processes in which CRD-causing genes are involved.

1.2 Symptoms of CRD

The following distinct clinical features characterize CRD patients: decreased visual acuity, increased sensitivity to bright lights (photophobia), impaired color vision (dyschromatopsia), blind spots in the central field (scotomas), and late peripheral vision loss when rods begin to degenerate (Aboshiha, Dubis, Carroll, Hardcastle, & Michaelides, 2016; Hamel, 2007; Michaelides, Hardcastle, Hunt, & Moore, 2006). Additionally,

individuals with CRD may develop involuntary eye movement (nystagmus) that can further limit their autonomy (Berger, Kloeckener-Gruissem, & Neidhardt, 2010; Thiadens et al., 2012).

The gold standard for distinguishing CRD from other overlapping retinal dystrophies is through electroretinography (ERG) (Hamel, 2007; Michaelides et al., 2006; Thiadens et al., 2012). ERG provides a characteristic biphasic response known as the a- and b-wave. The hyperpolarizing a-wave corresponds to photoreceptor response, whereas the depolarizing b-wave is the responses of ON-bipolar cell and other retinal neurons. The time interval between the light stimulus onset and the peak a-wave is known as the a-wave implicit time and the stimulus onset to the peak of the b-wave is the b-wave implicit time. Light stimulation of primarily rod photoreceptors under dark conditions provides scotopic ERG, whereas excitation of primarily cone photoreceptors provides photopic ERG.

In CRD patients, ERG implicit response times show that cone responses, in comparison to rods, are significantly delayed (Michaelides et al., 2006; Thiadens et al., 2012). Additionally, the a- and b-wave single flash amplitudes are severely reduced in cones and over time in rods (Michaelides et al., 2006; Thiadens et al., 2012). Fundus examinations show pigmentary deposits at the macular region and moderately attenuated retinal vessels (Michaelides et al., 2006; Thiadens et al., 2012).

1.2.1 Distinguishing CRD from overlapping retinal disorders

Deterioration of cone photoreceptor function and survival can happen at various stages of life in retinal disorders other than CRD. Complete achromatopsia (ACHM or rod monochromacy) is defined as congenital color blindness primarily because of cone

dysfunctions (S, M, and L) (Aboshiha et al., 2016; Remmer, Rastogi, Ranka, & Ceisler, 2015). Individuals present the inability to distinguish color, photophobia, impaired visual acuity, and nystagmus (Kohl & Hamel, 2013; Remmer et al., 2015; Zobor, Zobor, & Kohl, 2015). The clinical onset of ACHM is at infancy and thought to be nonprogressive over time (Remmer et al., 2015). ERG recordings show nondetectable or significantly diminished cone responses while rod responses remain normal (Kohl & Hamel, 2013; Remmer et al., 2015). The prevalence of ACHM is 1:30,000 worldwide. All ACHM mutations to date have been identified as autosomal recessive (Ansar et al., 2015; Kohl & Hamel, 2013; Remmer et al., 2015).

Leber congenital amaurosis (LCA) is the most severe form of IRD (den Hollander, Roepman, Koenekoop, & Cremers, 2008). LCA is commonly inherited as autosomal recessive and the population frequency of LCA is thought to be 1:81,000 (Chacon-Camacho & Zenteno, 2015; den Hollander et al., 2008). LCA is clinically characterized by severe and early visual loss before the age of one, absent electrical responses on ERG, sensory nystagmus, and amauric pupils (Chacon-Camacho & Zenteno, 2015; den Hollander et al., 2008). Visual function and acuity are severely diminished between 20/200 to light perception (den Hollander et al., 2008).

Stargardt disease (SD) is the most common form of inherited macular dystrophy. The prevalence of SD is 1:8000–10,000 (Tanna, Strauss, Fujinami, & Michaelides, 2016). SD is characterized by bilateral macular atrophy with lipofuscin-like subretinal deposits (Tanna et al., 2016). The hallmark of SD is the presence of dark choroid during fluorescein angiography (Tanna et al., 2016). Full-field and multifocal ERG is generally restricted to cones or the macula region and with normal scotopic response (Tanna et al., 2016). Both

autosomal recessive and dominant mutations have been reported in SD (Palejwala et al., 2016; Tanna et al., 2016).

Retinitis pigmentosa (RP) is the most common form of IRD. The prevalence of RP is 1:4,000 worldwide (Sahel, Marazova, & Audo, 2015). RP patients present primary rod photoreceptor loss and then followed by cone photoreceptor loss. Initial symptoms include night blindness and reduced peripheral visual field. RP progresses to reduced visual acuity and macular lesions (Sahel et al., 2015; Shintani, Shechtman, & Gurwood, 2009; Yokochi, Li, Horiguchi, & Kishi, 2012). ERG measurements show severely reduced or nondetectable rod responses (a-wave) and increased b-wave implicit times (Sahel et al., 2015; Shintani et al., 2009; Yokochi et al., 2012). RP is progressive with time and can affect cone function and survival. To date, many genes have been implicated to cause RP (Daiger, Bowne, & Sullivan, 2007).

1.3 Photoreceptor cellular processes related to known CRD genes

In this section, CRD genes are discussed based on the protein's primary roles within a given photoreceptor compartment (OS, CC, IS, cell body, and synaptic terminal).

1.3.1 The photoreceptor OS: structure, phototransduction, and visual cycle

The OS is a dynamic compartment that interacts with the retinal pigment epithelium (RPE). The RPE is a monolayer cellular tissue that is adjacent to the photoreceptor OS and functions in providing nutrients, lipid synthesis, retinoid cycle, and mechanisms against photo-oxidation stress (R. S. Molday & Moritz, 2015; Strauss, 2005).

1.3.1.1 Disk morphogenesis, alignment, and OS structure

In order for the photoreceptors to maintain a constant OS length, the base of the OS generates new disks while the distal region sheds old disks. The base of the photoreceptor OS evaginates or outpouches to produce new OS disks (Figure 1.2) (Arikawa, Molday, Molday, & Williams, 1992; Steinberg, Fisher, & Anderson, 1980; Volland et al., 2015). The membrane disks are then flattened and align properly for OS membrane proteins to associate with each other and function properly (R. S. Molday & Moritz, 2015). As the OS base generates new disks, the distal disks shed ~10% per day, which are phagocytosed by the RPE cells (R. S. Molday & Moritz, 2015).

- *CDHR1* and *PROM1* complex. Cadherin Related Family Member 1 (CDHR1 also known as PrCAD and PCDH21) interacts with Prominin-1 (PROM1). The complex of CDHR1 and PROM1 is thought to play a role in disk morphogenesis at the OS base (Rattner, Chen, & Nathans, 2004; Rattner et al., 2001). CDHR1 is a photoreceptor-specific calcium-dependent cell-adhesion protein. CDHR1 is found on nascent evaginating discs and holds six extracellular cadherin repeats and a transmembrane domain (Rattner et al., 2004; Rattner et al., 2001). PROM1 is a pentaspan-transmembrane glycoprotein also localized at the base of the OS (Kleinman & Ambati, 2008). PROM1 interacts with actin filaments and the complex of PROM1 and actin is predicted to stabilize and facilitate the formation of new disks (Kleinman & Ambati, 2008; Rattner et al., 2004; Yang et al., 2008).
- *PRPH2* and *ROM1* complex. Peripherin 2/Retinal Degeneration, Slow (*PRPH2*) is a transmembrane protein that forms a heterotetramer with ROM1 (rod outer segment protein-1) (Stuck, Conley, & Naash, 2016). ROM1 is also an integral membrane protein (Clarke et al., 2000). Both PRPH2 and ROM1 are found at the photoreceptor disk

rim via noncovalent and disulfide linkages (Stuck et al., 2016). The PRPH2 and ROM1 complex induces membrane curvature at the disk rim and facilitates membrane fusion events during disk development (Clarke et al., 2000; Stuck et al., 2016). This complex also flattens disks through their disulfide linkage and anchors the disks to the plasma membrane CNG channel (Figure 1.3) (Clarke et al., 2000; Stuck et al., 2016).

- *ADAM9.* ADAM Metallopeptidase Domain 9 (ADAM9) is a member of A Disintegrin and Metalloprotease domain family (Parry, Toomes, et al., 2009). This protein may have several functions in the retina. ADAM9 is thought to keep the OS and RPE in close contact by acting as an adhesion protein (Parry, Toomes, et al., 2009). ADAM9 is known to bind αvβ5 integrin, and *Adam9 null* mice show abnormal contact between the OS and the RPE (Parry, Toomes, et al., 2009; Zhou, Graham, Russell, & Croucher, 2001).

1.3.1.2 Phototransduction

The phototransduction cascade begins with light-stimulated isomerization of 11-cis retinal which causes conformational changes of the opsin protein. Rod and cone opsin proteins have an 11-cis retinal chromophore binding pocket and function as G protein-coupled receptors (GPCR). Light causes the photoisomerization of the chromophore 11-cis retinal to all-trans retinal (Fu & Yau, 2007; Mannu, 2014). Opsin molecules (meta II) in turn activate transducin (Mannu, 2014), which then activates phosphodiesterase 6 (PDE6), an enzyme that hydrolyzes cGMP to 5'-GMP (Fu & Yau, 2007). PDE6 is a heterotetrameric protein composed of α, β, and two γ subunits (Cote, 2004; Grau et al., 2011; Hamilton & Hurley, 1990; Li, Volpp, & Applebury, 1990). The γ subunit of PDE6 functions as an inhibitory subunit that significantly reduces hydrolysis of cGMP to the

basal level (Cote, 2004; Deng et al., 2013). Upon light activation, transducin displaces the γ subunit of PDE6, activates PDE6, and promotes the hydrolysis of cGMP (Fu & Yau, 2007; Mannu, 2014). Reduction of cGMP in the cytoplasm leads to closure of ion channels and hyperpolarization of the photoreceptors (Figure 1.4) (Fu & Yau, 2007; Mannu, 2014).

- *GUCY2D* and *GUCA1A*. Guanylyl cyclase 1 (Gucy2d/Ret-GC1 or GC1), a transmembrane protein that plays a role in the synthesis of cGMP (Kuhn, 2016; Palczewski, Sokal, & Baehr, 2004; Wen, Dizhoor, & Makino, 2014). Ret-GC1 is expressed in both rods and cones and forms a homodimer (Figure 1.4) (Palczewski et al., 2004; Sharma & Duda, 2014). Ret-GC1 activity is regulated by GCAPs (GCAP1 and GCAP2), which are Ca^{2+} binding proteins (Behnen, Dell'Orco, & Koch, 2010; Koch & Dell'Orco, 2015; Kuhn, 2016). GCAPs stimulate Ret-GC1 in low concentrations of Ca^{2+} when the cyclic nucleotide-gated (CNG) ion channels are closed (Koch & Dell'Orco, 2015; Kuhn, 2016; Sharma & Duda, 2014). Ret-GC1 restores the pool of cGMP in the dark state and cGMP reopens the CNG channels (Figure 1.4). GCAP1 (GUCA1A) is thought to be more active than GCAP2 due to its lower affinity to Ca^{2+} and plays a role in early photo-recovery (Ames & Ikura, 2002; Behnen et al., 2010; Hughes, Brzovic, Dizhoor, Klevit, & Hurley, 1998).

1.3.1.3 Visual cycle

The RPE participates in the regeneration of 11-cis retinal required by the opsin molecules to sense photons. The regeneration process begins after the dissociation of all-trans retinal from opsins. All-trans retinal (NRPE) is then transferred by the flippase ABCA4 into the cytoplasm (R. S. Molday, 2007; Pollock & Callaghan, 2011). In the cytoplasm, retinol dehydrogenases (RDH) reduce all-trans retinal to all-trans retinol

(vitamin A) (Kiser, Golczak, Maeda, & Palczewski, 2012; Pollock & Callaghan, 2011; Tsybovsky, Molday, & Palczewski, 2010). All-trans retinol is subsequently transferred to the RPE either by adjacent membrane crossing or by the interphotoreceptor retinoid binding protein (IRBP) (Beharry, Zhong, & Molday, 2004; R. S. Molday, 2015; Tsybovsky et al., 2010). All-trans retinol undergoes a series of the following modifications: 1. LRAT esterifies all-trans retinol to all-trans retinyl esters. 2. RPE65 hydrolyzes all-trans retinyl esters and isomerizes it to 11-cis retinol. 3. RDH5 oxidizes 11-cis retinol to 11-cis retinal. 4. 11-cis retinal reenters the photoreceptors via IRBPs (Figure 1.5) (Beharry et al., 2004; Maugeri et al., 2000; R. S. Molday, 2015; Tsybovsky et al., 2010).

- *ABCA4.* ATP Binding Cassette Subfamily A Member 4 (ABCA4) is a membrane-associated protein found on the rod disks and the cone OS membrane lamina (Figure 1.5) (L. L. Molday, Rabin, & Molday, 2000; R. S. Molday, 2007; Tsybovsky et al., 2010). ABC proteins function as extra- and intracellular molecular transporters (Tsybovsky et al., 2010). ABCA4 is a photoreceptor-specific protein. It binds NRPE, a product of all-trans retinal and phosphatidylethanolamine (Beharry et al., 2004; R. S. Molday, 2007; Tsybovsky et al., 2010), and transports NRPE to the cytoplasmic side of the photoreceptor OS disk (Beharry et al., 2004).

- *RDH5.* Retinol Dehydrogenase 5 *(*RDH5) forms a complex with RPE65 and catalyzes 11-cis retinol to 11-cis retinal through an NAD+-dependent reaction (Kiser et al., 2012; Simon, Hellman, Wernstedt, & Eriksson, 1995). RPE65 is an isomerohydrolase that converts the all-trans-retinyl ester to 11-cis retinol (Kiser et al., 2015). RDH5 holds a Gly-Cys-Asp-Ser-Gly-Phe-Gly motif within the cofactor binding site for NAD(H) and this motif is essential for its catalytic activity (Kiser et al., 2012; Simon

et al., 1995; Skorczyk-Werner et al., 2015).

- *SEMA4A.* Semaphorin 4A (SEMA4A) has a transmembrane domain and is a member of the semaphorin family (Nojima et al., 2013; Toyofuku et al., 2012). Semaphorins are known to play a role in axonal extension, neuronal morphogenesis/development, cell migration, and cell proliferation (Toyofuku et al., 2012). In the retina, SEMA4A has been implicated to play a role in Rab11/FIP2-mediated endosomal sorting in RPE cells (Nojima et al., 2013; Toyofuku et al., 2012; Tsuruma et al., 2012). SEMA4A has been shown to sort retinoid-binding proteins, specifically cellular retinaldehyde-binding protein (CRALBP) and cellular retinol-binding protein 1 (CRBP1), at the cell surface and endoplasmic reticulum (Nojima et al., 2013; Toyofuku et al., 2012; Tsuruma et al., 2012).

1.3.2 The photoreceptor CC: ciliogenesis and protein transport

Retinitis Pigmentosa GTPase Regulator (RPGR) is expressed at the CC in the cones and rods (Dutta & Seo, 2016; Rao, Zhang, Li, Anand, & Khanna, 2016). RPGR proteins have a guanine nucleotide exchange factor (GEF) domain and interact with RAB8a, a small GTPase. RPGR proteins promote GDP/GTP nucleotide exchange of RAB8a (Dutta & Seo, 2016; Rao et al., 2016; Wätzlich et al., 2013). Additionally, RPGRs interact with RPGR-interacting protein 1 (RPGRIP1) (Remans, Bürger, Vetter, & Wittinghofer, 2014). RPGRIP1 is required for the proper localization of RPGR proteins to the CC (Figure 1.6) (Patnaik, Raghupathy, Zhang, Mansfield, & Shu, 2015; Remans et al., 2014). RPGRIP1 and RPGR form homodimers and interact with PDE6D (Dutta & Seo, 2016; Patnaik et al., 2015; Rao et al., 2016; Wätzlich et al., 2013). RPGR proteins also have many Glu-Gly

tandem repeats, and tubulin tyrosine ligase like-5 (TTLL5) has been found to polyglutamylate Glu-Gly-rich repetitive region (Sergouniotis et al., 2014; Sun et al., 2016). *Ttll5* mutant mouse shows impaired glutamylation of RPGR and compromised RPGR function (Sergouniotis et al., 2014; Sun et al., 2016).

1.3.3 The photoreceptor IS: protein folding, modification, and transport

The photoreceptor IS is filled with ribosomes, long mitochondria, endoplasmic reticulum, and the Golgi apparatus. The endoplasmic reticulum is the site for protein and lipid synthesis, whereas the Golgi apparatus is the site for protein posttranslational modification, packaging, and sorting. All proteins destined for the OS are synthesized in the IS and transported to the OS (Insinna & Besharse, 2008).

- *AIPL1*. Aryl Hydrocarbon Receptor Interacting Protein Like-1 (AIPL1) is a protein that contains tetratricopeptide repeats and is known as a chaperone (Gopalakrishna, Boyd, Yadav, & Artemyev, 2016; Kolandaivelu, Singh, & Ramamurthy, 2014). AIPL1 interacts with all of the rod PDE6 subunits (α, β, and γ) and the cone PDE6 α' subunit (Figure 1.6) (Gopalakrishna et al., 2016; Kolandaivelu et al., 2014; Majumder, Gopalakrishna, Cheguru, Gakhar, & Artemyev, 2013; Ramamurthy et al., 2003). AIPL1's role in the photoreceptors is folding and stabilizing PDE6 (Gopalakrishna et al., 2016; Kolandaivelu et al., 2014).

- *ARL3* and *RP2*. Arf-like protein 3 (ADP-ribosylation factor-like 3 or ARL3) is a member of the small GTPase family (Hanke-Gogokhia et al., 2016). This protein has a role in trafficking lipid-binding proteins and axoneme formation (Hanke-Gogokhia et al., 2016; Wright et al., 2016; Wätzlich et al., 2013; Zhang et al., 2015). Specifically, ARL3

may function as a cargo displacement factor for lipidated protein (Hanke-Gogokhia et al., 2016; Zhang et al., 2015). ARL3 cycles from the inactive GDP-bound state to an active GTP-bound form (Hanke-Gogokhia et al., 2016; Wright et al., 2016). Retinitis pigmentosa 2 (RP2) is a GTPase-activating protein (GAP) and has been shown to accelerate the hydrolysis of GTP bound form of ARL3 (Zhang et al., 2015). Moreover, RP2 stimulates the GTPase activity of tubulin and may also participate in vesicular transport (Zhang et al., 2015).

- *UNC119.* Uncoordinated 119 protein (UNC119) is an acyl-binding chaperone (Constantine, Zhang, Gerstner, Frederick, & Baehr, 2012; Gopalakrishna et al., 2011). It functions in the solubilization and trafficking of acylated transducin-α subunit (Zhang et al., 2011). Transducin undergoes bidirectional translocations between the IS and OS under different light conditions. UNC119 interacts with the N-acylated GTP-bound transducin-α subunit in the dark (Figure 1.6) (Constantine et al., 2012; Gopalakrishna et al., 2011; Zhang et al., 2011). The binding of UNC119 to transducin may facilitate the separation of transducin-α subunit from the γ and β subunits (Gopalakrishna et al., 2011; Zhang et al., 2011).

- *KCNV2.* Potassium Voltage-Gated Channel Modifier Subfamily V Member 2 (KCVN2) is a subunit of a voltage-gated potassium channel found in the IS (Ottschytsch, Raes, Van Hoorick, & Snyders, 2002; Wu et al., 2006). It has six transmembrane domains and forms hetero-tetramers with KCNB1, KCNC1, and KCNF1. KCNV2 has a potassium-selective motif, GYG in the transmembrane loop (Czirják, Tóth, & Enyedi, 2007; Wu et al., 2006) and is predicted to have an essential role in ion homeostasis and cell repolarization (Czirják et al., 2007; Wu et al., 2006).

- *RAB28.* RAS-related protein RAB28 is a small GTPase. It has a farnesylation motif at the CaaX carboxyl terminus, while other RABs contain geranylgeranyl motifs at the same region (Roosing et al., 2013). RAB28 localizes at the basal body and ciliary rootlets in photoreceptors (Figure 1.6) (Roosing, Collin, den Hollander, Cremers, & Siemiatkowska, 2014; Roosing et al., 2013). In the unicellular organism, trypanosoma brucei, RAB28 may be involved in endocytosis, lysosomal sorting, and delivery of protein cargos (Lumb, Leung, Dubois, & Field, 2011).
- *CERKL*. Ceramide kinase-like (CERKL) is an antioxidant protein (Tuson, Garanto, Gonzàlez-Duarte, & Marfany, 2009). CERKL is expressed at the endoplasmic reticulum and on the Golgi (Li et al., 2014; Tuson et al., 2009). During hypoxia, CERKL is up-regulated and protects cells from apoptosis (Li et al., 2014; Tuson et al., 2009) by interacting with mitochondrial thioredoxin 2 (TRX2) and regulating its antioxidant pathway (Li et al., 2014).

1.3.4 The photoreceptor cell body: gene transcription and expression

The photoreceptor cell body holds the nucleus, the site for gene expression. As retinal precursor cells develop into various differentiated cell types, photoreceptor-specific gene expression in mice starts at approximately embryonic day 11 (E11) and finishes around postnatal day 10 (P10) (Brzezinski & Reh, 2015; Swaroop, Kim, & Forrest, 2010). The birth of photoreceptor cells is from central-to-peripheral retina where cone photoreceptors are born at ~E11 and peak at E14 in the central retina (Brzezinski & Reh, 2015). Rod photoreceptors are born at ~E14.5 and peak at P0 in the central retina and peak at P1 in the peripheral retina (Figure 1.7) (Brzezinski & Reh, 2015).

- *CRX* and *RAX2.* Cone-rod homeobox (CRX) is a photoreceptor-specific transcription factor (Furukawa, Morrow, & Cepko, 1997; Hennig, Peng, & Chen, 2008). It binds the upstream sequence 5-TAATC[CA]-3 and induces the expression of S-opsin (Opn1sw) and M-opsin (Opn1mw) (Figure 1.7) (Furukawa et al., 1997; Hennig et al., 2008). Therefore, retinal precursor cells that express CRX develop into cone photoreceptors (Furukawa et al., 1997; Hennig et al., 2008). The transactivation of CRX is increased by RAX2 (Retina and Anterior Neural Fold Homeobox 2) (Irie et al., 2015). RAX2 directly interacts with CRX and cooperatively transactivates rhodopsin and cone opsin genes (Irie et al., 2015; Reks, McIlvain, Zhuo, & Knox, 2014). Reduction of RAX2 leads to a significant reduction of the expression of *Opn1sw, Opn1mw, Gnat2, and Pde6c* genes (Irie et al., 2015).

1.3.5 The photoreceptor synaptic terminus: neurotransmitter release

Photoreceptors release the neurotransmitter L-glutamate in the absence of light, which is calcium-dependent. Upon depolarization in the dark, photoreceptors release L-glutamate into the synaptic cleft between photoreceptors and bipolar and horizontal cells. In the light, the closure of the CNG channels leads to photoreceptor hyperpolarization, which reduces calcium concentration in the synapse and thus L-glutamate release. Several cellular processes can affect Ca^{2+} level and glutamate release in rods and cones.

- *CACNA1F*, *CACNA2D4,* and *RIMS1*. L-type (long-lasting) $Ca_v1.4$ channels mediate voltage-dependent Ca^{2+} currents into the photoreceptor ribbon synapse that triggers exocytotic release of glutamate (Dolphin, 2016; Heidelberger, Thoreson, & Witkovsky, 2005). $Ca_v1.4$ channels are localized on the plasma membrane of the synaptic

terminus and are clustered near the presynaptic ribbon **(**Figure 1.8) (Davies et al., 2007; Dolphin, 2016). $Ca_v1.4$ channel is composed of α1, α2δ4, β, and γ subunits (Dolphin, 2016). CACNA1F is the alpha-1 (α1) and pore-forming subunit of the channel and can sustain calcium current over a large voltage range during synaptic transmission (Davies et al., 2007; Dolphin, 2012, 2016; Koschak et al., 2003; McRory et al., 2004). The alpha2delta 4 (CACNA2D4) is processed into two subunits, alpha-2 and delta-4, and is linked by a disulfide bond (Dolphin, 2012, 2016). CACNA2D4 acts as an auxiliary subunit that forms a complex with the α1 subunit (Dolphin, 2012, 2016). CACNA2D4 regulates the activity of the calcium channel by changing the properties of the α1 subunits (Dolphin, 2012, 2016; Koschak et al., 2003). Regulating Synaptic Membrane Exocytosis 1 (RIMS1) is a member of the RAS superfamily and is a synaptic active zone protein that regulates vesicle exocytosis (Castillo, Schoch, Schmitz, Südhof, & Malenka, 2002). RIMS1 is directly involved in the exocytosis of synaptic vesicles and has been found to enhance the influx of Ca^{2+} via $Ca_v1.4$ channels at the synaptic terminus (Figure 1.8) (Castillo et al., 2002; Grabner et al., 2015). Loss of RIMS1 leads to significant reduction in Ca^2 influx through $Ca_v1.4$ channels which suggests that RIMS1 may facilitate the opening of $Ca_v1.4$ channels, and thus the release of glutamate (Grabner et al., 2015). RIMS1 also interacts with RAB3 and facilitates synaptic-vesicle fusion (Castillo et al., 2002; Grabner et al., 2015).

1.3.6 Proteins encoded by CRD genes with poorly-understood functions

The functions of several proteins, encoded by CRD genes, in the retina are not clearly understood. These proteins are C8ORF37, C21ORF2, POC1B, PITPNM3, and CNNM4. Interestingly, a majority of these proteins are found at the base of the CC and are

postulated to have a ciliary role, such as C8ORF37 and C21ORF2 (Estrada-Cuzcano et al., 2012; Khan, Eisenberger, Nagel-Wolfrum, Wolfrum, & Bolz, 2015). C8ORF37 is also found in the cell body and the OPL of photoreceptors. The ciliary role of C8ORF37 and C21ORF2 has not yet been studied in detail. Similarly, POC1B is localized at the basal body near the periciliary region (Beck et al., 2014; Roosing, Lamers, et al., 2014). POC1B is thought to play a role in centriole assembly and ciliogenesis (Beck et al., 2014; Roosing, Lamers, et al., 2014).

Another protein, PITPNM3 is expressed in the photoreceptor IS and synaptic terminus as well as Muller cells in rodent retinas (Köhn et al., 2007). PITPNM3 is thought to transfer phosphatidylinositol and phosphatidylcholine across the plasma membranes (Köhn et al., 2007). Lastly, CNNM4 has four transmembrane domains, binds magnesium ions, and regulates metal ion homeostasis by interacting with cytochrome oxidase 11 (Parry, Mighell, et al., 2009; Polok et al., 2009). CNNM4 is localized to the photoreceptors (IS, OS, OPL), ganglion cells, and inner plexiform layer in the retina (Parry, Mighell, et al., 2009; Polok et al., 2009). Currently, how CNNM4 mutations lead to CRD remains unclear.

1.4 Conclusions

Rod and cone photoreceptors are highly specialized cells with structurally and functionally distinct subcellular compartments (OS, CC, IS, cell body, and synaptic terminus). The currently identified CRD-causing genes are involved in cellular processes in every subcellular compartment of these two types of photoreceptors. Perturbation in these cellular processes leads to photoreceptor dysfunction and degeneration. Proteins that

associate with CRD and function in the OS mainly have a role in phototransduction, OS morphogenesis, disk alignment, and retinoid cycle. Other CRD proteins are critical for protein transport in the CC, protein synthesis in the IS, gene transcription in the cell body, and neurotransmitter release in the synaptic terminus. Insights into the function of these CRD-causing genes have significantly accelerated our understanding of photoreceptor cell biology from light detection to synaptic transmission as well as the CRD pathogenic mechanism. However, the function of several CRD-causing genes still remain unknown. Future efforts should focus on understanding the molecular functions of these genes to better understand the light sensing neurons—the rod and cone photoreceptors under healthy and diseased conditions.

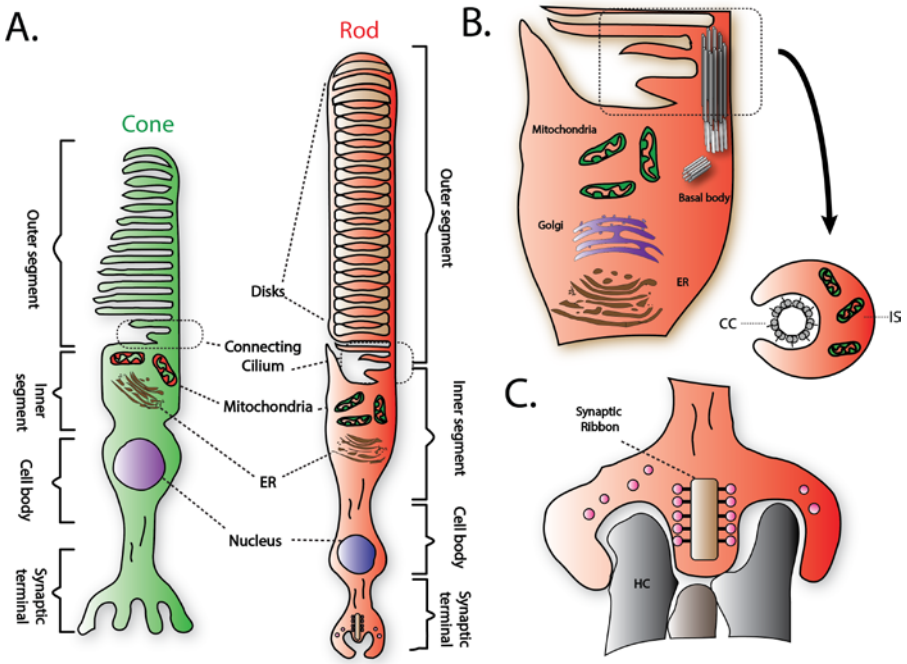

Figure 1.1: Schematic diagram of a cone and rod photoreceptor. (A) Rod and cone photoreceptor structures with labeled compartments. (B) The inner segment holds the mitochondria, endoplasmic reticulum, and the Golgi. In the right with the arrow is a magnified diagram of the cross-section of the connecting cilium (CC), showing a 9+0 microtubule doublet. Microtubule doublets are anchored to the basal body. (C) The synaptic terminal is for glutamate release to bipolar and horizontal cells (HC). Magnified schematic diagram of the synaptic terminal. The synaptic terminal contains specialized synaptic ribbons for fast glutamate release.

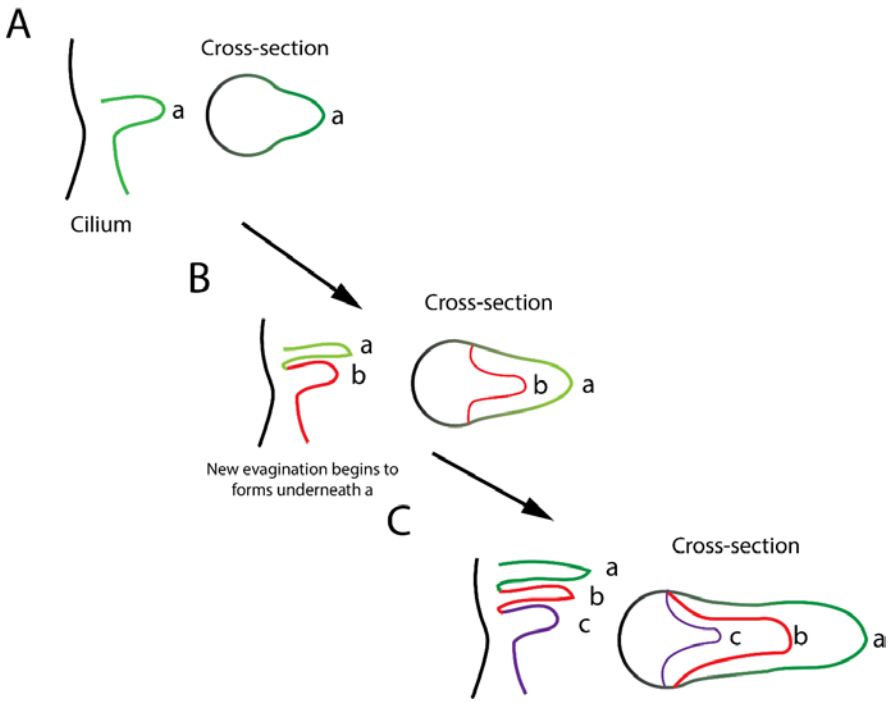

Figure 1.2: Schematic diagram of outer segment generation. (A) At the base of the cilium is where the OS membrane begins to evaginations or outpouch. (B) The outpouched membrane grows while subsequent newer disks form from below. (C) The expanding membranes reach an optimal length and can later become detached as free-floating discs in rods or remain attached to the outer segment membrane in cones (Steinberg et al., 1980).

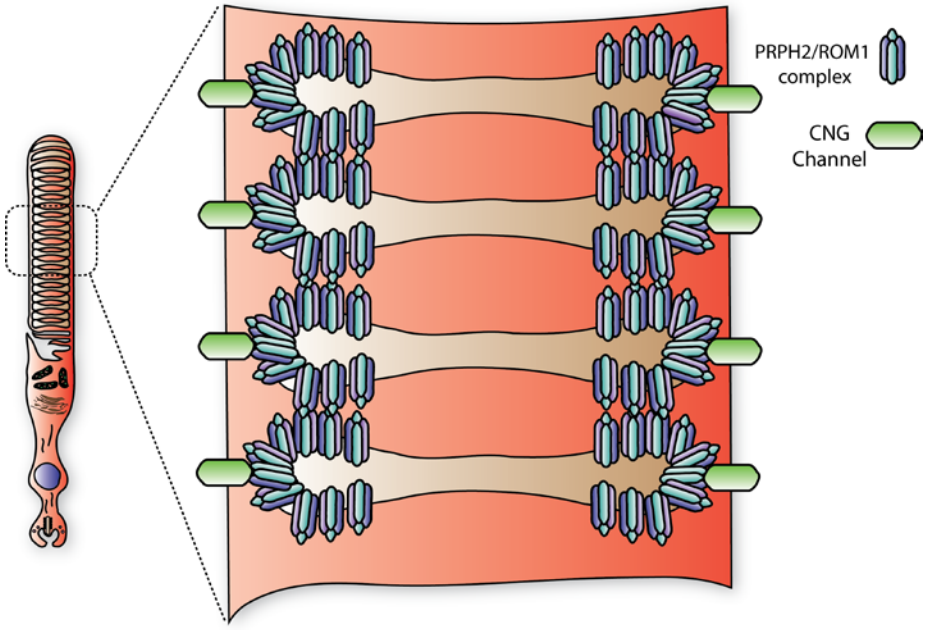

Figure 1.3: PRPH2/ROM1 complex. Both PRPH2 and ROM1 are transmembrane proteins that form a heterotetramer and found at the disk rim via noncovalent and disulfide linkages (Stuck et al., 2016). The PRPH2 and ROM1 complex plays a role in membrane curvature during nascent disk formation and at the disk rim. This complex also anchors the disks to the plasma membrane CNG channel (Stuck et al., 2016).

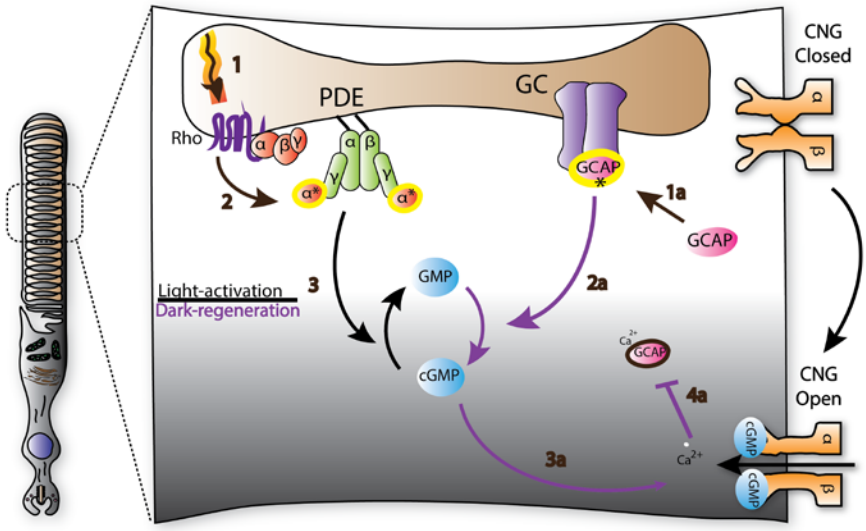

Figure 1.4: Schematic representation of the phototransduction cascade. 1. A wavelength of light induces the photoisomerization of the chromophore 11-cis retinal to all-trans retinal in the opsin protein and 2. transducin dissociates and then activates phosphodiesterase (PDE), an enzyme that hydrolyzes cGMP to 5'-GMP. 3. PDE reduces cGMP levels which leads to closure of cGMP-gated cation channels (CNG). 1a. Low Ca^{2+} concentration activate GCAP and it stimulates GC. 2a. GC resynthesizes cGMP. 3a. cGMP binds CNG channels and opens the channel. 4a. Increased Ca^{2+} concentration leads to reduced GCAP and GC activity (Fu & Yau, 2007; R. S. Molday & Moritz, 2015). Asterisks represent active state.

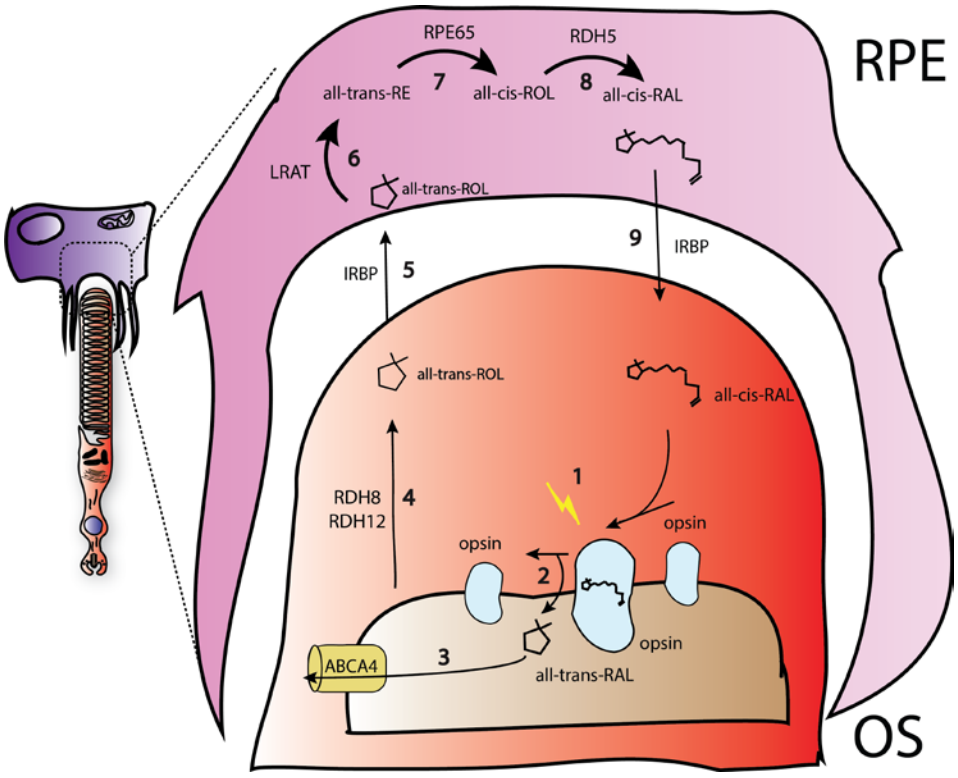

Figure 1.5: Schematic illustration of the visual cycle. 1. Photo-activation of opsin and isomerization of all-cis-RAL. 2. The dissociation of all-trans retinal. 3. All-trans retinal is transferred to the cytoplasm by the flippase ABCA4. 4. In the cytoplasm, RDH8/12 reduces all-trans retinal to all-trans retinol (vitamin A). 5. All-trans retinol is subsequently transferred to the RPE by interphotoreceptor retinoid binding protein (IRBP). 6. LRAT esterifies all-trans retinol to all-trans retinyl esters. 7. RPE65 isomerizes all-trans retinyl esters to 11-cis retinol. 8. RDH5 oxidizes 11-cis retinol to 11-cis retinal. 9. Lastly, 11-cis retinal reenters the photoreceptors via IRBPs (Kiser et al., 2012; Kiser et al., 2015; R. S. Molday, 2015; Pollock & Callaghan, 2011; Tsybovsky et al., 2010).

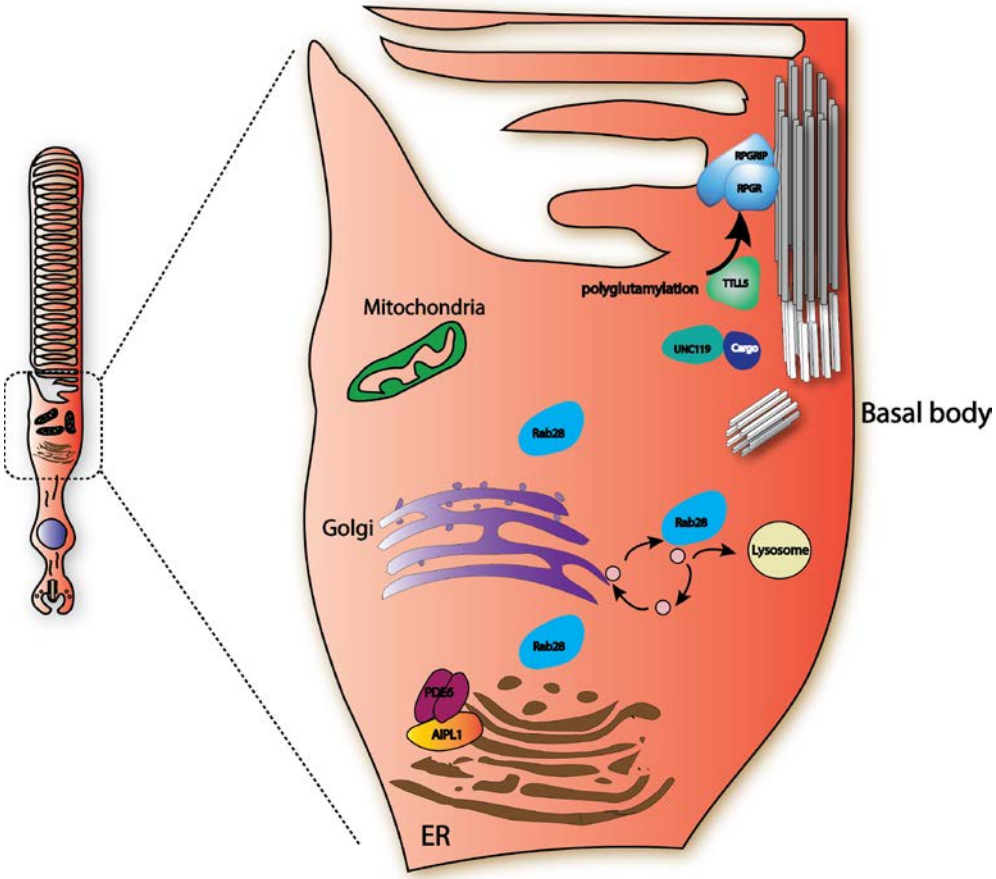

Figure 1.6: Schematic illustration of the inner segment. AIPL1 interacts with all of the PDE6 subunits and acts as a chaperone (Gopalakrishna et al., 2016; Ramamurthy et al., 2003). Similarly, UNC119 functions acts as a lipid-binding chaperone for transducing as it facilitates it transport (Gopalakrishna et al., 2011; Zhang et al., 2011). RAB28 may play a role in endocytosis and lysosomal delivery of protein cargo (Lumb et al., 2011; Roosing et al., 2013). RPGR is found at the photoreceptor connecting cilia and binds to the RPGR interacting protein 1 (RPGRIP1) (Patnaik et al., 2015). TTLL5 glutamylates RPGR for its proper function (Sergouniotis et al., 2014; Sun et al., 2016).

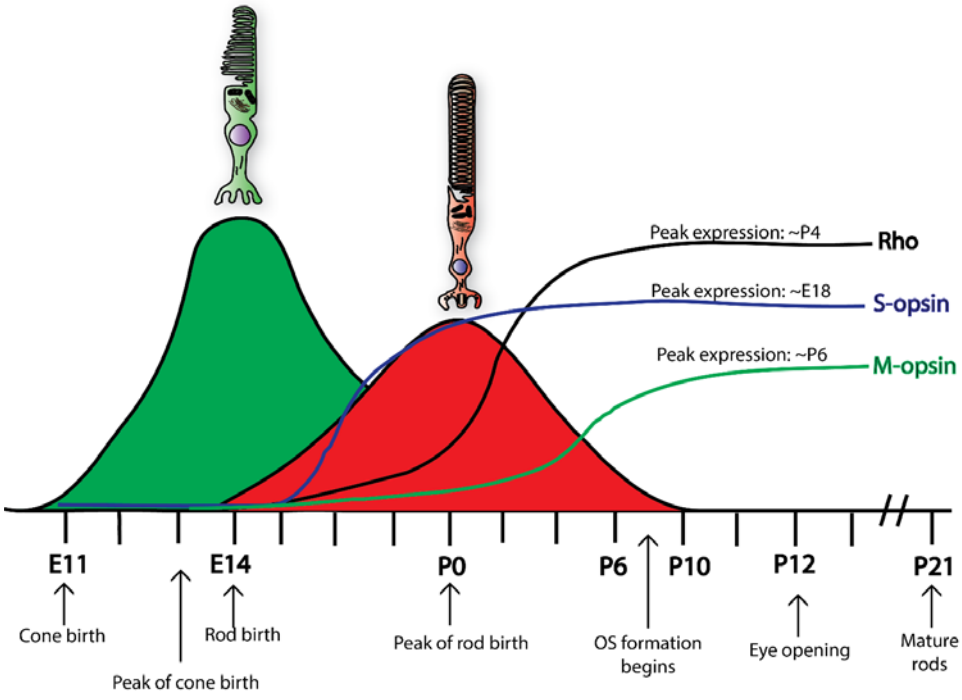

Figure 1.7: Photoreceptor birth and maturation in mice. From central-to-peripheral gradient, cone birth starts at embryonic day (E) 11.0 with production peaking at E14.0 (Brzezinski & Reh, 2015). Rods are born prenatally at E14 until postnatal P10. Rods birth peaks at P0 (Brzezinski & Reh, 2015). Area under curve equals 100%. Expression of S opsin begins at ~E18, M opsin at ~P6 (Cepko, 2014; Swaroop et al., 2010), and rhodopsin at ~P4 (Akimoto et al., 2006).

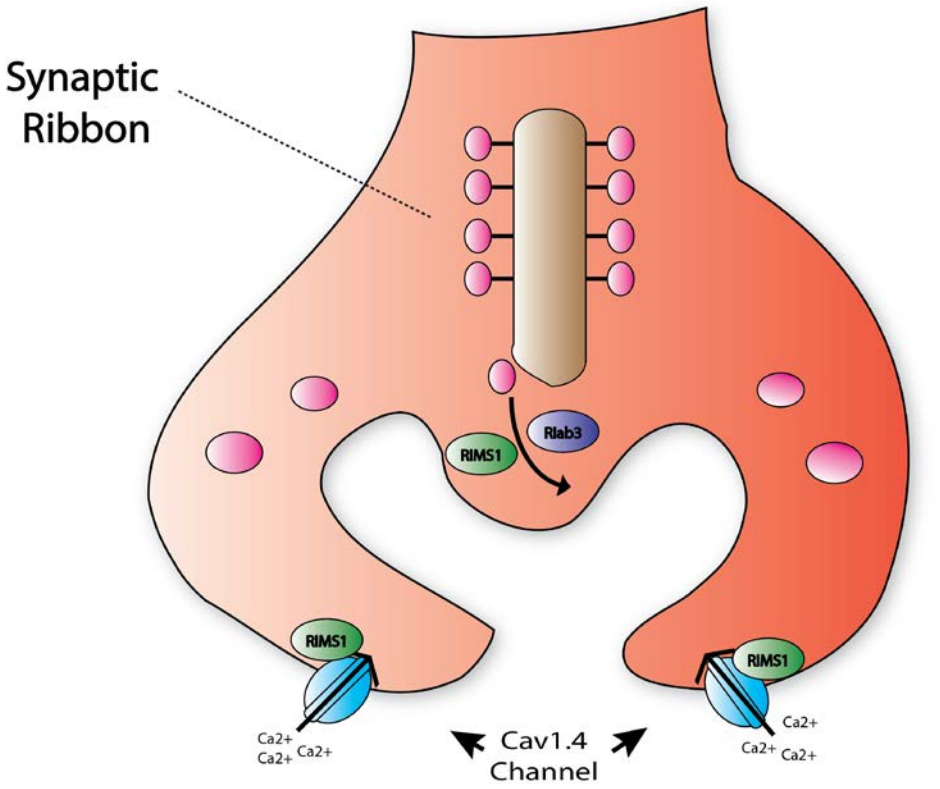

Figure 1.8: Synaptic transmission. Calcium voltage-gated channel $Ca_v1.4$ consists of several subunits including CACNA1F, the pore forming alpha-1 subunit and CACNA2D4, the auxiliary alpha2/delta-4 subunits (Joiner & Lee, 2015; Koschak et al., 2003). $Ca_v1.4$ uptakes Ca2+ ions and can sustain calcium current over a longer voltage range during synaptic transmission (Joiner & Lee, 2015; Koschak et al., 2003). RIMS1 interacts with rab3 for the release of synaptic vesicles (Castillo et al., 2002). RIM1/2 proteins also regulate the $Ca_v1.4$ channel opening (Grabner et al., 2015).

Table 1.1: Differences between human cones and rods

Characteristics	Cones[a,b]	Rods[a,b]
Optimal function	Bright light	Low light
Sensitivity	Low	High
Response	Fast	Slow
Dark adaptation	Fast	Slow
Shape	Short/wide/conical	Long/narrow/uniform
Abundance site	Fovea	Peripheral
Length OS (µm)-primate	13	25
Diameter OS (µm)--primate	3-base 1-tip	2

[a](Shichida & Matsuyama, 2009)

[b](Fu & Yau, 2007)

Table 1.2 CRD genes, loci, expression, and associated diseases

Gene name	Locus[a,b]	Expression [b]	Inheritance [b]	Retinal Diseases [b]
ABCA4	1p21-23	Cones, rods	Recessive	CRD,CD,STGD1, RP
ADAM9	8p11.23	RPE	Recessive	CRD
C21ORF2	21q22.3	Ubiquitous	Recessive	CRD
C8ORF37	8q22.1	Cones, rods	Recessive	CRD, RP
CACNA2D4	12p13.33	Ubiquitous	Recessive	CRD, CD
CDHR1	10q23.1	Ubiquitous	Recessive	CRD, RP
CERKL	2q31.3	Cones, rods	Recessive	CRD, RP
CNNM4	2q11.2	Ubiquitous	Recessive	CRD, JLL
KCNV2	9p24.2	Cones, rods	Recessive	CRD
POC1B	12q21.33	Ubiquitous	Recessive	CRD
RAB28	4p15.33	Ubiquitous	Recessive	CRD
RAX2	19p13.3	Retina, brain	Recessive	CRD
RDH5	12q13.2	RPE	Recessive	CRD, FA
RPGRIP1	14q11.2	Cones, rods	Recessive	CRD, LCA, RP
TTLL5	14q24.3	Retina, some tissues	Recessive	CRD, RP
AIPL1	17p13.1	Cones, rods	Dominant	CRD, LCA
ARL3	10q23.3	Retina	Dominant	CRD, RP
CRX	19q13.33	Cones, rods	Dominant	CRD, LCA, RP
GUCA1A	6p21.1	Cones, rods	Dominant	CRD, CD
GUCY2D	17p13.1	Cones, rods	Dominant	CRD, LCA, MD, RP
PITPNM3	17p13	Retina	Dominant	CRD, RP
PROM1	4p15.32	Ubiquitous	Dominant	CRD, STGD
PRPH2	6p21.1	Cones, rods	Dominant	CRD, MD, RP
RIMS1	6q12-q13	Retina, brain	Dominant	CRD
SEMA4A	1q22	Ubiquitous	Dominant	CRD, RP
UNC119	17q11.2	Neural retina	Dominant	CRD
RPGR	Xp11.4	Cones, rods	X-linked	CRD, MD, RP
CACNA1F	Xp11.23	Neural retina	X-linked	CRD, CSNB
RP2	Xp11.3	Ubiquitous	X-linked	CRD, RP

ACHM-Achromatopsia; CD-Cone dystrophy; CRD-Cone-rod dystrophy; CSNB-congenital stationary blindness; FA-Fundus Albipunctatus; JLL-Jalili syndrome; LCA- Leber congenital amaurisis; MD-Macular degeneration; RPE-retinal pigment epithelium; STGG-Stargardt disease. [a]www.genecard.com [b]Online Mendelian Inheritance in Man (OMIM)

1.5 References

Aboshiha, J., Dubis, A. M., Carroll, J., Hardcastle, A. J., & Michaelides, M. (2016). The cone dysfunction syndromes. *British Journal of Ophthalmology, 100*(1), 115-121. doi:10.1136/bjophthalmol-2014-306505

Akimoto, M., Cheng, H., Zhu, D., Brzezinski, J. A., Khanna, R., Filippova, E., Swaroop, A. (2006). Targeting of GFP to newborn rods by Nrl promoter and temporal expression profiling of flow-sorted photoreceptors. *Proceedings of the National Academy of Sciences USA, 103*(10), 3890-3895. doi:10.1073/pnas.0508214103

Ames, J. B., & Ikura, M. (2002). Structure and membrane-targeting mechanism of retinal Ca2+-binding proteins, recoverin and GCAP-2. *Advances in Experimental Medicine and Biology, 514*, 333-348.

Ansar, M., Santos-Cortez, R. L., Saqib, M. A., Zulfiqar, F., Lee, K., Ashraf, N. M., Genomics, U. o. W. C. f. M. (2015). Mutation of ATF6 causes autosomal recessive achromatopsia. *Human Genetics, 134*(9), 941-950. doi:10.1007/s00439-015-1571-4

Arikawa, K., Molday, L. L., Molday, R. S., & Williams, D. S. (1992). Localization of peripherin/rds in the disk membranes of cone and rod photoreceptors: relationship to disk membrane morphogenesis and retinal degeneration. *Journal of Cell Biology, 116*(3), 659-667.

Beck, B. B., Phillips, J. B., Bartram, M. P., Wegner, J., Thoenes, M., Pannes, A., Bolz, H. J. (2014). Mutation of POC1B in a severe syndromic retinal ciliopathy. *Human Mutatation, 35*(10), 1153-1162. doi:10.1002/humu.22618

Beharry, S., Zhong, M., & Molday, R. S. (2004). N-retinylidene-phosphatidylethanolamine is the preferred retinoid substrate for the photoreceptor-specific ABC transporter ABCA4 (ABCR). *Journal of Biological Chemistry, 279*(52), 53972-53979. doi:10.1074/jbc.M405216200

Behnen, P., Dell'Orco, D., & Koch, K. W. (2010). Involvement of the calcium sensor GCAP1 in hereditary cone dystrophies. *Biological Chemistry, 391*(6), 631-637. doi:10.1515/BC.2010.063

Berger, W., Kloeckener-Gruissem, B., & Neidhardt, J. (2010). The molecular basis of human retinal and vitreoretinal diseases. *Progress in Retinal and Eye Research, 29*(5), 335-375. doi:10.1016/j.preteyeres.2010.03.004

Brzezinski, J. A., & Reh, T. A. (2015). Photoreceptor cell fate specification in vertebrates. *Development, 142*(19), 3263-3273. doi:10.1242/dev.127043

Castillo, P. E., Schoch, S., Schmitz, F., Südhof, T. C., & Malenka, R. C. (2002). RIM1alpha is required for presynaptic long-term potentiation. *Nature, 415*(6869), 327-330. doi:10.1038/415327a

Cepko, C. (2014). Intrinsically different retinal progenitor cells produce specific types of progeny. *Nature Reviews Neuroscience, 15*(9), 615-627. doi:10.1038/nrn3767

Chacon-Camacho, O. F., & Zenteno, J. C. (2015). Review and update on the molecular basis of Leber congenital amaurosis. *World Journal of Clinical Cases, 3*(2), 112-124. doi:10.12998/wjcc.v3.i2.112

Clarke, G., Goldberg, A. F., Vidgen, D., Collins, L., Ploder, L., Schwarz, L.,McInnes, R. R. (2000). Rom-1 is required for rod photoreceptor viability and the regulation of disk morphogenesis. *Nature Genetics, 25*(1), 67-73. doi:10.1038/75621

Constantine, R., Zhang, H., Gerstner, C. D., Frederick, J. M., & Baehr, W. (2012). Uncoordinated (UNC)119: coordinating the trafficking of myristoylated proteins. *Vision Research, 75*, 26-32. doi:10.1016/j.visres.2012.08.012

Cote, R. H. (2004). Characteristics of photoreceptor PDE (PDE6): similarities and differences to PDE5. *International Journal of Impotence Research, 16 Suppl 1*, S28-33. doi:10.1038/sj.ijir.3901212

Curcio, C. A., Allen, K. A., Sloan, K. R., Lerea, C. L., Hurley, J. B., Klock, I. B., & Milam, A. H. (1991). Distribution and morphology of human cone photoreceptors stained with anti-blue opsin. *Journal of Comparative Neurology, 312*(4), 610-624. doi:10.1002/cne.903120411

Czirják, G., Tóth, Z. E., & Enyedi, P. (2007). Characterization of the heteromeric potassium channel formed by kv2.1 and the retinal subunit kv8.2 in Xenopus oocytes. *Journal of Neurophysiology, 98*(3), 1213-1222. doi:10.1152/jn.00493.2007

Daiger, S. P., Bowne, S. J., & Sullivan, L. S. (2007). Perspective on genes and mutations causing retinitis pigmentosa. *Archives of Ophthalmology, 125*(2), 151-158. doi:10.1001/archopht.125.2.151

Davies, A., Hendrich, J., Van Minh, A. T., Wratten, J., Douglas, L., & Dolphin, A. C. (2007). Functional biology of the alpha(2)delta subunits of voltage-gated calcium channels. *Trends in Pharmacological Sciences, 28*(5), 220-228. doi:10.1016/j.tips.2007.03.005

den Hollander, A. I., Roepman, R., Koenekoop, R. K., & Cremers, F. P. (2008). Leber congenital amaurosis: genes, proteins and disease mechanisms. *Progress in Retinal and Eye Research, 27*(4), 391-419. doi:10.1016/j.preteyeres.2008.05.003

Deng, W. T., Sakurai, K., Kolandaivelu, S., Kolesnikov, A. V., Dinculescu, A., Li, J., Hauswirth, W. W. (2013). Cone phosphodiesterase-6α' restores rod function and confers distinct physiological properties in the rod phosphodiesterase-6β-deficient rd10 mouse. *Journal of Neuroscience, 33*(29), 11745-11753. doi:10.1523/JNEUROSCI.1536-13.2013

Dolphin, A. C. (2012). Calcium channel auxiliary α2δ and β subunits: trafficking and one step beyond. *Nature Reviews Neuroscience, 13*(8), 542-555. doi:10.1038/nrn3311

Dolphin, A. C. (2016). Voltage-gated calcium channels and their auxiliary subunits: physiology and pathophysiology and pharmacology. *Journal of Physiology*. doi:10.1113/JP272262

Dutta, N., & Seo, S. (2016). RPGR, a prenylated retinal ciliopathy protein, is targeted to cilia in a prenylation- and PDE6D-dependent manner. *Biology Open*. doi:10.1242/bio.020461

Estrada-Cuzcano, A., Neveling, K., Kohl, S., Banin, E., Rotenstreich, Y., Sharon, D., Consortium, E. R. D. (2012). Mutations in C8orf37, encoding a ciliary protein, are associated with autosomal-recessive retinal dystrophies with early macular involvement. *American Journal of Human Genetics, 90*(1), 102-109. doi:10.1016/j.ajhg.2011.11.015

Fu, Y., & Yau, K. W. (2007). Phototransduction in mouse rods and cones. *Pflugers Archiv, 454*(5), 805-819. doi:10.1007/s00424-006-0194-y

Furukawa, T., Morrow, E. M., & Cepko, C. L. (1997). Crx, a novel otx-like homeobox gene, shows photoreceptor-specific expression and regulates photoreceptor differentiation. *Cell, 91*(4), 531-541.

Gopalakrishna, K. N., Boyd, K., Yadav, R. P., & Artemyev, N. O. (2016). Aryl Hydrocarbon Receptor-interacting Protein-like 1 Is an Obligate Chaperone of Phosphodiesterase 6 and Is Assisted by the γ-Subunit of Its Client. *Journal of Biological Chemistry, 291*(31), 16282-16291. doi:10.1074/jbc.M116.737593

Gopalakrishna, K. N., Doddapuneni, K., Boyd, K. K., Masuho, I., Martemyanov, K. A., & Artemyev, N. O. (2011). Interaction of transducin with uncoordinated 119 protein (UNC119): implications for the model of transducin trafficking in rod photoreceptors. *Journal of Biological Chemistry, 286*(33), 28954-28962. doi:10.1074/jbc.M111.268821

Grabner, C. P., Gandini, M. A., Rehak, R., Le, Y., Zamponi, G. W., & Schmitz, F. (2015). RIM1/2-Mediated Facilitation of Cav1.4 Channel Opening Is Required for Ca2+-Stimulated Release in Mouse Rod Photoreceptors. *Journal of Neuroscience, 35*(38), 13133-13147. doi:10.1523/JNEUROSCI.0658-15.2015

Grau, T., Artemyev, N. O., Rosenberg, T., Dollfus, H., Haugen, O. H., Cumhur Sener, E., Kohl, S. (2011). Decreased catalytic activity and altered activation properties of PDE6C mutants associated with autosomal recessive achromatopsia. *Human Molecular Genetics, 20*(4), 719-730. doi:10.1093/hmg/ddq517

Hamel, C. P. (2007). Cone rod dystrophies. *Orphanet Journal of Rare Diseases, 2*, 7. doi:10.1186/1750-1172-2-7

Hamilton, S. E., & Hurley, J. B. (1990). A phosphodiesterase inhibitor specific to a subset of bovine retinal cones. *Journal of Biological Chemistry, 265*(19), 11259-11264.

Hanke-Gogokhia, C., Wu, Z., Gerstner, C. D., Frederick, J. M., Zhang, H., & Baehr, W. (2016). Arf-like protein 3 (ARL3) regulates protein trafficking and ciliogenesis in mouse photoreceptors. *Journal of Biological Chemistry, 291*(13), 7142-7155. doi:10.1074/jbc.M115.710954

Heidelberger, R., Thoreson, W. B., & Witkovsky, P. (2005). Synaptic transmission at retinal ribbon synapses. *Progress in Retinal and Eye Research, 24*(6), 682-720. doi:10.1016/j.preteyeres.2005.04.002

Hennig, A. K., Peng, G. H., & Chen, S. (2008). Regulation of photoreceptor gene expression by Crx-associated transcription factor network. *Brain Research, 1192*, 114-133. doi:10.1016/j.brainres.2007.06.036

Hughes, R. E., Brzovic, P. S., Dizhoor, A. M., Klevit, R. E., & Hurley, J. B. (1998). Ca2+-dependent conformational changes in bovine GCAP-2. *Protein Science, 7*(12), 2675-2680. doi:10.1002/pro.5560071222

Imamoto, Y., & Shichida, Y. (2014). Cone visual pigments. *Biochimica et Biophysica Acta, 1837*(5), 664-673. doi:10.1016/j.bbabio.2013.08.009

Ingram, N. T., Sampath, A. P., & Fain, G. L. (2016). Why are rods more sensitive than cones? *Journal of Physiology, 594*(19), 5415-5426. doi:10.1113/JP272556

Insinna, C., & Besharse, J. C. (2008). Intraflagellar transport and the sensory outer segment of vertebrate photoreceptors. *Developmental Dynamics, 237*(8), 1982-1992. doi:10.1002/dvdy.21554

Irie, S., Sanuki, R., Muranishi, Y., Kato, K., Chaya, T., & Furukawa, T. (2015). Rax homeoprotein regulates photoreceptor cell maturation and survival in association with Crx in the postnatal mouse retina. *Molecular and Cellular Biology, 35*(15), 2583-2596. doi:10.1128/MCB.00048-15

Joiner, M. L., & Lee, A. (2015). Voltage-Gated Cav1 channels in disorders of vision and hearing. *Current Molecular Pharmacology, 8*(2), 143-148.

Khan, A. O., Eisenberger, T., Nagel-Wolfrum, K., Wolfrum, U., & Bolz, H. J. (2015). C21orf2 is mutated in recessive early-onset retinal dystrophy with macular staphyloma and encodes a protein that localises to the photoreceptor primary cilium. *British Journal of Ophthalmology, 99*(12), 1725-1731. doi:10.1136/bjophthalmol-2015-307277

Kiser, P. D., Golczak, M., Maeda, A., & Palczewski, K. (2012). Key enzymes of the retinoid (visual) cycle in vertebrate retina. *Biochimica et Biophysica Acta, 1821*(1), 137-151. doi:10.1016/j.bbalip.2011.03.005

Kiser, P. D., Zhang, J., Badiee, M., Li, Q., Shi, W., Sui, X., Palczewski, K. (2015). Catalytic mechanism of a retinoid isomerase essential for vertebrate vision. *Nature Chemical Biology, 11*(6), 409-415. doi:10.1038/nchembio.1799

Kleinman, M. E., & Ambati, J. (2008). Fifty years later: the disk goes to the prom. *Journal of Clinical Investigation, 118*(8), 2681-2684. doi:10.1172/JCI36515

Koch, K. W., & Dell'Orco, D. (2015). Protein and signaling networks in vertebrate photoreceptor cells. *Frontiers in Molecular Neuroscience, 8*, 67. doi:10.3389/fnmol.2015.00067

Kohl, S., & Hamel, C. (2013). Clinical utility gene card for: Achromatopsia - update 2013. *European Journal of Human Genetics, 21*(11). doi:10.1038/ejhg.2013.44

Kolandaivelu, S., Singh, R. K., & Ramamurthy, V. (2014). AIPL1, A protein linked to blindness, is essential for the stability of enzymes mediating cGMP metabolism in cone photoreceptor cells. *Human Molecular Genetics, 23*(4), 1002-1012. doi:10.1093/hmg/ddt496

Koschak, A., Reimer, D., Walter, D., Hoda, J. C., Heinzle, T., Grabner, M., & Striessnig, J. (2003). Cav1.4alpha1 subunits can form slowly inactivating dihydropyridine-sensitive L-type Ca2+ channels lacking Ca2+-dependent inactivation. *Journal of Neuroscience, 23*(14), 6041-6049.

Kuhn, M. (2016). Molecular physiology of membrane guanylyl cyclase receptors. *Physiological Reviews, 96*(2), 751-804. doi:10.1152/physrev.00022.2015

Köhn, L., Kadzhaev, K., Burstedt, M. S., Haraldsson, S., Hallberg, B., Sandgren, O., & Golovleva, I. (2007). Mutation in the PYK2-binding domain of PITPNM3 causes autosomal dominant cone dystrophy (CORD5) in two Swedish families. *European Journal of Human Genetics, 15*(6), 664-671. doi:10.1038/sj.ejhg.5201817

Li, C., Wang, L., Zhang, J., Huang, M., Wong, F., Liu, X., Liu, M. (2014). CERKL interacts with mitochondrial TRX2 and protects retinal cells from oxidative stress-induced apoptosis. *Biochimica et Biophysica Acta, 1842*(7), 1121-1129. doi:10.1016/j.bbadis.2014.04.009

Li, T. S., Volpp, K., & Applebury, M. L. (1990). Bovine cone photoreceptor cGMP phosphodiesterase structure deduced from a cDNA clone. *Proceedings of the National Academy of Sciences USA, 87*(1), 293-297.

Lumb, J. H., Leung, K. F., Dubois, K. N., & Field, M. C. (2011). Rab28 function in trypanosomes: interactions with retromer and ESCRT pathways. *Journal of Cell Science, 124*(Pt 22), 3771-3783. doi:10.1242/jcs.079178

Majumder, A., Gopalakrishna, K. N., Cheguru, P., Gakhar, L., & Artemyev, N. O. (2013). Interaction of aryl hydrocarbon receptor-interacting protein-like 1 with the farnesyl moiety. *Journal of Biological Chemistry, 288*(29), 21320-21328. doi:10.1074/jbc.M113.476242

Mannu, G. S. (2014). Retinal phototransduction. *Neurosciences (Riyadh), 19*(4), 275-280.

Maugeri, A., Klevering, B. J., Rohrschneider, K., Blankenagel, A., Brunner, H. G., Deutman, A. F., Cremers, F. P. (2000). Mutations in the ABCA4 (ABCR) gene are the major cause of autosomal recessive cone-rod dystrophy. *American Journal of Human Genetics, 67*(4), 960-966. doi:10.1086/303079

McRory, J. E., Hamid, J., Doering, C. J., Garcia, E., Parker, R., Hamming, K., . . . Snutch, T. P. (2004). The CACNA1F gene encodes an L-type calcium channel with unique biophysical properties and tissue distribution. *Journal of Neuroscience, 24*(7), 1707-1718. doi:10.1523/JNEUROSCI.4846-03.2004

Michaelides, M., Hardcastle, A. J., Hunt, D. M., & Moore, A. T. (2006). Progressive cone and cone-rod dystrophies: phenotypes and underlying molecular genetic basis. *Survey of Ophthalmology, 51*(3), 232-258. doi:10.1016/j.survophthal.2006.02.007

Molday, L. L., Rabin, A. R., & Molday, R. S. (2000). ABCR expression in foveal cone photoreceptors and its role in stargardt macular dystrophy. *American Journal of Ophthalmology, 130*(5), 689.

Molday, R. S. (2007). ATP-binding cassette transporter ABCA4: molecular properties and role in vision and macular degeneration. *Journal of Bioenergetics and Biomembranes, 39*(5-6), 507-517. doi:10.1007/s10863-007-9118-6

Molday, R. S. (2015). Insights into the molecular properties of ABCA4 and its role in the visual cycle and stargardt disease. *Progress in Molecular Biology and Translational Science, 134*, 415-431. doi:10.1016/bs.pmbts.2015.06.008

Molday, R. S., & Moritz, O. L. (2015). Photoreceptors at a glance. *Journal of Cell Science, 128*(22), 4039-4045. doi:10.1242/jcs.175687

Mustafi, D., Engel, A. H., & Palczewski, K. (2009). Structure of cone photoreceptors. *Progress in Retinal and Eye Research, 28*(4), 289-302. doi:10.1016/j.preteyeres.2009.05.003

Nojima, S., Toyofuku, T., Kamao, H., Ishigami, C., Kaneko, J., Okuno, T., . . . Kumanogoh, A. (2013). A point mutation in Semaphorin 4A associates with defective endosomal sorting and causes retinal degeneration. *Nature Communications, 4*, 1406. doi:10.1038/ncomms2420

Ottschytsch, N., Raes, A., Van Hoorick, D., & Snyders, D. J. (2002). Obligatory heterotetramerization of three previously uncharacterized Kv channel alpha-subunits identified in the human genome. *Proceedings of the National Academy of Sciences USA, 99*(12), 7986-7991. doi:10.1073/pnas.122617999

Packer, O., Hendrickson, A. E., & Curcio, C. A. (1989). Photoreceptor topography of the retina in the adult pigtail macaque (Macaca nemestrina). *Journal of Comparative Neurology, 288*(1), 165-183. doi:10.1002/cne.902880113

Palczewski, K., Sokal, I., & Baehr, W. (2004). Guanylate cyclase-activating proteins: structure, function, and diversity. *Biochem Biophys Res Commun, 322*(4), 1123-1130. doi:10.1016/j.bbrc.2004.07.122

Palejwala, N. V., Gale, M. J., Clark, R. F., Schlechter, C., Weleber, R. G., & Pennesi, M. E. (2016). Insights into autosomal dominat Stargardt-like macular dystrophy through multimodality diagnostic imaging. *Retina, 36*(1), 119-130. doi:10.1097/IAE.0000000000000659

Parry, D. A., Mighell, A. J., El-Sayed, W., Shore, R. C., Jalili, I. K., Dollfus, H., Inglehearn, C. F. (2009). Mutations in CNNM4 cause Jalili syndrome, consisting of autosomal-recessive cone-rod dystrophy and amelogenesis imperfecta. *American Journal of Human Genetics, 84*(2), 266-273. doi:10.1016/j.ajhg.2009.01.009

Parry, D. A., Toomes, C., Bida, L., Danciger, M., Towns, K. V., McKibbin, M., Inglehearn, C. F. (2009). Loss of the metalloprotease ADAM9 leads to cone-rod dystrophy in humans and retinal degeneration in mice. *American Journal of Human Genetics, 84*(5), 683-691. doi:10.1016/j.ajhg.2009.04.005

Patnaik, S. R., Raghupathy, R. K., Zhang, X., Mansfield, D., & Shu, X. (2015). The role of RPGR and its interacting proteins in ciliopathies. *Journal of Ophthalmology, 2015*, 414781. doi:10.1155/2015/414781

Pollock, N. L., & Callaghan, R. (2011). The lipid translocase, ABCA4: seeing is believing. *FEBS J, 278*(18), 3204-3214. doi:10.1111/j.1742-4658.2011.08169.x

Polok, B., Escher, P., Ambresin, A., Chouery, E., Bolay, S., Meunier, I., Schorderet, D. F. (2009). Mutations in CNNM4 cause recessive cone-rod dystrophy with

amelogenesis imperfecta. *American Journal of Human Genetics, 84*(2), 259-265. doi:10.1016/j.ajhg.2009.01.006

Ramamurthy, V., Roberts, M., van den Akker, F., Niemi, G., Reh, T. A., & Hurley, J. B. (2003). AIPL1, a protein implicated in Leber's congenital amaurosis, interacts with and aids in processing of farnesylated proteins. *Proceedings of the National Academy of Sciences USA, 100*(22), 12630-12635. doi:10.1073/pnas.2134194100

Rao, K. N., Zhang, W., Li, L., Anand, M., & Khanna, H. (2016). Prenylated retinal ciliopathy protein RPGR interacts with PDE6δ and regulates ciliary localization of Joubert Syndrome-associated protein INPP5E. *Human Molecular Genetics*. doi:10.1093/hmg/ddw281

Rattner, A., Chen, J., & Nathans, J. (2004). Proteolytic shedding of the extracellular domain of photoreceptor cadherin. Implications for outer segment assembly. *Journal of Biological Chemistry, 279*(40), 42202-42210. doi:10.1074/jbc.M407928200

Rattner, A., Smallwood, P. M., Williams, J., Cooke, C., Savchenko, A., Lyubarsky, A., Nathans, J. (2001). A photoreceptor-specific cadherin is essential for the structural integrity of the outer segment and for photoreceptor survival. *Neuron, 32*(5), 775-786. doi:S0896-6273(01)00531-1 [pii]

Reks, S. E., McIlvain, V., Zhuo, X., & Knox, B. E. (2014). Cooperative activation of Xenopus rhodopsin transcription by paired-like transcription factors. *BMC Molecular Biology, 15*, 4. doi:10.1186/1471-2199-15-4

Remans, K., Bürger, M., Vetter, I. R., & Wittinghofer, A. (2014). C2 domains as protein-protein interaction modules in the ciliary transition zone. *Cell Reports, 8*(1), 1-9. doi:10.1016/j.celrep.2014.05.049

Remmer, M. H., Rastogi, N., Ranka, M. P., & Ceisler, E. J. (2015). Achromatopsia: a review. *Current Opinion in Ophthalmology, 26*(5), 333-340. doi:10.1097/ICU.0000000000000189

Roosing, S., Collin, R. W., den Hollander, A. I., Cremers, F. P., & Siemiatkowska, A. M. (2014). Prenylation defects in inherited retinal diseases. *Journal of Medical Genetics, 51*(3), 143-151. doi:10.1136/jmedgenet-2013-102138

Roosing, S., Lamers, I. J., de Vrieze, E., van den Born, L. I., Lambertus, S., Arts, H. H., Group, P. B. S. (2014). Disruption of the basal body protein POC1B results in autosomal-recessive cone-rod dystrophy. *American Journal of Human Genetics, 95*(2), 131-142. doi:10.1016/j.ajhg.2014.06.012

Roosing, S., Rohrschneider, K., Beryozkin, A., Sharon, D., Weisschuh, N., Staller, J., Consortium, E. R. D. (2013). Mutations in RAB28, encoding a farnesylated small

GTPase, are associated with autosomal-recessive cone-rod dystrophy. *American Journal of Human Genetics, 93*(1), 110-117. doi:10.1016/j.ajhg.2013.05.005

Sahel, J. A., Marazova, K., & Audo, I. (2015). Clinical characteristics and current therapies for inherited retinal degenerations. *Cold Spring Harbor Perspectives in Medicine, 5*(2), a017111. doi:10.1101/cshperspect.a017111

Sergouniotis, P. I., Chakarova, C., Murphy, C., Becker, M., Lenassi, E., Arno, G., Consortium, U.-E. (2014). Biallelic variants in TTLL5, encoding a tubulin glutamylase, cause retinal dystrophy. *American Journal of Human Genetics, 94*(5), 760-769. doi:10.1016/j.ajhg.2014.04.003

Sharma, R. K., & Duda, T. (2014). Membrane guanylate cyclase, a multimodal transduction machine: history, present, and future directions. *Frontiers in Molecular Neuroscience, 7*, 56. doi:10.3389/fnmol.2014.00056

Shichida, Y., & Matsuyama, T. (2009). Evolution of opsins and phototransduction. *Philosophical Transactions of the Royal Society B: Biological Sciences, 364*(1531), 2881-2895. doi:10.1098/rstb.2009.0051

Shintani, K., Shechtman, D. L., & Gurwood, A. S. (2009). Review and update: current treatment trends for patients with retinitis pigmentosa. *Optometry, 80*(7), 384-401. doi:10.1016/j.optm.2008.01.026

Simon, A., Hellman, U., Wernstedt, C., & Eriksson, U. (1995). The retinal pigment epithelial-specific 11-cis retinol dehydrogenase belongs to the family of short chain alcohol dehydrogenases. *Journal of Biological Chemistry, 270*(3), 1107-1112.

Skorczyk-Werner, A., Pawłowski, P., Michalczuk, M., Warowicka, A., Wawrocka, A., Wicher, K., Krawczyński, M. R. (2015). Fundus albipunctatus: review of the literature and report of a novel RDH5 gene mutation affecting the invariant tyrosine (p.Tyr175Phe). *Journal of Applied Genetics, 56*(3), 317-327. doi:10.1007/s13353-015-0281-x

Steinberg, R. H., Fisher, S. K., & Anderson, D. H. (1980). Disc morphogenesis in vertebrate photoreceptors. *Journal of Comparative Neurology, 190*(3), 501-508. doi:10.1002/cne.901900307

Strauss, O. (2005). The retinal pigment epithelium in visual function. *Physiological Reviews, 85*(3), 845-881. doi:10.1152/physrev.00021.2004

Stuck, M. W., Conley, S. M., & Naash, M. I. (2016). PRPH2/RDS and ROM-1: Historical context, current views and future considerations. *Progress in Retinal and Eye Research, 52*, 47-63. doi:10.1016/j.preteyeres.2015.12.002

Sun, X., Park, J. H., Gumerson, J., Wu, Z., Swaroop, A., Qian, H., Li, T. (2016). Loss of RPGR glutamylation underlies the pathogenic mechanism of retinal dystrophy caused by TTLL5 mutations. *Proceedings of the National Academy of Sciences USA, 113*(21), E2925-2934. doi:10.1073/pnas.1523201113

Swaroop, A., Kim, D., & Forrest, D. (2010). Transcriptional regulation of photoreceptor development and homeostasis in the mammalian retina. *Nature Reviews Neuroscience, 11*(8), 563-576. doi:10.1038/nrn2880

Tanna, P., Strauss, R. W., Fujinami, K., & Michaelides, M. (2016). Stargardt disease: clinical features, molecular genetics, animal models and therapeutic options. *British Journal of Ophthalmology*. doi:10.1136/bjophthalmol-2016-308823

Thiadens, A. A., Phan, T. M., Zekveld-Vroon, R. C., Leroy, B. P., van den Born, L. I., Hoyng, C. B., Consortium, W. C. f. t. C. D. S. G. (2012). Clinical course, genetic etiology, and visual outcome in cone and cone-rod dystrophy. *Ophthalmology, 119*(4), 819-826. doi:10.1016/j.ophtha.2011.10.011

Toyofuku, T., Nojima, S., Ishikawa, T., Takamatsu, H., Tsujimura, T., Uemura, A., Kumanogoh, A. (2012). Endosomal sorting by Semaphorin 4A in retinal pigment epithelium supports photoreceptor survival. *Genes and Development, 26*(8), 816-829. doi:10.1101/gad.184481.111

Tsuruma, K., Nishimura, Y., Kishi, S., Shimazawa, M., Tanaka, T., & Hara, H. (2012). SEMA4A mutations lead to susceptibility to light irradiation, oxidative stress, and ER stress in retinal pigment epithelial cells. *Investigative Ophthalmology and Visual Science, 53*(10), 6729-6737. doi:10.1167/iovs.11-9378

Tsybovsky, Y., Molday, R. S., & Palczewski, K. (2010). The ATP-binding cassette transporter ABCA4: structural and functional properties and role in retinal disease. *Advances in Experimental Medicine and Biology, 703*, 105-125. doi:10.1007/978-1-4419-5635-4_8

Tuson, M., Garanto, A., Gonzàlez-Duarte, R., & Marfany, G. (2009). Overexpression of CERKL, a gene responsible for retinitis pigmentosa in humans, protects cells from apoptosis induced by oxidative stress. *Molecular Vision, 15*, 168-180.

Volland, S., Hughes, L. C., Kong, C., Burgess, B. L., Linberg, K. A., Luna, G., Williams, D. S. (2015). Three-dimensional organization of nascent rod outer segment disk membranes. *Proceedings of the National Academy of Sciences USA, 112*(48), 14870-14875. doi:10.1073/pnas.1516309112

Wen, X. H., Dizhoor, A. M., & Makino, C. L. (2014). Membrane guanylyl cyclase complexes shape the photoresponses of retinal rods and cones. *Frontiers in Molecular Neuroscience, 7*, 45. doi:10.3389/fnmol.2014.00045

Wensel, T. G., Zhang, Z., Anastassov, I. A., Gilliam, J. C., He, F., Schmid, M. F., & Robichaux, M. A. (2016). Structural and molecular bases of rod photoreceptor morphogenesis and disease. *Progress in Retinal and Eye Research*. doi:10.1016/j.preteyeres.2016.06.002

Wright, Z. C., Singh, R. K., Alpino, R., Goldberg, A. F., Sokolov, M., & Ramamurthy, V. (2016). ARL3 regulates trafficking of prenylated phototransduction proteins to the rod outer segment. *Human Molecular Genetics, 25*(10), 2031-2044. doi:10.1093/hmg/ddw077

Wu, H., Cowing, J. A., Michaelides, M., Wilkie, S. E., Jeffery, G., Jenkins, S. A., Webster, A. R. (2006). Mutations in the gene KCNV2 encoding a voltage-gated potassium channel subunit cause "cone dystrophy with supernormal rod electroretinogram" in humans. *American Journal of Human Genetics, 79*(3), 574-579. doi:10.1086/507568

Wätzlich, D., Vetter, I., Gotthardt, K., Miertzschke, M., Chen, Y. X., Wittinghofer, A., & Ismail, S. (2013). The interplay between RPGR, PDEδ and Arl2/3 regulate the ciliary targeting of farnesylated cargo. *EMBO Reports, 14*(5), 465-472. doi:10.1038/embor.2013.37

Yang, Z., Chen, Y., Lillo, C., Chien, J., Yu, Z., Michaelides, M., . . . Zhang, K. (2008). Mutant prominin 1 found in patients with macular degeneration disrupts photoreceptor disk morphogenesis in mice. *Journal of Clinical Investigation, 118*(8), 2908-2916. doi:10.1172/JCI35891

Yokochi, M., Li, D., Horiguchi, M., & Kishi, S. (2012). Inverse pattern of photoreceptor abnormalities in retinitis pigmentosa and cone-rod dystrophy. *Documenta Ophthalmologica, 125*(3), 211-218. doi:10.1007/s10633-012-9348-8

Zhang, H., Constantine, R., Vorobiev, S., Chen, Y., Seetharaman, J., Huang, Y. J., Baehr, W. (2011). UNC119 is required for G protein trafficking in sensory neurons. *Nature Neuroscience, 14*(7), 874-880. doi:10.1038/nn.2835

Zhang, H., Hanke-Gogokhia, C., Jiang, L., Li, X., Wang, P., Gerstner, C. D., Baehr, W. (2015). Mistrafficking of prenylated proteins causes retinitis pigmentosa 2. *FASEB J, 29*(3), 932-942. doi:10.1096/fj.14-257915

Zhou, M., Graham, R., Russell, G., & Croucher, P. I. (2001). MDC-9 (ADAM-9/Meltrin gamma) functions as an adhesion molecule by binding the alpha(v)beta(5) integrin. *Biochemical and Biophysical Research Communications, 280*(2), 574-580. doi:10.1006/bbrc.2000.4155

Zobor, D., Zobor, G., & Kohl, S. (2015). Achromatopsia: on the doorstep of a possible therapy. *Ophthalmic Research, 54*(2), 103-108. doi:10.1159/000435957

CHAPTER 2

C8ORF37 IS REQUIRED FOR PHOTORECEPTOR OUTER SEGMENT DISC MORPHOGENESIS BY MAINTAINING OUTER SEGMENT MEMBRANE PROTEIN EXPRESSION

Jun Yang designed the original study. I began the C8ORF37 project when I joined the lab. I generated *C8orf37* knockout mice and contributed to almost all of the experiments. Lab members assisted with experiments throughout the process. Jun Yang wrote the manuscript and I helped write the methods section and revised the manuscript. Jun Yang and I analyzed the data.

*The chapter is not a reprint and is intended to be published. Acknowledgements include Dongmei Yu, Stuart Loertscher, Kevin Nguyen, Pranav Dinesh Mathur, Anna M. Clark, Junhuang Zou, Ekaterina S. Lobanova, Vadim Y. Arshavsky, and Jun Yang

2.1 Abstract

C8ORF37 is a causative gene for cone-rod dystrophy, retinitis pigmentosa, and Bardet-Biedl syndrome, three clinical forms of incurable retinal degeneration. The unknown function of *C8ORF37* hinders understanding the pathogenicity of *C8ORF37* mutations. To address this problem, we performed a thorough phenotypical characterization of a *C8orf37* knockout mouse generated by the CRISPR/Cas9 technology. The *C8orf37* knockout mice exhibited progressive retinal degeneration with ~60% photoreceptor loss by 26 weeks of age. This cell loss was accompanied with reduction and prolongation of scotopic and photopic electroretinograms, indicating simultaneous rod and cone degeneration. However, the *C8orf37* knockout was not associated with any evident nonocular phenotype that is manifested in Bardet-Biedl syndrome. Therefore, *C8orf37* knockout mice recapitulate only the retinal phenotype of *C8ORF37*-deficient patients. The major ultrastructural feature of the *C8orf37* knockout photoreceptors is massive disorganization of the outer segment (OS) membrane discs observed from the onset of disc morphogenesis. The amounts of multiple OS-specific membrane proteins, including proteins involved in membrane disc organization, were reduced, although these proteins were normally targeted to the OS. Considering the localization of C8ORF37 in the photoreceptor cell body but not the OS, these findings suggest that C8ORF37 is required for OS disc formation by participating in the secretory pathway of OS membrane proteins, thereby maintaining their expression homeostasis. This study sheds new light on the role of *C8ORF37* in photoreceptors and on the pathogenic mechanism underlying retinal degeneration in *C8ORF37*-deficient patients.

2.2 Significance statement

Inherited retinal degeneration is a group of incurable conditions with poorly-understood underlying molecular mechanisms. Here, we investigated *C8ORF37*, a causative gene for three retinal degenerative conditions: retinitis pigmentosa, cone-rod dystrophy, and Bardet-Biedl syndrome. *C8ORF37* encodes a protein with no known functional domains, and thus its biological function is unpredictable. Using the CRISPR/Cas9 approach, we knocked out the *C8ORF37* ortholog in mice, which resulted in a retinal phenotype similar to that observed in patients. Further studies demonstrate that C8ORF37 is required for photoreceptor outer segment disc formation, a process poorly understood but critical for photoreceptor function. This study has an impact on understanding the pathogenesis of retinal degeneration and will contribute to therapeutic development by providing a valuable mouse model.

2.3 Introduction

Inherited retinal degeneration is a group of heterogeneous diseases affecting mainly photoreceptors. To date, more than 200 genes have been identified to be responsible for inherited retinal degeneration. However, little is known about the function of a significant number of these genes, and this knowledge gap hinders the development of effective treatments. *C8ORF37*, named by its position on human chromosome 8, is a causative gene for autosomal recessive retinitis pigmentosa (RP), cone-rod dystrophy (CRD), and Bardet-Biedl syndrome (BBS) (Estrada-Cuzcano et al., 2011; Heon et al., 2016; Jinda et al., 2014; Katagiri et al., 2014; Khan, Decker, Bachmann, Bolz, & Bergmann, 2016; Lazar et al., 2015; Rahner, Nuernberg, Finis, Nuernberg, & Royer-Pokora, 2016; Ravesh et al., 2015;

van Huet et al., 2013). RP is the most common inherited retinal degenerative disease (Hartong, Berson, & Dryja, 2006). Blindness in RP patients results initially from loss of rod photoreceptors followed by loss of cones. BBS is a syndromic form of RP and is also classified as a ciliopathy, characterized by childhood-onset rod-cone dystrophy, polydactyly, obesity, mental retardation, renal dysfunction, and hypogenitalism (Hartong et al., 2006; Zaghloul & Katsanis, 2009). Finally, CRD is characterized by a cone-mediated vision impairment followed by rod degeneration, or simultaneous degeneration of cones and rods (Thiadens et al., 2012). Currently, no obvious genotype-phenotype correlation has been observed in *C8ORF37*-deficient patients.

The function of the C8ORF37 protein is unknown and unpredictable, because this protein has no known functional domains or motifs and does not belong to any known protein family. The human C8ORF37 protein has 207 amino acids. Two thirds of its C-terminal sequence is highly conserved from mammals to unicellular flagellates and oomycetes (Estrada-Cuzcano et al., 2011). Like in humans, the knockdown of *C8ORF37* ortholog in zebrafish impairs vision (Heon et al., 2016). This evolutionary conservation in sequence and phenotype indicates a functional significance of C8ORF37. In hTERT-RPE1 cells, C8ORF37 is localized at the base of the primary cilium and in the cytoplasm, and in mouse photoreceptors, C8ORF37 is enriched at the base of the connecting cilium and along the ciliary rootlet (Estrada-Cuzcano et al., 2011). Furthermore, *c8orf37* knockdown zebrafish have a small Kuppfer's vesicle, a ciliated organ responsible for left-right body asymmetry establishment during development, and have a slow retrograde melanosome transport in melanophores (Heon et al., 2016). These phenotypes, combined with the localization of C8ORF37 at the ciliary apparatus and its association with BBS, suggest that

C8ORF37 may contribute to the function of the primary cilium.

In the retina, the photoreceptor outer segment (OS) is a large specialized primary cilium harboring the phototransduction machinery on the tightly-stacked membrane discs. The integrity of this organelle and the tight disc alignment are crucial for photoreceptor function and survival (Ding et al., 2004; Pearring, Salinas, Baker, & Arshavsky, 2013; Zhang et al., 2009). OS proteins are synthesized in the photoreceptor inner segment (IS) and transported to their destination during OS morphogenesis and subsequent renewal (Young, 1967). However, the mechanisms underlying the synthesis, sorting and transport of OS proteins in the IS remain poorly understood (Pearring et al., 2013). In this report, we knocked out the mouse ortholog of *C8ORF37* (*C8orf37*, aka 2610301B20Rik), which produced retinal phenotype similar to that in *C8ORF37*-deficient patients. We demonstrated that C8ORF37 is required for maintaining normal expression levels of OS membrane proteins and lack of C8ORF37 results in severe abnormalities in photoreceptor disc formation and subsequent photoreceptor cell death

2.4 Results

2.4.1 Generation of *C8orf37* knockout mice using the CRISPR/Cas9 technology

We cloned two CRISPR/Cas9 plasmids carrying small guide RNA sequences targeting exon 1 and exon 5 of the mouse *C8orf37* gene (Figure 2.S1A). To increase the mutagenesis efficiency, these plasmids were simultaneously injected into 349 mouse zygotes. Among the 71 screened founder mice, 32 exhibited INDEL mutations in exon 1; 10 showed INDEL mutations in exon 5; and 7 had a deletion of ~12-kb genomic DNA

fragments between exons 1 and 5. Through crossing with C57BL/6 mice, three homozygous mutant mouse lines were established: *C8orf37*$^{ex1/ex1}$, *C8orf37*$^{ex5/ex5}$, and *C8orf37*$^{del/del}$ (Figure 2.S1B-D). The *C8orf37*$^{ex1/ex1}$ mouse carried a 6-bp deletion including the ATG translation start codon in exon 1; the *C8orf37*$^{ex5/ex5}$ mouse had a 10-bp deletion in exon 5; and the *C8orf37*$^{del/del}$ mouse missed a large genomic fragment between exons 1 and 5, which also included the translation start codon. Immunoblotting analysis using a custom-made rabbit antibody demonstrated the absence of C8ORF37 or its truncated protein fragments in all three *C8orf37* mutant retinas (Figure 2.1A), indicating that *C8orf37*$^{ex1/ex1}$, *C8orf37*$^{ex5/ex5}$, and *C8orf37*$^{del/del}$ mice were *C8orf37*-null. The absence of C8ORF37 truncated fragment in *C8orf37*$^{ex5/ex5}$ mice was probably due to nonsense-mediated decay, which occurred in a patient with a *C8ORF37* nonsense mutation (Heon et al., 2016).

C8orf37$^{ex1/ex1}$, *C8orf37*$^{ex5/ex5}$, and *C8orf37*$^{del/del}$ mice were viable and indistinguishable from their wild-type littermates in reproductive performance and general health. Specifically, male and female mice of these three knockout lines showed normal body weights compared with their heterogeneous littermates up to 6 months of age (Figure 2.S2A). In *C8orf37*$^{del/del}$ mice, no defects were observed in forelimb and hindlimb digit numbers (Figure 2.S2B, n = 70 mice, at various ages), kidney morphology and weight (Figure 2.S2C, n = 9 mice, at P28-P60) or left-right body asymmetry (n = 23 mice, at P0-P4). Therefore, all three *C8orf37* knockout mouse lines did not seem to have nonocular phenotypes that are manifested in BBS patients.

2.4.2 Abnormal retinal function in *C8orf37* knockout mice

To assess the retinal function of *C8orf37*$^{ex1/ex1}$, *C8orf37*$^{ex5/ex5}$ and *C8orf37*$^{del/del}$ mice, we performed electroretinography (ERG). In all three knockout mice at 5 weeks of age, the amplitudes of scotopic ERG a- and b-waves (Figure 2.1B, D, and E) and the amplitude of photopic ERG b-wave (Figure 2.1C and F) were reduced by ~60%, 45%, and 35%, respectively, at various light intensities. At 12 weeks of age, the amplitudes of scotopic ERG a- and b-waves (Figure 2.S3A and B) and the amplitude of photopic ERG b-wave (Figure 2.S3C) were further reduced by ~75%, 55%, and 50%, respectively. At the same age, the implicit time of scotopic ERG a-wave became prolonged (Figure 2.S3D), while the implicit times of scotopic and photopic ERG b-waves were generally normal, except the increased implicit time of the photopic ERG b-wave in *C8orf37*$^{ex1/ex1}$ mice at 10 dB (Figure 2.S3E and F). These findings demonstrate that both rods and cones are affected by the *C8orf37* knockout. The similar changes of ERG responses in the three knockout lines suggest that the ERG phenotype is caused specifically by the *C8orf37* knockout but not by any random off-target mutations, which is a general concern when using the CRISPR/cas9 genome engineering technology.

Since the genotyping procedure was relatively simple for *C8orf37*$^{del/del}$ mice compared with *C8orf37*$^{ex1/ex1}$ and *C8orf37*$^{ex5/ex5}$ mice, we next focused on the phenotypical characterization of this mouse line only. *C8orf37*$^{del/del}$ mice exhibited reduced scotopic and photopic ERG responses as early as 3 weeks of age, the earliest time point to record reliable ERG responses (Figure 2.1G-I). In addition, the reduction (Figure 2.1G-I) and prolongation (Figure 2.S3G-I) of scotopic and photopic ERG responses were progressive up to 26 weeks of age, the latest time point examined. Therefore, the dysfunction of rods and cones occurs

simultaneously and is progressive in *C8orf37* knockout mice.

2.4.3 Retinal degeneration in *C8orf37* knockout mice

To investigate whether *C8orf37* knockout causes retinal degeneration characterized by photoreceptor cell loss, we conducted noninvasive spectral domain optical coherence tomography (SD-OCT) and histological analysis of retinal plastic sections. SD-OCT analysis showed that 2-month-old *C8orf37*$^{del/del}$ mice lost the photoreceptor IS/OS junction line (Figure 2.S4A), which was an indicator of retinal abnormality (Mitamura et al., 2012) and was previously observed in patients carrying *C8ORF37* mutations (Heon et al., 2016; Katagiri et al., 2014). In *C8orf37*$^{del/del}$ mice at the same age, the outer nuclear layer (ONL) containing photoreceptor nuclei appeared to be slightly thinner (Figure 2.S4A), indicating a small loss of photoreceptors. Further examination of 6-month-old *C8orf37*$^{del/del}$ mice revealed that, in addition to the loss of the IS/OS line, the ONL thickness was significantly reduced (Figure 2.S4A), leading to the decreased thickness of the entire retinas in comparison to *C8orf37*$^{+/del}$ mice (Figure 2.S4B). Therefore, *C8orf37*$^{del/del}$ mice undergo photoreceptor cell loss in the retina.

Consistent with SD-OCT findings, histological examination of retinal cross-sections showed that the various retinal layers of *C8orf37*$^{del/del}$ mice were grossly normal at postnatal days 13 and 16 (P13 and P16) (Figure 2.2A). In *C8orf37*$^{del/del}$ mice, at P49, the photoreceptor OS length and ONL thickness were reduced by 29% and 17%, respectively, at the mid-peripheral retinas (Figure 2.2). At P208, further ONL thinning and OS shortening were observed. At the mid-peripheral region, quantification by both ONL thickness and nuclear number showed ~60% reduction in the ONL; the OS layer was too

short and distorted to be reliably measured (Figure 2.2). Together with the ERG data, SD-OCT and histological analyses demonstrate that *C8orf37*$^{del/del}$ mice exhibit a retinal degenerative phenotype similar to that in RP and CRD patients carrying mutations in the *C8ORF37* gene.

2.4.4 Disorganization of photoreceptor OS discs in *C8orf37* knockout mice

To examine the morphology and ultrastructure of *C8orf37*$^{del/del}$ photoreceptors, we performed scanning (SEM) and transmission (TEM) electron microscopy, respectively. SEM performed at P10 revealed that developing rudimentary OSs had an abnormal shape (Figure 2.S5A). They were generally swollen but also constricted at some spots. Further examination at P30 revealed that the *C8orf37*$^{del/del}$ OS was about 30% wider than the *C8orf37*$^{+/del}$ OS (Figure 2.S5B and D). Likely to reflect an increase in the average OS diameter, the OS density in *C8orf37*$^{del/del}$ mice was ~20% less than that in *C8orf37*$^{+/del}$ mice (Figure 2.S5B and D). *C8orf37*$^{del/del}$ OS also displayed a larger variation in diameter than *C8orf37*$^{+/del}$ OS (Figure 2.S5B and D).

TEM revealed massive disorganization of membrane discs inside the *C8orf37*$^{del/del}$ OS from P13 to P60. While membranous discs in the *C8orf37*$^{+/del}$ OS were organized in a single stack perpendicular to the long OS axis (Figure 2.3A), additional disc stacks parallel to the long axis (Figure 2.3B, E, and F) and membranous whirls (Figure 2.3C) were observed in the *C8orf37*$^{del/del}$ OS. These vertically aligned disc membranes appeared to extend from the horizontally aligned discs (Figure 2.3E), and no plasma membrane was observed between the vertical and horizontal disc membrane clusters (Figure 2.3F). These

observations indicate that the two types of the membrane structures coexist in the *C8orf37*$^{del/del}$ OS and explain the wide and variable diameter of the *C8orf37*$^{del/del}$ OS documented by SEM (Figure 2.S5). Occasionally, abnormal vesicular clusters were found at the IS/OS junction of *C8orf37*$^{del/del}$ photoreceptors (Figure 2.3D). Other subcellular structures and compartments of photoreceptor cells, including the connecting cilium (Figs. 2.S5C and 3G), basal body (Figure 2.3G), ciliary rootlet (Figure 2.3G), and synaptic terminus (Figure 2.3H), displayed no obvious ultrastructural defects.

2.4.5 Reduction of photoreceptor OS membrane proteins in *C8orf37* knockout mice

To characterize the defects in *C8orf37*$^{del/del}$ photoreceptors at the molecular level, we examined the photoreceptor protein expression by semiquantitative immunoblotting analysis. At P30, the amounts of OS membrane proteins, including rhodopsin, cone opsins (S/M-opsins), guanylate cyclase 1 (GC1), peripherin 2/RDS (RDS), cyclic nucleotide gated channel α1- and β1-subunits (CNGA1 and CNGB1), and ATP- binding cassette subfamily A member 4 (ABCA4) were reduced by 30-70% compared with control littermates (Figure 2.4). Similarly, the amounts of nonmembrane proteins associated with GC1 and CNGB1 were also reduced, which were guanylate cyclase-activating protein 1 and 2 (GCAP1 and GCAP2) and CNGB1 splice isoform glutamic acid-rich protein 2 (GARP2) (Figure 2.4).

On the contrary, two OS membrane proteins, guanylate cyclase 2 (GC2) and protocadherin-21 (PCDH21) were not affected by the *C8orf37* knockout. The expression of membrane-associated transducin α-subunit (GNAT1), cytoplasmic protein arrestin and cytoskeletal protein β-tubulin remained normal (Figure 2.4). Consistent with the normal

structure of photoreceptor ciliary apparatus, the expression levels of the axoneme-binding protein RP1 and basal body protein γ-tubulin were normal as well (Figure 2.4)

The semiquantitative immunoblotting analysis of photoreceptor proteins was also conducted at P49 (Figure 2.S6) and yielded results generally similar to those obtained at P30. At P49, OS GC2 was reduced in addition to OS membrane proteins reduced at P30. The extent of OS membrane protein reduction varied between 34-82%. Again, the OS membrane-associated proteins, phosphodiesterase 6 α/β-subunits (PDE6α/β) and GNAT1, had normal (95%) or close to normal (82%) expression levels, respectively (Figure 2.S6).

In the above proteins whose expression levels were affected by the *C8orf37* knockout, rhodopsin is the main building component of the OS membrane (Filipek, Stenkamp, Teller, & Palczewski, 2003; Heitzmann, 1972; Robinson, Gordon-Walker, & Bownds, 1972), and its protein level is positively proportional to the OS volume (Price et al., 2012). Thus, the ~25% reduction of rhodopsin in P30 *C8orf37*$^{del/del}$ retinas may indicate a ~25% reduction in the OS volume at this age, which is generally in agreement with a ~29% thinning of the OS layer found by our histological analysis at P49 (Figure 2.2). Several OS proteins had a reduction level larger than 25% at P30 and 29% at P49, such as the proteins involved in OS membrane disc formation, RDS, CNGB1, and GARP2. The reduction degrees of RDS, CNGB1, and GARP2 expression were similar to each other at both P30 and P49, indicating that the ratio of their relative expression levels is not altered by *C8orf37* knockout. Therefore, a group of OS proteins, especially the membrane proteins, are reduced at their expression levels in *C8orf37*$^{del/del}$ retinas. Furthermore, the reduction degrees of these OS membrane proteins are not the same.

2.4.6 Onset of membrane protein reduction at the OS morphogenesis in *C8orf37* knockout mice

C8ORF37 protein was found to be expressed in the mouse retina as early as P0 (Figure 2.5A), suggesting that C8ORF37 may play a role during mouse photoreceptor postnatal development. During this process, the connecting cilium growth occurs at P3-P6 followed by robust OS extension at P8-P21, when a large amount of OS discs are formed (Caley, Johnson, & Liebelt, 1972; De Robertis, 1956). Immunoblotting analysis demonstrated that the rhodopsin reduction in *C8orf37*$^{del/del}$ retinas began at the onset of rhodopsin expression at P5 (Figure 2.5A and C). Additionally, GC1, RDS, and S/M-opsins were expressed at a much lower level than rhodopsin during development. Their reduction in *C8orf37*$^{del/del}$ retinas occurred at P12, P14, and P16, respectively (Figure 2.5B and C), later than their expression onset times but during OS disc morphogenesis when their demands are increasing. Therefore, in *C8orf37*$^{del/del}$ retinas, the rhodopsin reduction begins at the very beginning of OS morphogenesis before the OS disc formation, indicating that the rhodopsin reduction found in mature *C8orf37*$^{del/del}$ retinas at P30 probably leads to but not results from the OS shortening. Combined with our semiquantitative immunoblotting analysis at P30 and P49, these findings indicate that *C8orf37* knockout causes the reduction of a group of OS membrane proteins.

2.4.7 Localization of C8ORF37 in the photoreceptor cell body but not OS

Immunoblotting analysis showed that C8ORF37 was expressed in multiple mouse tissues, including the brain, kidney, lung, spleen, heart, trachea, and testis (Figure 2.S7A).

In mouse photoreceptors, C8ORF37 was previously reported to be enriched at the basal body and ciliary rootlet by immunofluorescence using a commercial antibody (Estrada-Cuzcano et al., 2011). Using the same commercial antibody as well as our custom-made C8ORF37 antibodies, we could not detect a specific signal for C8ORF37 in *C8orf37*$^{+/del}$ photoreceptors, since *C8orf37*$^{del/del}$ photoreceptors exhibited a similar immunoreactivity pattern, presumably reflecting antibody cross-reactivity (Figure 2.S7B). To solve this problem, we transfected *C8orf37*$^{del/del}$ photoreceptors with a DNA construct coding GFP-tagged C8ORF37 using the technique of *in vivo* electroporation at P0 (Matsuda & Cepko, 2004). At P21, GFP-C8ORF37 was evenly distributed throughout the photoreceptor cell volume, except for the OS, which was marked by rhodopsin or S-opsin (Figure 2.6A). In the IS, immunostaining of the ciliary rootlet using a rootletin antibody showed that GFP-C8ORF37 was present at the basal body region on the top of the ciliary rootlet (Figure 2.6B). No C8ORF37 enrichment was observed at or around the basal body or ciliary rootlet. This result indicates that C8ORF37 is broadly distributed in photoreceptors and only restricted from OS. Consistently, in serum-starved IMCD3 cells, we observed transfected GFP-C8ORF37 evenly distributed in the cytoplasm but not in the primary cilium (Figure 2.S7C), an analog of the photoreceptor OS.

Another independent evidence for C8ORF37 localization throughout the photoreceptor cell body was obtained using the technique following the protein distribution in serial tangential sections through the photoreceptor layer of a flat-mounted retina (Sokolov et al., 2002). The C8ORF37 expression profile in the serial sections, determined by immunoblotting analysis, was comparable to that of the photoreceptor cell body marker phosducin (PDC), but not the expression profile of the photoreceptor OS marker RDS

(Figure 2.6C). All these results support the notion that C8ORF37 is localized to the photoreceptor cell body including the basal body, IS and synaptic terminus but not the OS.

2.4.8 Normal targeting of most OS membrane proteins in *C8orf37* knockout photoreceptors

The data obtained so far indicate that the major phenotype of the *C8orf37* knockout is in the photoreceptor OS, while C8ORF37 is localized outside this cellular compartment. This suggests that C8ORF37 participates in a cellular process related to the OS morphogenesis but taking place in the photoreceptor cell body, where OS proteins are synthesized, sorted, and transported. We therefore examined whether *C8orf37* knockout was associated with any defects in the cellular localization of OS membrane proteins.

Immunostaining analysis showed that rhodopsin, CNGA1, RDS, CNGB1, and GC1 were normally distributed in the *C8orf37*$^{del/del}$ OS at P21 (Figure 2.7A-E), so were the OS membrane proteins prominin-1 and PCDH21 and the connecting cilium cytoskeletal protein acetylated α-tubulin (Figure 2.S8). Therefore, C8ORF37 is not involved or at least is not critical for the OS targeting of these membrane and cytoskeletal proteins. Since RDS, GC1, prominin-1, PCDH21, and acetylated α-tubulin are expressed in both rods and cones (Arikawa, Molday, Molday, & Williams, 1992; Rattner et al., 2001; R. B. Yang et al., 1999; Zacchigna et al., 2009), the lack of any cells where these proteins are mislocalized indicates that the above conclusion is applied to both rods and cones.

The only proteins whose intracellular localization was affected in the *C8orf37*$^{del/del}$ retinas were S/M-opsins. *C8orf37*$^{del/del}$ retinas consistently displayed some cones with S/M-opsins partially mislocalized to the cell body and synaptic terminus (Figure 2.7F and G).

Quantification analysis showed that ~6% and 55% of *C8orf37*$^{+/del}$ and *C8orf37*$^{del/del}$ cones had cone opsin mislocalization, respectively. This suggests that C8ORF37 may participate in either cone opsin processing in the biosynthetic membranes or its OS transport and that C8ORF37 may have a different functional mechanism for assisting the processing of cone opsins than other OS membrane proteins.

2.5 Discussion

C8ORF37 is a protein of unknown function whose mutations are associated with an array of visual disorders. The central result obtained in this study is that C8ORF37 knockout results in a major defect in the structural organization of photoreceptor OS membrane discs, ultimately leading to cell death. This result is striking and not immediately intuitive because in wild-type photoreceptors C8ORF37 is essentially excluded from OS and, instead, is evenly distributed throughout the cytoplasm of the rest of the cell. The reduction of OS membrane proteins in the absence of C8ORF37 suggests that C8ORF37 plays a role in the homeostasis of these proteins while they are being synthesized and processed inside the photoreceptor cell body.

A critical observation in support of this hypothesis is that *C8orf37* knockout results in a variable reduction in the expression levels of several proteins known to participate in the process of photoreceptor disc morphogenesis. For example, at P30 RDS, CNGB1, and GARP2 were present at ~50% of the control level, whereas PCDH21 was not reduced at all. Furthermore, rhodopsin, the major OS protein building block, was reduced by only ~25% at this age, which creates a mismatch in the molar ratio among all these critical proteins. The fact that such a mismatch can lead to abnormal photoreceptor morphology

has been established in at least two examples. First, photoreceptor disc misalignment similar to that observed in our study was documented in photoreceptors expressing a single copy of the *Rds* gene (Chakraborty, Conley, Al-Ubaidi, & Naash, 2014; Hawkins, Jansen, & Sanyal, 1985). Second, long stacks of misaligned discs were also observed in *Cngb1*$^{-/-}$ photoreceptors (Chakraborty, Conley, Pittler, & Naash, 2016; Zhang et al., 2009). The relative reduction of these proteins to rhodopsin may explain the OS disc overgrowth and vertical alignment observed in *C8orf37* knockout photoreceptors.

How could a cytoplasmic protein coordinate the relative expression levels of multiple OS membrane proteins? A previous study using *c8orf37* knockdown zebrafish suggested a role of C8ORF37 in melanosome transport (Heon et al., 2016). However, our observation that OS localization of all tested membrane proteins in rods is unaffected by the *C8orf37* knockout argues against C8ORF37 involvement in the motor protein-mediated protein transport. Since the majority of proteins affected by the *C8orf37* knockout are membrane proteins, C8ORF37 highly likely functions in the membrane protein secretory pathway from their synthesis to sorting. One hypothetical possibility is that C8orf37 serves as a part of molecular chaperone machinery assisting the final folding stages of multiple proteins affected by its knockout. Alternatively, C8ORF37 may participate in inhibiting the degradation of these proteins during their synthesis, processing, and transport. Sorting out these and other alternatives is an exciting goal of future investigations.

In addition to causing a mismatch in the expression levels of RDS, CNGB1, GARP2, PCDH21, and rhodopsin, our study revealed two phenotypes related to the expression of rod and cone visual pigments. The earlies phenotype observed in *C8orf37* knockout photoreceptors is the reduction of rhodopsin content at P5. This may suggest that

the subsequently observed reduction in the expression levels of RDS, CNGB1, and GARP2 is merely a consequence of rhodopsin reduction. However, the phenotype of *Rho*$^{+/-}$ mouse rods argues against this idea. *Rho*$^{+/-}$ rods contain ~50% of the normal amount of rhodopsin (Chakraborty et al., 2016; Lem et al., 1999; Price et al., 2012), however, their RDS content is normal (Chakraborty et al., 2016). The *Rho*$^{+/-}$ OS is shorter and thinner, yet its disc alignment is normal (Hollingsworth & Gross, 2013; Lem et al., 1999; Liang et al., 2004; Price et al., 2012). Therefore, the *Rho*$^{+/-}$ phenotype is very different from that observed in *C8orf37* knockout photoreceptors, indicating that the reduction of other OS membrane proteins in *C8orf37* knockout photoreceptors is a primary defect which does not rely on the reduction of rhodopsin.

An even stronger phenotype of the *C8orf37* knockout was revealed upon examining the intracellular localization of cone opsins, which were partially mislocalized in a large fraction of cone photoreceptors. This hints for the existence of subtle differences in the intracellular processing of visual pigments in the two photoreceptor types and a potential difference in their C8ORF37-dependent control.

Importantly, our finding that C8ORF37 knockout mice have both rod and cone phenotypes is consistent with clinical findings in RP and CRD patients. Among the 22 reported *C8ORF37*-deficient patients (Estrada-Cuzcano et al., 2011; Heon et al., 2016; Jinda et al., 2014; Katagiri et al., 2014; Khan et al., 2016; Lazar et al., 2015; Rahner et al., 2016; Ravesh et al., 2015; van Huet et al., 2013), 8 were diagnosed as CRD (Estrada-Cuzcano et al., 2011; Lazar et al., 2015; Rahner et al., 2016; van Huet et al., 2013), 5 as RP with early maculopathy (Estrada-Cuzcano et al., 2011; Jinda et al., 2014; van Huet et al., 2013), and 2 as either CRD or RP with early maculopathy (Katagiri et al., 2014).

Maculopathy is a symptom indicating defective cones, thus, the majority of patients showed early symptoms of both rod and cone degeneration. On the other hand, the reason for absence of nonocular phenotype in *C8orf37* knockout mice is unclear. In humans, *C8ORF37* is a rare causative gene for BBS (Heon et al., 2016); only two *C8ORF37*-deficient patients were diagnosed as BBS (Heon et al., 2016; Khan et al., 2016). One carried a benign BBS4 heterozygous mutation (Heon et al., 2016) and the other carried a mutation exactly the same as in other four CRD patients (Estrada-Cuzcano et al., 2011; Khan et al., 2016; Lazar et al., 2015). Therefore, it is possible that the nonocular phenotype of *C8ORF37* mutations is modified by other genes or is not fully penetrant. Alternatively, there may be a species difference for the requirement of C8ORF37 in the nonocular tissues, which has been documented for other BBS-associated mutations (Novas, Cardenas-Rodriguez, Irigoin, & Badano, 2015).

In summary, our study demonstrated that C8ORF37 is a protein expressed in photoreceptor cell body, which is required for maintaining the physiological level of OS membrane proteins. Loss of C8ORF37 leads to misalignment of photoreceptor discs and subsequent retinal degeneration. This degeneration is progressive and has a sufficient time window for therapeutic intervention. The knockout mouse generated in our study provides an accurate representation of the retinal phenotype in patients and is a valid animal model for future pathophysiological and therapeutic studies.

2.6 Materials and methods

2.6.1 Animals

C8orf37 knockout mice were generated using CRISPR/Cas9 approach at the University of Utah Transgenic and Gene Targeting Mouse Core and the Mutation Generation and Detection Core. Specifically, small guide RNA sites that targeted exon 1 and exon 5 of *C8orf37* and were compatible with the U6 promoter (Figure 2.S1A) were identified using ZiFit Targeter (Version 4.2, http://zifit.partners.org/ZiFiT/) (Hwang et al., 2013; Mali et al., 2013; Sander et al., 2010; Sander, Zaback, Joung, Voytas, & Dobbs, 2007), with potential off targets analyzed using CasOT (http://eendb.zfgenetics.org/casot/) (Xiao et al., 2014). Pairs of oligonucleotides corresponding to the chosen small guide RNA sites (Table 2.S1) were synthesized, annealed and cloned into the pX330-U6-Chimeric_BB-CBh-hSpCas9 vector, a gift from Feng Zhang (Addgene plasmid # 42230), according to the protocol detailed in Le Cong et al (Cong et al., 2013). Both CRISPR/Cas9 plasmids targeting exon 1 and exon 5 were simultaneously injected into F1 (B6/CBA) mouse strain embryos at a concentration of 5, 25, or 50 ng/ul. F_0 founder mice were screened by high-resolution melting analysis (HRMA) (LightScanner® instrument, Biofire Diagnostics, Salt Lake City, Utah) using primers listed in Table 2.S1. Three F_0 founder mice carrying deletions in exon 1, exon 5, and between exons 1 and 5 were crossed with C57BL mice (Jackson Laboratory, Bar Harbor, ME) to achieve germline transmission. *C8orf37*$^{ex1/ex1}$, *C8orf37*$^{ex5/ex5}$ and *C8orf37*$^{del/del}$ mouse lines were eventually established. Their exact mutations in the genome were verified by sequencing of the polymerase chain reaction (PCR) products containing the mutations. The three *C8orf37* mutant mouse lines were then maintained and examined according to the protocol approved by the Institutional

Animal Care and Use Committee (IACUC) at the University of Utah. Routine genotyping was carried out by PCR of the genomic DNA (*C8orf37*$^{del/del}$) followed by DNA sequencing (*C8orf37*$^{ex1/ex1}$ and *C8orf37*$^{ex5/ex5}$). Female Long-Evans rats (P50-P60) were purchased from Charles River Laboratories (Wilmington, MA) and handled according to the protocol approved by the IACUC at Duke University.

2.6.2 Antibodies

Full-length *C8orf37* cDNA (NM_026005) was cloned from mouse retinas by reverse transcription-PCR into the pET28 (EMD Millipore, Billerica, MA) and pGEX4t-1 (GE Healthcare Life Sciences, Pittsburgh, PA) vectors for fusion with His and GST tags, respectively. These two *C8orf37* constructs were transformed into BL21-CodonPlus (DE3)-RIPL cells (Agilent Technologies, Santa Clara, CA) to generate recombinant proteins. His-tagged C8ORF37 protein was purified from the inclusion body after IPTG induction using Ni-NTA agarose (Qiagen, Valencia, CA) in the presence of 6 M urea or guanidine. The purified His-C8ORF37 protein was used as an antigen to immunize rabbits and chicken (Cocalico Biologicals, Stevens, PA). GST-tagged C8ORF37 protein was purified from the soluble fraction of cell lysates using GST•Bind™ resin (EMD Millipore, Billerica, MA). This GST-C8ORF37 protein was immobilized to agarose beads using the AminoLink™ Plus Immobilization kit (Pierce Biotechnology, Rockford, IL) and was used to affinity-purify the sera obtained from rabbits and chicken. The specificity of C8ORF37 antibodies was verified by immunoblotting analysis using *C8orf37* knockout retinas as a negative control. Mouse monoclonal antibody against rhodopsin (1D4), chicken antibodies against S- and M-opsins, rootletin, and RDS were described previously (Liu et al., 2004; J.

Yang et al., 2005). Mouse monoclonal antibodies against GC1 (GC 2H6), ROM-1 (Rom 1C6), RDS (Per 5H2), ABCA4 (Rim 3F4), CNGA1 (PMC 1D1), GARP (GARP 4B1) were gifts from Robert Molday (University of British Columbia). Mouse monoclonal antibody against GC1 (1S4) and rabbit antibodies against GC2 (L-670), GCAP1 (UW14 and UW101), GCAP2 (UW50), and arrestin were gifts from Wolfgang Baehr (University of Utah) and Krzysztof Palczewski (Case Western Reserve University). Rabbit antibodies against RDS, PCDH21 and CNGB1 were gifts from Andrew Goldberg (Oakland University), Amir Rattner (Johns Hopkins University), and Steven Pittler (University of Alabama), respectively. Chicken antibody against RP1 was a gift from Qin Liu (Harvard Medical School). Mouse monoclonal antibodies against acetylated α-tubulin (6-11B-1), β-tubulin (D66) and γ-tubulin (GTU-88) were purchased from Sigma-Aldrich (St. Louis, MO). Goat antibody against ABCA4 (M-18) and rabbit antibody against rod transducin α (K-20) were from Santa Cruz Biotechnology (Dallas, TX). Mouse monoclonal antibody against CNGB1 (5A5.1), rat monoclonal antibody against prominin 1 (13A4), and rabbit antibody against rod PDE (MOE) were from EMD Millipore (Billerica, MA), Affymetrix eBioscience (San Diego, CA) and CytoSignal (Irvine, CA), respectively. Alexa fluorochrome-conjugated secondary antibodies and Hoechst dye 33342 were obtained from Invitrogen (Carlsbad, CA). Horseradish peroxidase-conjugated secondary antibodies were purchased from Jackson ImmunoResearch Laboratories, Inc. (AffiniPure, West Grove, PA).

2.6.3 Cell culture, transfection, immunostaining, and immunoblotting analyses

IMCD3 cells were cultured according to the ATCC protocol and transfected by Lipofectamine® 2000 Transfection Reagent (Thermo Fisher Scientific, Waltham, MA). Retinal *in vivo* transfection (Matsuda & Cepko, 2004) and immunostaining of cultured cells and mouse retinal sections (Wang, Zou, Shen, Song, & Yang, 2012) were conducted as described previously. To quantify S/M-opsin mislocalization in the retina, immunostaining using mixed S- and M-opsin antibodies was conducted. Cone photoreceptors with S/M-opsin immunostaining signals mislocalized in the IS, ONL, and synaptic terminus were counted in a region of retinal cross-sections, which was 211 μm wide and ~900 μm away from the optical nerve head.

Serial tangential sectioning of rat retinas at 20 μm and immunoblotting analysis of proteins in sections were performed according to the procedure reported previously (Lobanova et al., 2008). Other immunoblotting analysis was carried out using our previous procedure (Wang et al., 2012). Specifically, immunoblotting of S/M-opsins was conducted using a mixture of S- and M-opsin antibodies. The intensity of immunoblotting signals was quantified by ImageJ using the Gels feature under the Analyze menu. The intensity of bands of interest was normalized by the intensity of loading control bands (e.g., γ-tubulin) in the same lanes on the same blots.

2.6.4 Electroretinography (ERG) and spectral domain optical coherence tomography (SD-OCT)

ERG tests were performed using a UTAS-E3000 instrument (LKC Technologies, Gaithersburg, MD) as described previously (Zou et al., 2011). After dark adaptation overnight, mice were anesthetized by intraperitoneal injection of ketamine and xylazine (0.1 mg and 0.01 mg per g body weight), and pupils were dilated with 1% tropicamide. Full-field scotopic retinal electrical responses were recorded in the dark upon a series of white light stimuli at increasing intensities. Full-field photopic retinal electrical responses were subsequently recorded after light adaptation at 33.25 cd/m^2 for 10 min. The a-wave amplitude of scotopic ERGs was measured from the baseline to the peak of the cornea-negative wave, while the b-wave amplitude of scotopic and photopic ERGs was measured from the peak of the cornea-negative wave to the peak of the major cornea-positive wave. The implicit times of a- and b-waves were measured from the onset of the light stimulus to the peaks of a- and b-waves, respectively.

SD-OCT images were acquired on anesthetized mice using Spectralis® HRA + OCT instrument (Heidelberg Engineering, Carlsbad, CA), with super luminescence diode light at an average wavelength of 870 nm. Cross-sectional two-dimensional B-scans of 1536 A-scans (5.3 mm) were captured with a rate of 40 kHz and a scan depth of 1.9 mm at the high-resolution mode. The measurement of the retinal thickness was conducted using the analysis tool in the Heidelberg Eye Explorer software platform (version 6.0.12.0).

2.6.5 Histology, transmission (TEM) and scanning (SEM) electron microscopy

Mouse eye cups, with the anterior segments and lens removed, were fixed in 1% formaldehyde and 2.5% glutaraldehyde in 0.1 M cacodylate buffer (pH 7.5) overnight. After washed with 0.1 M cacodylate buffer, the eye cups were post-fixed in 2% osmium tetroxide, dehydrated through a graded alcohol series and embedded in Epon. Half-micron cross-sections were stained with 1% methylene blue/azure II or 1% toluidine blue. The thicknesses of the OS and ONL layers were measured along the retinal vertical meridian at three evenly-separated locations on each side of the optic nerve head. The subsequent procedures for TEM were described previously (J. Yang et al., 2002). For SEM, retinas were dissected and fixed in 2.5% glutaraldehyde/PBS overnight. After washes with PBS buffer, the retinas were postfixed by alternative incubations in 1% osmium tetroxide (40 min for three times) and 0.3% thiocarbohydrizide (10 min for two times). The retinas were then dehydrated with a graded alcohol series, critical point dried using hexamethyldisilazane, and examined using Hitachi 4800 scanning electron microscope. OS density was calculated by the number of OSs divided by the retinal tangential width the OSs occupied. OS thickness was calculated by averaging the diameters measured from the top, middle, and bottom of the same OS. OS uniformity was calculated by the difference between the smallest and largest diameters of the same OS.

2.6.6 Statistical analyses

All measurements in this study were conducted by an individual blind to genotype. GraphPad PRISM® Version 4.00 was used for two-way ANOVA and Bonferroni posttests

to compare values between *C8orf37* heterozygous and homozygous groups. Microsoft Office Excel 2013 was used to conduct two-tailed Student's *t*-tests, assuming equal variances of *C8orf37* heterozygous and homozygous groups. A *p*-value of < 0.05 was considered to indicate a significant difference between the values from two genotype groups.

2.7 Acknowledgments

The authors thank Wolfgang Baehr (University of Utah), Krzysztof Palczewski (Case Western Reserve University), Robert Molday (University of British Columbia), Tiansen Li (National Eye Institute), Andrew Goldberg (Oakland University), Qin Liu (Harvard Medical School), and Amir Rattner (Johns Hopkins University) for providing antibodies. The authors are grateful to Robert Marc, Jia-hui Yang, Kevin Rapp, and Carl Watt at the University of Utah for their assistance in transmission electron microscopy. The authors appreciate Susan Tamowski at the Transgenic Gene Targeting Mouse Core and Timothy Dahlem at the Mutation Generation and Detection Core for assisting us in generating *C8orf37* knockout mice. The authors also acknowledge Wolfgang Baehr, Monica Vetter, Yukio Saijoh, and Michael Deans at the University of Utah for their insightful comments on the first version of this manuscript. This work was supported by National Eye Institute grants EY020853 (J.Y.), EY024234 (A.S.S), EY022959 (V.Y.A), EY12859 (V.Y.A), EY05722 (V.Y.A), and EY014800 (core grant to the Department of Ophthalmology and Visual Sciences, University of Utah), Research to Prevent Blindness, Inc. (J.Y. and the Departments of Ophthalmology and Visual Sciences at the University of Utah and Duke University), an incentive seed grant from the University of Utah Research

Foundation (J.Y.), and a startup package from the Moran Eye Center, University of Utah (J.Y.).

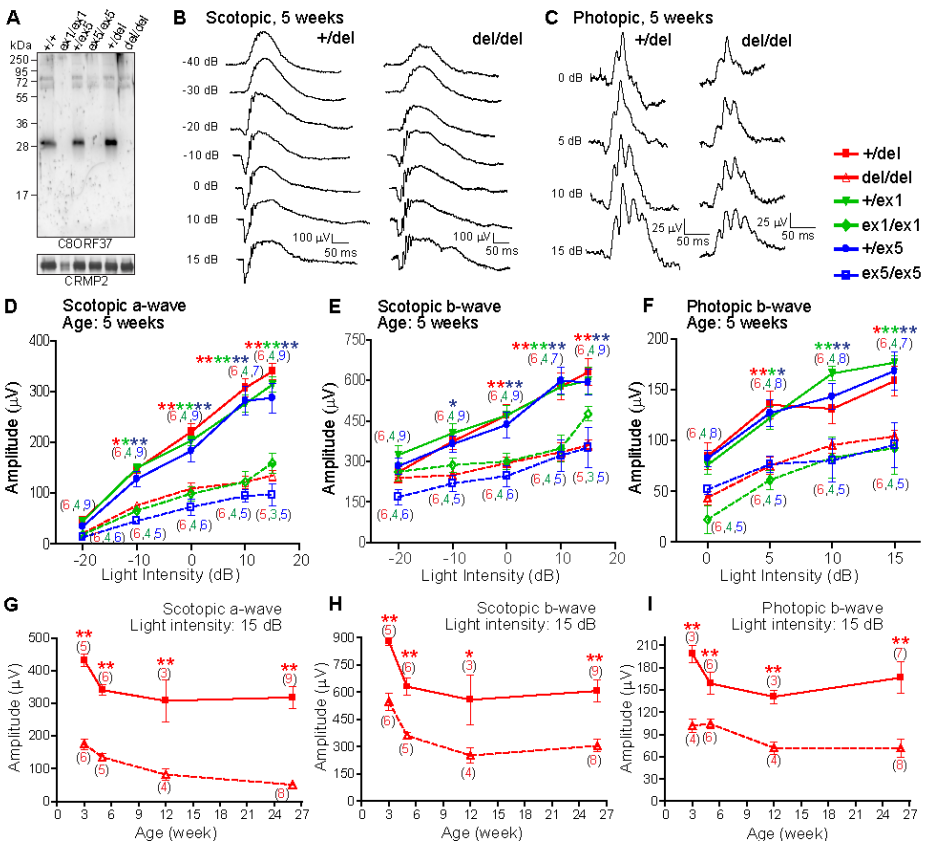

Figure 2.1: *C8orf37* knockout mice have reduced scotopic and photopic ERG responses. (A) Immunoblotting analysis showed that *C8orf37*$^{ex1/ex1}$, *C8orf37*$^{ex5/ex5}$ and *C8orf37*$^{del/del}$ retinas expressed no C8ORF37 protein or fragment. The blot of CRMP2 was used as a loading control. (B) Representative scotopic ERG responses at various light intensities from 5-week-old *C8orf37*$^{+/del}$ and *C8orf37*$^{del/del}$ littermates. (C) Representative photopic ERG responses at various light intensities from 5-week-old *C8orf37*$^{+/del}$ and *C8orf37*$^{del/del}$ littermates. (D - F) Reduced scotopic ERG a-wave amplitude (C), b-wave amplitude (E) and photopic ERG b-wave amplitude (F) of 5-week-old *C8orf37*$^{ex1/ex1}$, *C8orf37*$^{ex5/ex5}$ and *C8orf37*$^{del/del}$ mice, compared with their heterozygous littermates. (G - I) Changes of scotopic ERG a-wave amplitude (G), b-wave amplitude (*H*) and photopic ERG b-wave amplitude (I) at 15 dB in *C8orf37*$^{+/del}$ and *C8orf37*$^{del/del}$ littermates from 3 to 26 weeks of age. Legends for each genotype are shown on top right. Data are presented as mean ± *SEM*. *, $p < 0.05$; **, $p < 0.01$. Numbers in the parentheses are numbers of animals tested at each light intensity or age point. Color of the numbers and asterisks matches the color of the heterozygous and homozygous genotypes. 0 dB = 2.4 cds/m^2.

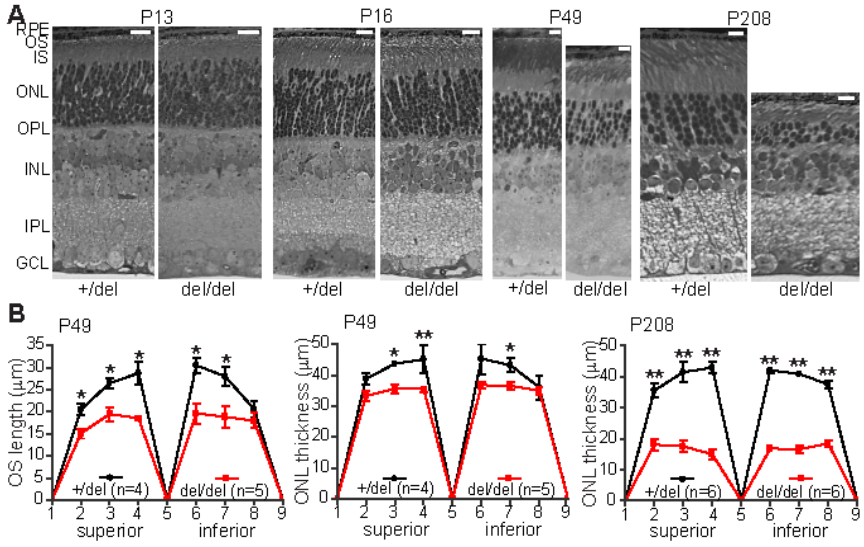

Figure 2.2: *C8orf37*$^{del/del}$ mice show progressive retinal degeneration. (A) The photoreceptor ONL and OS layers become thinner with age in *C8orf37*$^{del/del}$ mice. Retinal sections were stained with methylene blue and azure II at P13 and P16, and were stained with toluidine blue at P49 and P208. RPE, retinal pigment epithelium; OPL, outer plexiform layer; INL, inner nuclear layer; IPL, inner plexiform layer; GCL, ganglion cell layer; scale bars, 10 μm. (B) Quantification of OS and ONL thicknesses at P49 (left and middle) and ONL thickness at P208 (right) along the retinal vertical meridian in *C8orf37*$^{+/del}$ and *C8orf37*$^{del/del}$ retinas. Data are presented as mean ± *SEM*. *n*, number of animals analyzed; *, $p < 0.05$; **, $p < 0.01$.

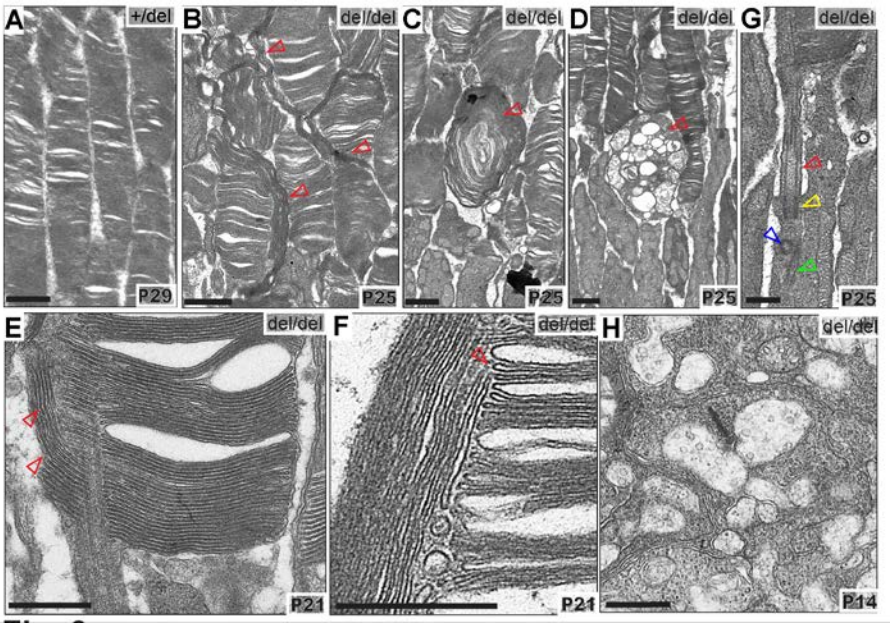

Figure 2.3: The *C8orf37*$^{del/del}$ OS has disorganized membrane discs. (A) The membrane discs are stacked tightly and horizontally in the control *C8orf37*$^{+/del}$ OS. (B) The membrane discs are wide and sometimes extend vertically (arrows) in the *C8orf37*$^{del/del}$ OS. (C) A membrane whirl (arrow) is shown in the *C8orf37*$^{del/del}$ OS layer. (D) An abnormal multivesicular body–like structure (arrow) is present between the IS and OS layers in the *C8orf37*$^{del/del}$ retina. (E) Extension of vertical membrane discs from the edge of horizontal membrane discs (arrows) in the *C8orf37*$^{del/del}$ OS. (F) No existence of a plasma membrane between the horizontal and vertical membrane discs (arrow) in the *C8orf37*$^{del/del}$ OS. (G) *C8orf37*$^{del/del}$ photoreceptors have a normal connecting cilium (red arrow), basal body (yellow arrow), daughter centriole (blue arrow) and ciliary rootlet (green arrow). (H) *C8orf37*$^{del/del}$ rod photoreceptors have a normal synaptic terminus. Age of photoreceptors is labeled at the bottom-left corner of each image. Scale bars, 1 μm (A-D) and 0.5 μm (E-H).

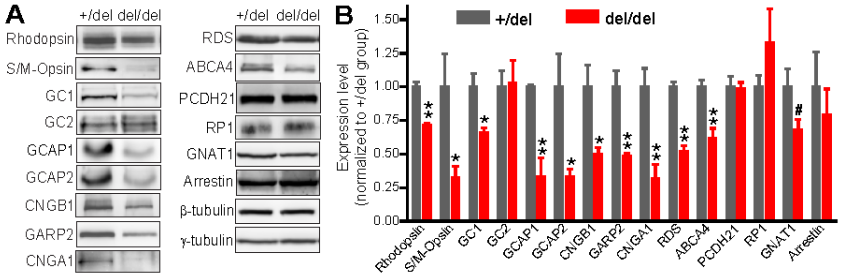

Figure 2.4: Many OS membrane proteins and their associated proteins are reduced in *C8orf37*$^{del/del}$ retinas. (A) Representative immunoblots of proteins expressed in *C8orf37*$^{+/del}$ and *C8orf37*$^{del/del}$ retinas at P30. (B) Quantification of OS protein expression in *C8orf37*$^{+/del}$ and *C8orf37*$^{del/del}$ retinas at P30. The expression of each protein was first normalized by its corresponding loading control, γ-tubulin, and then normalized by the mean value of the *C8orf37*$^{+/del}$ group. Data are presented as mean ± *SEM*. Four mice were analyzed for each genotype. $^{\#}$, $p < 0.1$; *, $p < 0.05$; **, $p < 0.01$.

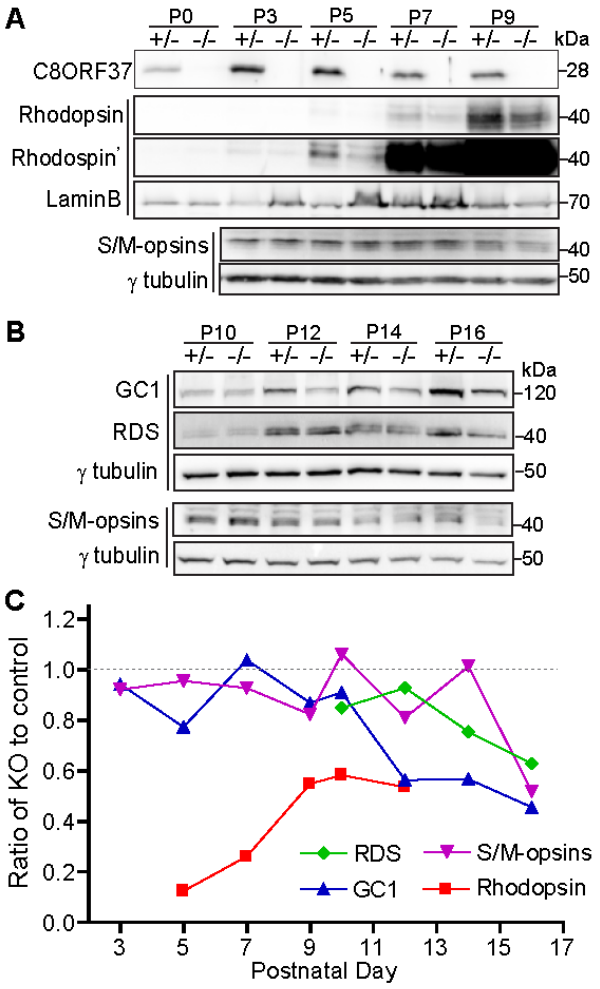

Figure 2.5: Onset of OS membrane protein reduction before and during OS disc morphogenesis in *C8orf37*$^{del/del}$ retinas. (A) Expression of C8ORF37, rhodopsin and S/M-opsin proteins in *C8orf37*$^{+/del}$ and *C8orf37*$^{del/del}$ retinas before OS disc morphogenesis. The blots labeled with rhodopsin and rhodopsin' are the same blot, but the signal intensity on the rhodopsin' blot was significantly enhanced to show the rhodopsin signals at P5. (B) Expression of GC1, RDS, and S/M-opsin proteins in *C8orf37*$^{+/del}$ and *C8orf37*$^{del/del}$ retinas during OS disc morphogenesis. (C) Ratios of rhodopsin, S/M-opsin, GC1 and RDS protein expression in *C8orf37*$^{del/del}$ retinas to that in *C8orf37*$^{+/del}$ retinas from P3 to P16. Lamin B and γ-tubulin are loading controls. Immunoblots labeled by the same vertical bars are from the same blots.

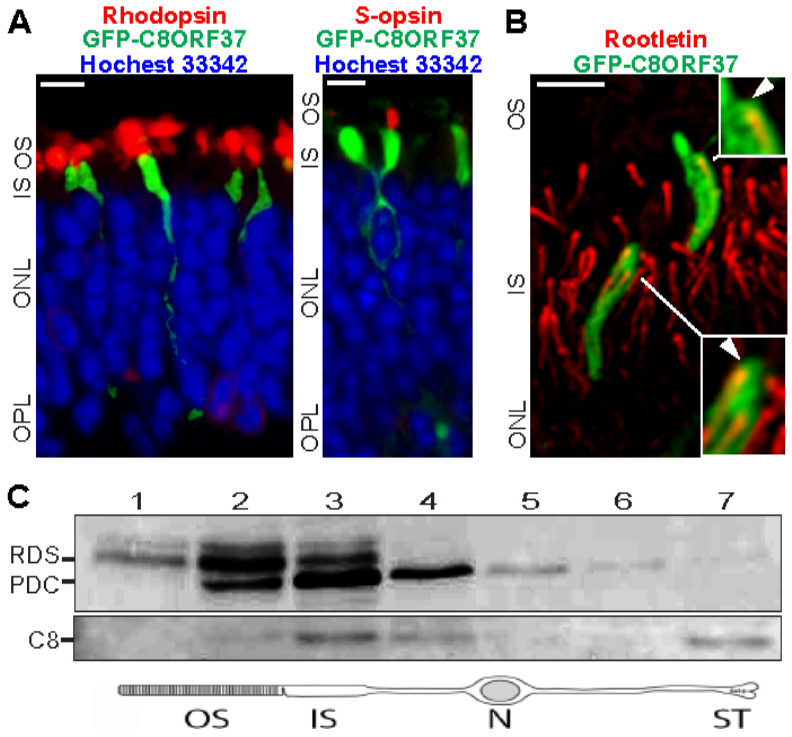

Figure 2.6: C8ORF37 is localized to the cell body but not the OS in photoreceptors. (A) Transfected GFP-C8ORF37 (green) is localized to the rod (left) and cone (right) photoreceptor cell body in the IS, ONL and outer plexiform layer (OPL) of *C8orf37*$^{del/del}$ retinas at P21. Rhodopsin and S-opsin (red) are markers for the rod and cone OS, respectively. Hoechst 33342 dye (blue) labels the nuclei. (B) GFP-C8ORF37 is evenly distributed in the IS, marked by rootletin (red). Insets, GFP-C8ORF37 is present in the region above the apical tip of the rootletin signal, where the basal body is located (arrows). Scale bars for A and B, 5 µm. (C) The distribution of C8ORF37 in seven 20-µm serial tangential sections throughout the photoreceptor layer of a flat-mounted rat retina. Relative contents of C8ORF37, phosducin (PDC, a cell body marker) and RDS (an OS marker) were analyzed by immunoblotting with corresponding antibodies. A cartoon of a photoreceptor beneath the immunoblotting panels is used to depict the subcellular origin of each section. Note that portions of OS and IS naturally overlap in sections #2 and 3. N, nucleus; ST, synaptic terminus.

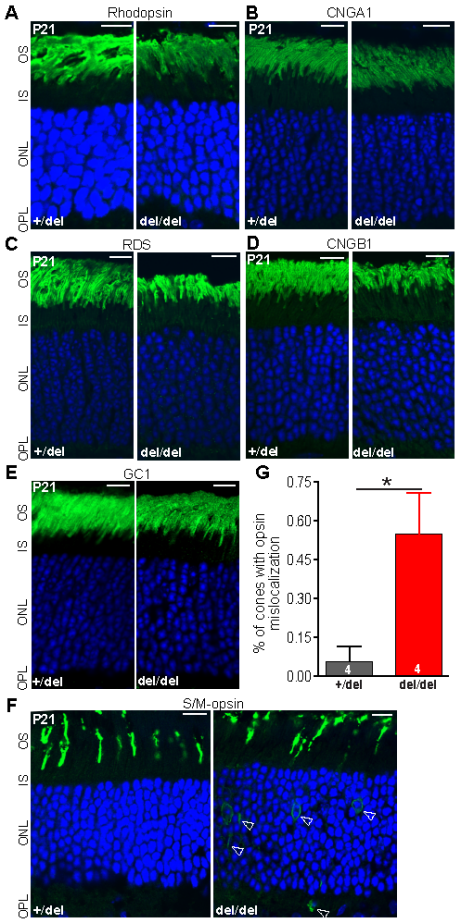

Figure 2.7: OS membrane proteins except S/M-opsins are distributed normally in *C8orf37*$^{del/del}$ photoreceptors. (A-E) Immunostaining demonstrated that rhodopsin (green, A), CNGA1 (green, B), RDS (green, C), CNGB1 (green, D) and GC1 (green, E) are localized normally to the *C8orf37*$^{del/del}$ OS at P21. (F) Immunostaining revealed partial mislocalization of S/M-opsins (arrows) in some *C8orf37*$^{del/del}$ cones at P21. (G) Quantification of cones with mislocalized S/M-opsins in littermate P21 *C8orf37*$^{+/del}$ and *C8orf37*$^{del/del}$ retinas. Data are presented as mean ± *SEM*. Numbers in the bottom of bars are numbers of mice analyzed. **, $p < 0.01$. Nuclei were stained by Hoechst 33342 (blue). Scale bars, 10 μm.

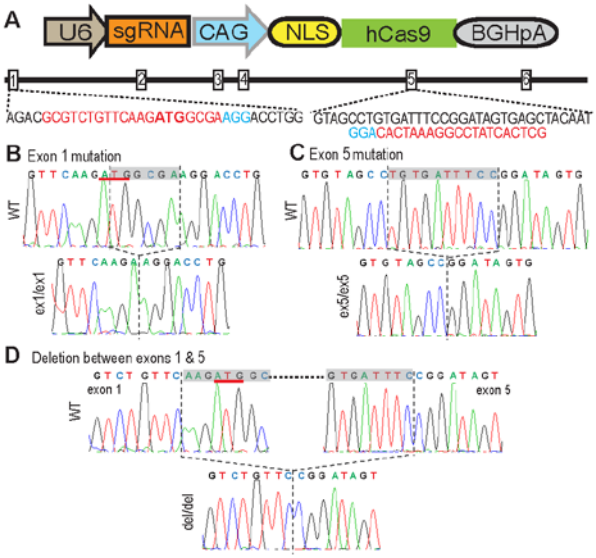

Figure 2.S1: *C8orf37* knockout mice were generated. (A) Packing of small guide RNA (sgRNA) and Cas9 in the pX330-U6-Chimeric_BB-CBh-hSpCas9 vector (top). The sequence and target position of sgRNAs used in this study are shown in the bottom. Rectangles labeled with numerals denote mouse *C8orf37* exons. (B-D) DNA sequencing chromatograms of wild-type and *C8orf37* mutant mice for *C8orf37*$^{ex1/ex1}$ (B), *C8orf37*$^{ex5/ex5}$ (C) and *C8orf37*$^{del/del}$ (D) alleles. Deleted regions in these three mutant alleles are highlighted in gray. The translation start codons are underlined in red. U6, U6 promoter; CAG, a hybrid of the cytomegalovirus early enhancer element and chicken beta-actin promoter; NLS, nuclear localization signal; and BGHpA, bovine growth hormone polyadenylation signal.

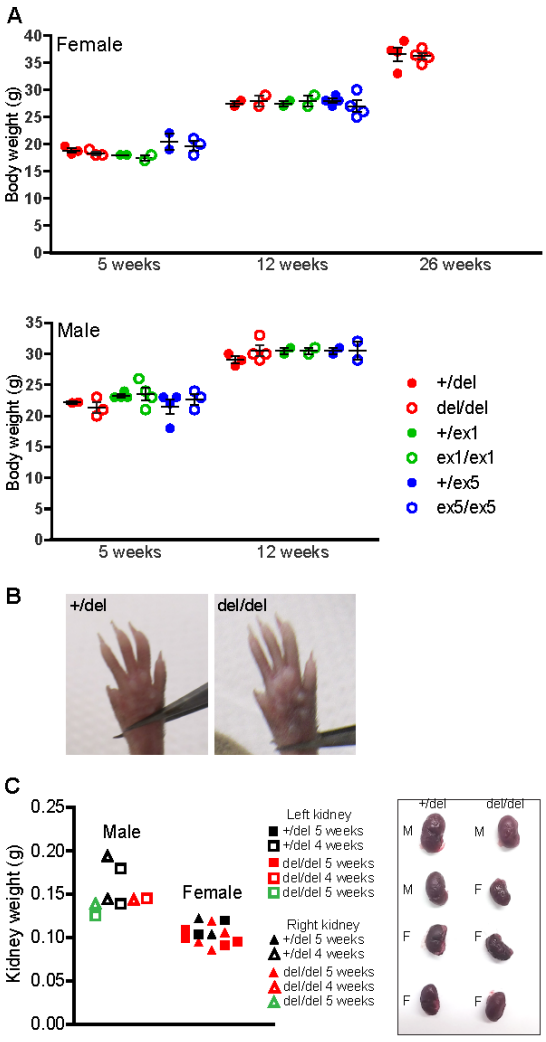

Figure 2.S2: Normal body weight, digit number and kidney in *C8orf37* knockout mice. (A) The body weight of female (top) and male (bottom) *C8orf37*$^{ex1/ex1}$, *C8orf37*$^{ex5/ex5}$ and *C8orf37*$^{del/del}$ mice is comparable to that of their heterozygous littermates up to 26 weeks of age. Data are shown as mean ± *SEM* as well as individual data points. (B) No polydactyly was observed in ~70 *C8orf37*$^{del/del}$ mice or ~50 *C8orf37*$^{+/del}$ mice. (C) Left, kidney weight is normal in male and female *C8orf37*$^{del/del}$ mice, compared with littermate *C8orf37*$^{+/del}$ mice at 4-5 weeks of age. Data are shown as individual data points. Right, the morphology of kidney appears normal in male (M) and female (F) *C8orf37*$^{del/del}$ mice.

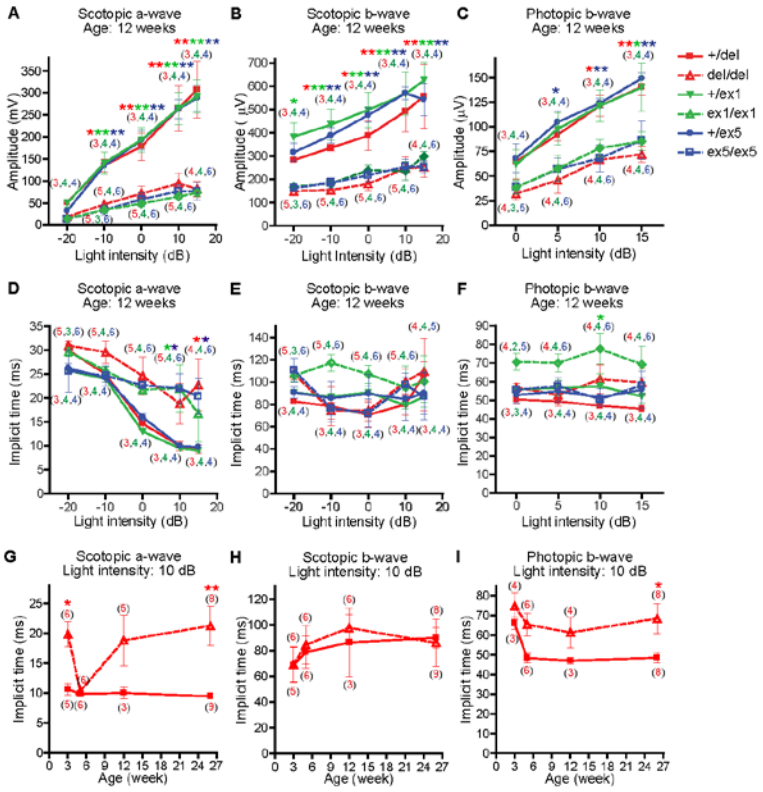

Figure 2.S3: *C8orf37* knockout mice have reduced and prolonged scotopic and photopic ERG responses. (A-C) *C8orf37*$^{ex1/ex1}$, *C8orf37*$^{ex5/ex5}$ and *C8orf37*$^{del/del}$ mice have reduced scotopic ERG a-wave amplitude (A), b-wave amplitude (B) and photopic ERG b-wave amplitude (C) at 12 weeks of age, compared with their heterozygous littermates. (D) *C8orf37*$^{ex1/ex1}$, *C8orf37*$^{ex5/ex5}$ and *C8orf37*$^{del/del}$ mice have prolonged scotopic a-wave implicit time at the light intensities of 10 and 15 dB at 12 weeks of age. (E) The scotopic b-wave implicit time is not changed in *C8orf37*$^{ex1/ex1}$, *C8orf37*$^{ex5/ex5}$ or *C8orf37*$^{del/del}$ mice at 12 weeks of age. (F) The photopic b-wave implicit time is not changed in *C8orf37*$^{ex1/ex1}$, *C8orf37*$^{ex5/ex5}$ or *C8orf37*$^{del/del}$ mice at 12 weeks of age, except the increased photopic b-wave implicit time in *C8orf37*$^{ex1/ex1}$ mice at 10 dB. (G-H) The implicit time of scotopic ERG a-wave (G) but not b-wave (H) at 10 dB is increased in *C8orf37*$^{del/del}$ mice at 3 and 26 weeks of age. (I) The implicit time of photopic ERG b-wave at 10 dB is prolonged in *C8orf37*$^{del/del}$ mice at 26 weeks of age. Data are presented as mean ± *SEM*. *, $p < 0.05$; **, $p < 0.01$. Legends for each genotype are shown on top right. Numbers in the parentheses are numbers of animals tested at each light intensity or age point. The color of numbers and asterisks matches the color of heterozygous and homozygous genotypes. 0 dB = 2.4 cds/m^2.

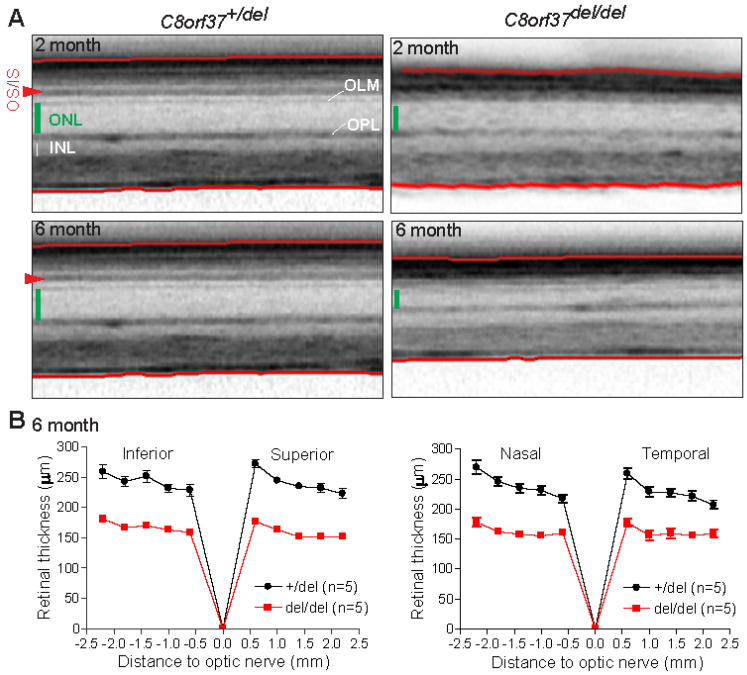

Figure 2.S4: Progressive retinal degeneration in *C8orf37*$^{del/del}$ mice revealed by SD-OCT. (A) Representative SD-OCT images of *C8orf37*$^{+/del}$ and *C8orf37*$^{del/del}$ retinas at 2 and 6 months of age. Red arrows point to the OS and IS junction line. Green lines mark the ONL thickness. OPL, outer plexiform layer; INL, inner nuclear layer; OLM, outer limiting membrane. (B) Quantification of the entire retinal thickness along the vertical (left) and horizontal (right) meridians from *C8orf37*$^{+/del}$ and *C8orf37*$^{del/del}$ SD-OCT images at 6 months of age. Data are presented as mean ± *SEM*. *n*, number of mice measured.

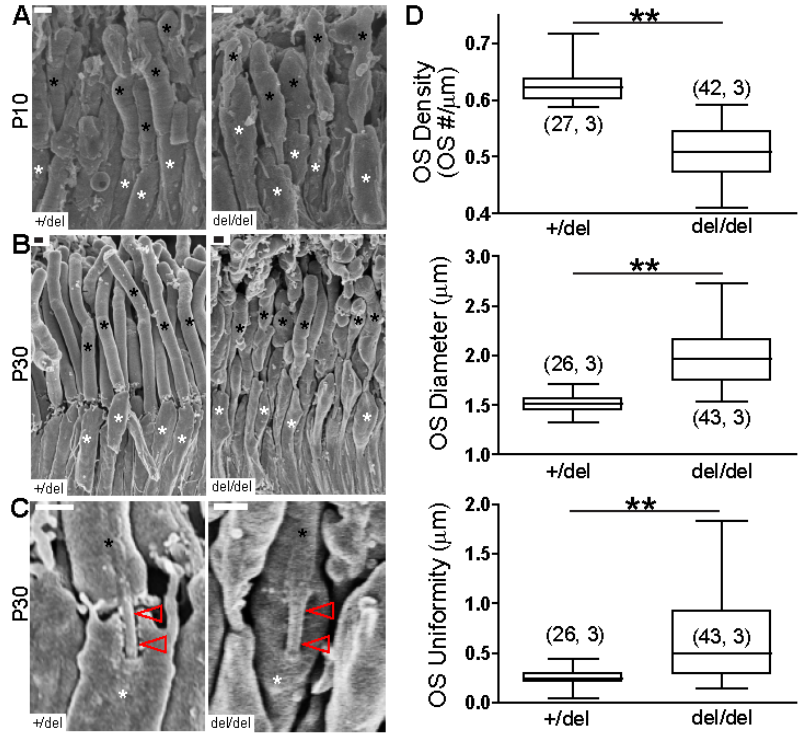

Figure 2.S5: *C8orf37*$^{del/del}$ mice have an abnormal photoreceptor OS shape. (A) SEM images showing abnormal OS shape in *C8orf37*$^{del/del}$ photoreceptors at P10, compared with littermate *C8orf37*$^{+/del}$ photoreceptors. (B) SEM images showing swollen OSs with uneven diameter in *C8orf37*$^{del/del}$ photoreceptors at P30. (C) SEM views of the connecting cilium (arrows) in *C8orf37*$^{+/del}$ and *C8orf37*$^{del/del}$ photoreceptors at P30. (D) Box-and-whisker plots of the OS density (top), diameter (middle) and uniformity (bottom) in *C8orf37*$^{+/del}$ and *C8orf37*$^{del/del}$ mice at P30. The upper and lower edges of the boxes represent the 25th and 75th percentiles, respectively, while the line in the boxes is the median. The top and bottom of the vertical lines mark the highest and lowest values, respectively. The numbers in the parentheses are the numbers of retinal regions or OSs (before the comma) and the numbers of animals (after the comma) measured in the assay. **, $p < 0.01$. Black and white asterisks mark the OS and IS, respectively. Scale bars, 1 μm.

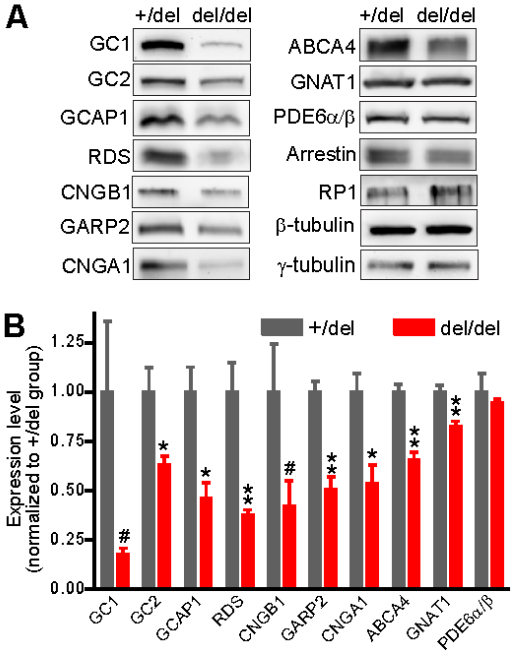

C

OS protein	+/del	del/del	*p*-value
GC1	1.00 ± 0.36	0.18 ± 0.03	0.062#
GC2	1.00 ± 0.12	0.63 ± 0.05	0.032*
GCAP1	1.00 ± 0.13	0.46 ± 0.08	0.012*
RDS	1.00 ± 0.15	0.38 ± 0.03	0.007**
CNGB1	1.00 ± 0.24	0.42 ± 0.13	0.081#
GARP2	1.00 ± 0.05	0.51 ± 0.06	0.001**
CNGA1	1.00 ± 0.10	0.53 ± 0.09	0.013*
ABCA4	1.00 ± 0.04	0.66 ± 0.04	0.001**
GNAT1	1.00 ± 0.04	0.82 ± 0.03	0.008**
PDE6α/β	1.00 ± 0.09	0.95 ± 0.02	0.588

Figure 2.S6: The expression of many photoreceptor OS membrane proteins is reduced in *C8orf37*$^{del/del}$ retinas. (A) Representative immunoblots of various proteins expressed in *C8orf37*$^{+/del}$ and *C8orf37*$^{del/del}$ retinas at P49. (B-C) Quantification of immunoblot signals at P49 showed reduction of many photoreceptor OS membrane proteins and their associated proteins in *C8orf37*$^{del/del}$ retinas. Data are presented as mean ± *SEM* in both the bar chart (B) and the table (C). Four mice were analyzed for each genotype. $^{\#}$, $p < 0.1$; *, $p < 0.05$; and **, $p < 0.01$.

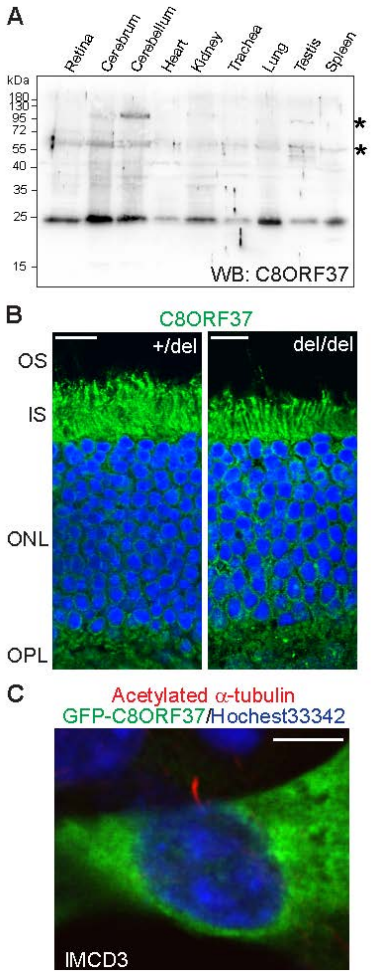

Figure 2.S7: Expression of C8ORF37 protein in multiple tissues and cultured cells. (A) Immunoblotting analysis showed that C8ORF37 is present in various tissues of adult mice. Asterisks denote nonspecific bands, which appeared inconsistently between duplicate experiments. (B) Immunostaining using our custom-made C8ORF37 antibody showed an immunoreactivity (green) throughout the *C8orf37*$^{+/del}$ photoreceptor layers except the OS layer; however, a similar immunoreactivity pattern was also observed in *C8orf37*$^{del/del}$ photoreceptors. (C) Transfected GFP-C8ORF37 (green) is evenly distributed in the cytoplasm but not the primary cilium, labeled by acetylated α-tubulin (red), in a serum-starved IMCD3 cell. Blue, nuclear staining from Hoechst 33342. Scale bars, 10 μm (B) and 5 μm (C).

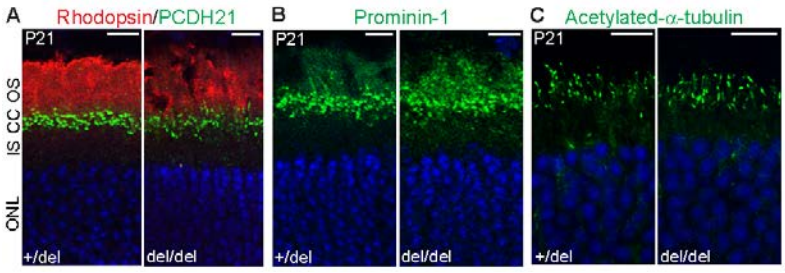

Figure 2.S8: The distribution of PCDH21 (green, A), prominin-1 (green, B) and acetylated α-tubulin (green, C) in *C8orf37*$^{del/del}$ photoreceptors is comparable to that in *C8orf37*$^{+/del}$ photoreceptors. Red signal in A is from rhodopsin antibody staining. Blue signal from Hoechst 33342 labels the nucleus. Scale bars, 10 μm.

Table 2.S1: DNA primer information.

Primer name	Primer sequence
CRISPR/Cas9 plasmid construction	
C8-E1-S1-F	CACCGCGTCTGTTCAAGATGGCGA
C8-E1-S1-R	AAACTCGCCATCTTGAACAGACGC
C8-E5-S10-F	CACCGCTCACTATCCGGAAATCAC
C8-E5-S10-R	AAACGTGATTTCCGGATAGTGAGC
HRMA analysis and genotyping (*C8orf37*$^{ex1/ex1}$ and *C8orf37*$^{ex5/ex5}$)	
FWD1.1-Exon1	GTTGCCGTGGAAACCACCGGCC
RVS1.1-Exon1	CCAGCCTCAAGGGGTCGAGTCTGC
FWD5.1-Exon5	TCTCTCTGAGCAGAGCATGTGA
RVS5.1-Exon5	GGCGAAACTCTTCAGAAACATACC
Genotyping (*C8orf37*$^{del/del}$)	
FWRDEX1	GCTCCCGGGCGCGTCGGTTTC
FWRDEX5	GCCCTACCTGGCTTAGAACTCAC
RVSEX5	CAAGGAGGTTCCCGAGCAAACATC

2.8 References

Arikawa, K., Molday, L. L., Molday, R. S., & Williams, D. S. (1992). Localization of peripherin/rds in the disk membranes of cone and rod photoreceptors: relationship to disk membrane morphogenesis and retinal degeneration. *Journal of Cell Biology, 116*(3), 659-667.

Caley, D. W., Johnson, C., & Liebelt, R. A. (1972). The postnatal development of the retina in the normal and rodless CBA mouse: a light and electron microscopic study. *American Journal of Anatomy, 133*(2), 179-212. doi:10.1002/aja.1001330205

Chakraborty, D., Conley, S. M., Al-Ubaidi, M. R., & Naash, M. I. (2014). Initiation of rod outer segment disc formation requires RDS. *PLoS One, 9*(6), e98939. doi:10.1371/journal.pone.0098939

Chakraborty, D., Conley, S. M., Pittler, S. J., & Naash, M. I. (2016). Role of RDS and rhodopsin in cngb1-related retinal degeneration. *Investigative Ophthalmology and Visual Science, 57*(3), 787-797. doi:10.1167/iovs.15-18516

Cong, L., Ran, F. A., Cox, D., Lin, S., Barretto, R., Habib, N., Zhang, F. (2013). Multiplex genome engineering using CRISPR/Cas systems. *Science, 339*(6121), 819-823. doi:10.1126/science.1231143

De Robertis, E. (1956). Morphogenesis of the retinal rods; an electron microscope study. *Journal of Biophysical and Biochemical Cytology, 2*(4 Suppl), 209-218.

Ding, X. Q., Nour, M., Ritter, L. M., Goldberg, A. F., Fliesler, S. J., & Naash, M. I. (2004). The R172W mutation in peripherin/rds causes a cone-rod dystrophy in transgenic mice. *Human Molecular Genetics, 13*(18), 2075-2087. doi:10.1093/hmg/ddh211

Estrada-Cuzcano, A., Neveling, K., Kohl, S., Banin, E., Rotenstreich, Y., Sharon, D., Cremers, F. P. (2011). Mutations in C8orf37, encoding a ciliary protein, are associated with autosomal-recessive retinal dystrophies with early macular involvement. *American Journal of Human Genetics, 90*(1), 102-109. doi:S0002-9297(11)00493-9 [pii]10.1016/j.ajhg.2011.11.015

Filipek, S., Stenkamp, R. E., Teller, D. C., & Palczewski, K. (2003). G protein-coupled receptor rhodopsin: a prospectus. *Annual Review of Physiology, 65*, 851-879. doi:10.1146/annurev.physiol.65.092101.142611

Hartong, D. T., Berson, E. L., & Dryja, T. P. (2006). Retinitis pigmentosa. *Lancet, 368*(9549), 1795-1809.

Hawkins, R. K., Jansen, H. G., & Sanyal, S. (1985). Development and degeneration of retina in rds mutant mice: photoreceptor abnormalities in the heterozygotes. *Experimental Eye Research, 41*(6), 701-720.

Heitzmann, H. (1972). Rhodopsin is the predominant protein of rod outer segment membranes. *Nature New Biology, 235*(56), 114.

Heon, E., Kim, G., Qin, S., Garrison, J. E., Tavares, E., Vincent, A., . . . Sheffield, V. C. (2016). Mutations in C8ORF37 cause Bardet Biedl syndrome (BBS21). *Human Molecular Genetics, 25*(11), 2283-2294. doi:10.1093/hmg/ddw096

Hollingsworth, T. J., & Gross, A. K. (2013). The severe autosomal dominant retinitis pigmentosa rhodopsin mutant Ter349Glu mislocalizes and induces rapid rod cell death. *Journal of Biological Chemistry, 288*(40), 29047-29055. doi:10.1074/jbc.M113.495184

Hwang, W. Y., Fu, Y., Reyon, D., Maeder, M. L., Tsai, S. Q., Sander, J. D., Joung, J. K. (2013). Efficient genome editing in zebrafish using a CRISPR-Cas system. *Nature Biotechnology, 31*(3), 227-229. doi:10.1038/nbt.2501

Jinda, W., Taylor, T. D., Suzuki, Y., Thongnoppakhun, W., Limwongse, C., Lertrit, P., Atchaneeyasakul, L. O. (2014). Whole exome sequencing in Thai patients with retinitis pigmentosa reveals novel mutations in six genes. *Investigative Ophthalmology and Visual Science, 55*(4), 2259-2268. doi:10.1167/iovs.13-13567

Katagiri, S., Hayashi, T., Yoshitake, K., Akahori, M., Ikeo, K., Gekka, T., Iwata, T. (2014). Novel C8orf37 Mutations in Patients with Early-onset Retinal Dystrophy, Macular Atrophy, Cataracts, and High Myopia. *Ophthalmic Genetics*, 37(1) 1-8. doi:10.3109/13816810.2014.949380

Khan, A. O., Decker, E., Bachmann, N., Bolz, H. J., & Bergmann, C. (2016). C8orf37 is mutated in Bardet-Biedl syndrome and constitutes a locus allelic to non-syndromic retinal dystrophies. *Ophthalmic Genetics, 37*(3), 290-293. doi:10.3109/13816810.2015.1066830

Lazar, C. H., Mutsuddi, M., Kimchi, A., Zelinger, L., Mizrahi-Meissonnier, L., Marks-Ohana, D., Banin, E. (2015). Whole exome sequencing reveals GUCY2D as a major gene associated with cone and cone-rod dystrophy in Israel. *Investigative Ophthalmology and Visual Science, 56*(1), 420-430. doi:10.1167/iovs.14-15647

Lem, J., Krasnoperova, N. V., Calvert, P. D., Kosaras, B., Cameron, D. A., Nicolo, M., Sidman, R. L. (1999). Morphological, physiological, and biochemical changes in rhodopsin knockout mice. *Proceedings of the National Academy of Sciences USA*, *96*(2), 736-741.

Liang, Y., Fotiadis, D., Maeda, T., Maeda, A., Modzelewska, A., Filipek, S., Palczewski, K. (2004). Rhodopsin signaling and organization in heterozygote rhodopsin knockout mice. *Journal of Biological Chemistry, 279*(46), 48189-48196. doi:10.1074/jbc.M408362200

Liu, X., Bulgakov, O. V., Wen, X. H., Woodruff, M. L., Pawlyk, B., Yang, J., Li, T. (2004). AIPL1, the protein that is defective in Leber congenital amaurosis, is essential for the biosynthesis of retinal rod cGMP phosphodiesterase. *Proceedings of the National Academy of Sciences USA, 101*(38), 13903-13908.

Lobanova, E. S., Finkelstein, S., Herrmann, R., Chen, Y. M., Kessler, C., Michaud, N. A., Arshavsky, V. Y. (2008). Transducin gamma-subunit sets expression levels of alpha- and beta-subunits and is crucial for rod viability. *Journal of Neuroscience, 28*(13), 3510-3520. doi:10.1523/JNEUROSCI.0338-08.2008

Mali, P., Yang, L., Esvelt, K. M., Aach, J., Guell, M., DiCarlo, J. E., Church, G. M. (2013). RNA-guided human genome engineering via Cas9. *Science, 339*(6121), 823-826. doi:10.1126/science.1232033

Matsuda, T., & Cepko, C. L. (2004). Electroporation and RNA interference in the rodent retina in vivo and in vitro. *Proceedings of the National Academy of Sciences USA, 101*(1), 16-22.

Mitamura, Y., Mitamura-Aizawa, S., Nagasawa, T., Katome, T., Eguchi, H., & Naito, T. (2012). Diagnostic imaging in patients with retinitis pigmentosa. *Journal of Medical Investigation, 59*(1-2), 1-11.

Novas, R., Cardenas-Rodriguez, M., Irigoin, F., & Badano, J. L. (2015). Bardet-Biedl syndrome: Is it only cilia dysfunction? *FEBS Letters, 589*(22), 3479-3491. doi:10.1016/j.febslet.2015.07.031

Pearring, J. N., Salinas, R. Y., Baker, S. A., & Arshavsky, V. Y. (2013). Protein sorting, targeting and trafficking in photoreceptor cells. *Progress in Retinal and Eye Research, 36*, 24-51.

Price, B. A., Sandoval, I. M., Chan, F., Nichols, R., Roman-Sanchez, R., Wensel, T. G., & Wilson, J. H. (2012). Rhodopsin gene expression determines rod outer segment size and rod cell resistance to a dominant-negative neurodegeneration mutant. *PLoS One, 7*(11), e49889. doi:10.1371/journal.pone.0049889

Rahner, N., Nuernberg, G., Finis, D., Nuernberg, P., & Royer-Pokora, B. (2016). A novel C8orf37 splice mutation and genotype-phenotype correlation for cone-rod dystrophy. *Ophthalmic Genetics, 37*(3), 294-300. doi:10.3109/13816810.2015.1071408

Rattner, A., Smallwood, P. M., Williams, J., Cooke, C., Savchenko, A., Lyubarsky, A., Nathans, J. (2001). A photoreceptor-specific cadherin is essential for the structural integrity of the outer segment and for photoreceptor survival. *Neuron, 32*(5), 775-786. doi:S0896-6273(01)00531-1 [pii]

Ravesh, Z., El Asrag, M. E., Weisschuh, N., McKibbin, M., Reuter, P., Watson, C. M., Ali, M. (2015). Novel C8orf37 mutations cause retinitis pigmentosa in consanguineous families of Pakistani origin. *Molecular Vision, 21,* 236-243.

Robinson, W. E., Gordon-Walker, A., & Bownds, D. (1972). Molecular weight of frog rhodopsin. *Nature New Biology, 235*(56), 112-114.

Sander, J. D., Maeder, M. L., Reyon, D., Voytas, D. F., Joung, J. K., & Dobbs, D. (2010). ZiFiT (Zinc Finger Targeter): an updated zinc finger engineering tool. *Nucleic Acids Research, 38*(Web Server issue), W462-468. doi:10.1093/nar/gkq319

Sander, J. D., Zaback, P., Joung, J. K., Voytas, D. F., & Dobbs, D. (2007). Zinc Finger Targeter (ZiFiT): an engineered zinc finger/target site design tool. *Nucleic Acids Research, 35*(Web Server issue), W599-605. doi:10.1093/nar/gkm349

Sokolov, M., Lyubarsky, A. L., Strissel, K. J., Savchenko, A. B., Govardovskii, V. I., Pugh, E. N., Jr., & Arshavsky, V. Y. (2002). Massive light-driven translocation of transducin between the two major compartments of rod cells: a novel mechanism of light adaptation. *Neuron, 34*(1), 95-106. doi:S0896627302006360 [pii]

Thiadens, A. A., Phan, T. M., Zekveld-Vroon, R. C., Leroy, B. P., van den Born, L. I., Hoyng, C. B., . . . Lotery, A. J. (2012). Clinical course, genetic etiology, and visual outcome in cone and cone-rod dystrophy. *Ophthalmology, 119*(4), 819-826. doi:10.1016/j.ophtha.2011.10.011

van Huet, R. A., Estrada-Cuzcano, A., Banin, E., Rotenstreich, Y., Hipp, S., Kohl, S., Klevering, B. J. (2013). Clinical characteristics of rod and cone photoreceptor dystrophies in patients with mutations in the C8orf37 gene. *Investigative Ophthalmology and Visual Science, 54*(7), 4683-4690. doi:10.1167/iovs.12-11439

Wang, L., Zou, J., Shen, Z., Song, E., & Yang, J. (2012). Whirlin interacts with espin and modulates its actin-regulatory function: an insight into the mechanism of Usher syndrome type II. *Human Molecular Genetics, 21*(3), 692-710. doi:ddr503 [pii] 10.1093/hmg/ddr503

Xiao, A., Cheng, Z., Kong, L., Zhu, Z., Lin, S., Gao, G., & Zhang, B. (2014). CasOT: a genome-wide Cas9/gRNA off-target searching tool. *Bioinformatics, 30*(8), 1180-1182. doi:10.1093/bioinformatics/btt764

Yang, J., Gao, J., Adamian, M., Wen, X. H., Pawlyk, B., Zhang, L., Li, T. (2005). The ciliary rootlet maintains long-term stability of sensory cilia. *Molecular and Cellular Biology, 25*(10), 4129-4137.

Yang, J., Liu, X., Yue, G., Adamian, M., Bulgakov, O., & Li, T. (2002). Rootletin, a novel coiled-coil protein, is a structural component of the ciliary rootlet. *Journal of Cell Biology, 159*(3), 431-440.

Yang, R. B., Robinson, S. W., Xiong, W. H., Yau, K. W., Birch, D. G., & Garbers, D. L. (1999). Disruption of a retinal guanylyl cyclase gene leads to cone-specific dystrophy and paradoxical rod behavior. *Journal of Neuroscience, 19*(14), 5889-5897.

Young, R. W. (1967). The renewal of photoreceptor cell outer segments. *Journal of Cell Biology, 33*(1), 61-72.

Zacchigna, S., Oh, H., Wilsch-Brauninger, M., Missol-Kolka, E., Jaszai, J., Jansen, S., Carmeliet, P. (2009). Loss of the cholesterol-binding protein prominin-1/CD133 causes disk dysmorphogenesis and photoreceptor degeneration. *Journal of Neuroscience, 29*(7), 2297-2308. doi:10.1523/JNEUROSCI.2034-08.2009

Zaghloul, N. A., & Katsanis, N. (2009). Mechanistic insights into Bardet-Biedl syndrome, a model ciliopathy. *Journal of Clinical Investigation, 119*(3), 428-437. doi:10.1172/JCI37041

Zhang, Y., Molday, L. L., Molday, R. S., Sarfare, S. S., Woodruff, M. L., Fain, G. L., Pittler, S. J. (2009). Knockout of GARPs and the beta-subunit of the rod cGMP-gated channel disrupts disk morphogenesis and rod outer segment structural integrity. *Journal of Cell Science, 122*(Pt 8), 1192-1200. doi:10.1242/jcs.042531

Zou, J., Luo, L., Shen, Z., Chiodo, V. A., Ambati, B. K., Hauswirth, W. W., & Yang, J. (2011). Whirlin replacement restores the formation of the USH2 protein complex in whirlin knockout photoreceptors. *Investigative Ophthalmology and Visual Science, 52*(5), 2343-2351.

CHAPTER 3

TO DECIPHER THE C8ORF37-INVOLVED CELLULAR PATHWAYS BY INVESTIGATING C8ORF37-BINDING PROTEINS

3.1 Abstract

C8ORF37 encodes domains/motifs with no known functions and belongs to no known protein family. The C8ORF37 orthologs, however, are highly conserved from lower eukaryotes to humans. I generated *C8orf37* knockout mice and found progressive retinal dysfunction and retinal degeneration. In *C8orf37* knockout mice, photoreceptor OS membrane discs were massively disorganized from the onset of OS extension. Notably, some OS discs in *C8orf37* knockout mice are aligned parallel with the plasma membrane. *C8orf37* knockout also decreased the amounts of several OS membrane proteins, including proteins involved in membrane disc organization. How does *C8orf37* knockout lead to the decreased amounts of OS membrane proteins? In order to study the function of C8ORF37, my aim was to identify C8ORF37-interating proteins. Several biochemical approaches were applied, including GST pull-down from bovine retinal lysates, yeast-two-hybrid, and immunoprecepitation from mouse retinal lysate. GST pull-down assay identified CRMP2, β-tubulin, α-enolase, and β-actin as C8ORF37-interacting candidates. Yeast-two-hybrid assay identified dynactin 6 (DCTN6), syntaxin 8 (STX8), S-arrestin, and retinol-binding protein 3 (RBP3/IRBP) as interacting candidates. Further studies revealed that C8ORF37 weakly interacted only with α-enolase and β-actin. Lastly, immunoprecepitation from mouse retinal lysate identified promising candidates (RAB28, KTN1, UCHL1, and PSMD14) that suggests that C8ORF37 may have a role in protein homeostasis.

3.2 Introduction

Mutations in *C8ORF37* were identified to cause autosomal recessive retinitis pigmentosa (RP), cone-rod dystrophy (CRD), and Bardet-Biedl syndrome (BBS) (Estrada-

Cuzcano et al., 2012; Heon et al., 2016). The *C8ORF37* gene consists of six exons that encode a polypeptide with 207 amino acids (Estrada-Cuzcano et al., 2012). In human tissues, mRNA expression of *C8ORF37* is abundant in the brain, heart, and retina (Estrada-Cuzcano et al., 2012). C8ORF37 does not have any functionally known domains or motifs, and C8ORF37 does not belong to any protein family. However, *C8ORF37* orthologs are highly conserved from lower eukaryotes to humans, suggesting that C8ORF37 has a significant role in cellular processes. Our lab has showed that C8ORF37 is localized in the inner segment (IS), cell body, and synaptic terminus of the mouse photoreceptors.

To determine the role of C8ORF37 and to study the consequence of *C8ORF37* disruption in the retina, I generated and characterized *C8orf37* knockout mice. *C8orf37* knockout mice exhibit early-onset visual dysfunction and progressive photoreceptor degeneration. Further studies identified that the photoreceptor OS morphology and disc morphogenesis are significantly perturbed. Moreover, immunoblotting analyses showed that the amounts of several OS membrane proteins, including rhodopsin (RHO), cone opsins (S/M-opsins), guanylate cyclases 1 and 2 (GC1 and GC2), peripherin 2/RDS (RDS), cyclic nucleotide gated channel α1 and β1 subunits (CNGA1 and CNGB1), and ATP-binding cassette subfamily A member 4 (ABCA4), were significantly reduced in knockout mice when compared with control littermates. To understand why *C8orf37* knockout leads to decreased amounts of OS membrane proteins, three biochemical approaches were applied. To identify C8ORF37-interacting proteins, glutathione S-transferase (GST) pull-down assay from bovine retinal lysates, yeast-two-hybrid screen of mouse brain and retinal cDNA libraries, and immunoprecipitation from mouse retinal lysates were performed.

3.3 Results and discussion

3.3.1 Characterization of the C8ORF37 protein

C8ORF37 consists of 207 amino acids (aa) in humans and 209 aa in mice, with 78% identity in residue sequence between the two species (Figure 3.1A). An online software for protein structure and function prediction, Iterative Threading ASSEmbly Refinement (I-TASSER), was used to analyze the C8ORF37 protein. I-TASSER predicted a very small number of alpha-helixes and beta-strands in C8ORF37, while a significant portion of this protein has unknown secondary structure (Figure 3.1B). The C-terminus of C8ORF37 has been named the retinal maintenance protein (RMP) domain in the Pfam database, because it is highly conserved across many species. Interestingly, we found that C8ORF37 binds Zn^{2+} ions using inductively coupled plasma (ICP) analysis, a mass spectrometry technique to measure metal ions in protein and tissue samples. *In silico* studies using COACH software predicted that the cysteines located in residue 132, 135, 183, and 204 in the mouse RMP domain are the potential sites for binding Zn^{2+}. To determine if zinc deficiency or toxicity could be a cause underlying retinal degeneration, zinc levels in the *C8orf37*$^{+/del}$ and *C8orf37*$^{del/del}$ retinas were measured by ICP analysis. The Zn^{2+} level in the knockout mice was normal, indicating that Zn^{2+} deficiency or toxicity is not the cause of retinal degeneration in the knockout retinas.

3.3.2 Determining C8ORF37-interacting proteins

My aim in identifying C8ORF37-binding partners is to understand the cellular pathways of C8ORF37 in photoreceptors. Currently, no C8ORF37-binding partners have been reported. To discover the C8ORF37-interacting proteins, I participated in the GST

pull-down experiments, in which GST-tagged C8ORF37 full length (FL) and exon 6 (E6) proteins were used as baits and purified GST protein was used as a negative control. GST pull-down assay was performed from bovine retinal lysates and the proteins pulled down together with GST proteins were identified by mass spectrometry. We identified four proteins from bovine retinal lysates (Figure 3.2-3.5A). They are collapsing response mediator protein 2 (CRMP2), β-tubulin, α-enolase, and actin. All these proteins exist in the reported proteome of photoreceptor sensory cilium, a microtubule-based structure (Liu et al., 2007). CRMP2 is known to bind to β-tubulin and promotes microtubule assembly (Lin, Chan, Hall, & Manser, 2011). CRMP2 functions by enhancing the heterodimer formation of β- and α-tubulin by regulating the GTPase binding site of β-tubulin (Fukata et al., 2002). Moreover, CRMP2 interacts with kinesin light chain 1 and dynein heavy chain and is suggested to regulate β-tubulin trafficking and microtubule assembly (Arimura et al., 2009; Kimura, Watanabe, Iwamatsu, & Kaibuchi, 2005). α-enolase is found at the centrosome and also interacts with microtubules (Gitlits, Toh, Loveland, & Sentry, 2000; Keller et al., 2007). α-enolase may also play a role in cellular differentiation (Gitlits et al., 2000; Keller et al., 2007). Therefore, the pull-down of these proteins with C8ORF37 suggests that C8ORF37 may form a complex with tubulin, CRMP2, and α-enolase and may regulate microtubule dynamics. I generated an antibody against CRMP2 and immunofluorescence using this antibody found that CRMP2 localized along the ciliary rootlet in the photoreceptors (Figure 3.3). Coimmunoprecipitation (CoIP) using FLAG-C8ORF37 and EGFP-tagged C8ORF37-interacting candidates, double transfected in HEK293 cells, confirmed a weak interaction of C8ORF37 with α-enolase but no obvious interaction with CRMP2 or β-tubulin (Figure 3.4). These results suggest that C8ORF37 may indirectly

interact with CRMP2 and β-tubulin via a protein complex or that perhaps C8ORF37 does not interact with these proteins at all.

GST pull-down and mass spectrometry analysis also showed that C8ORF37 may interact with actin (Figure 3.5A). Two cytoplasmic actins exist in mammalian nonmuscle tissues—β- and γ-actins. Both actins play a role in cytoskeleton remodeling; however, β-actin is more dynamic and has a higher polymerization rate than γ-actin. There are only 4 residues different between β- and γ-actin at their N-terminus. Our mass spectrometry data was unable to distinguish the two actins, because no peptide at the small N-terminus region was detected by mass spectrometry. Immunoblotting analysis of control and *C8orf37* knockout retinas using pan-actin antibody revealed that the actin protein level in *C8orf37* knockout retinas was significantly increased from P18 to P30 (Figure 3.5B). In *C8orf37*$^{del/del}$ retinas at P30, the β-actin protein level was doubled, whereas there was no change in the γ-actin protein level (Figure 3.6). These results suggest that C8ORF37 might be involved in actin polymerization especially at the dynamic region of the actin filaments. The increase in actin in *C8orf37* knockout retinas may be due to disruption of a direct interaction between actin and C8ORF37 or a secondary adaptive response in the retina to *C8orf37* knockout.

To further study the potential interaction between C8ORF37 and actin, HEK293 cells were transfected with actin and *C8orf37* expressing vectors. The overexpression of *C8orf37* in HEK293 cells decreased pan-actin protein expression, consistent with the actin increase in *C8orf37*$^{del/del}$ retinas. Additionally, using actin bundle- and filament-binding biochemical assays, C8ORF37 cosedimented with actin filaments and bundles (Figure 3.5C). Lastly, the binding of C8ORF37 to monomer or polymer actin was analyzed using

C8ORF37 protein expressed and purified from E.coli. After incubation, C8ORF37 protein weakly bound to nonmuscle actin filaments (Figure 3.7). Actin filaments are localized in the CC and IS of photoreceptors and studies have shown that actin may be important for disc morphogenesis (Goldberg, Moritz, & Williams, 2016; Vaughan & Fisher, 1989; Williams, Linberg, Vaughan, Fariss, & Fisher, 1988; Yang et al., 2008). Immunostaining using phalloidin to detect actin filaments in control and *C8orf37*$^{del/del}$ retinas revealed abnormal actin cytoskeleton in *C8orf37*$^{del/del}$ retinas. Actin cytoskeleton in the IS of *C8orf37*$^{del/del}$ photoreceptors was thicker and appeared shorter (Figure 3.8).

I then generated β-actin conditional knockout (CKO) mice by crossing *six3Cre* (sine oculis-related homeobox 3) mice with β-actin floxed mice, because whole body β-actin knockout is lethal (Figure 3.9) (Perrin, Sonnemann, & Ervasti, 2010; Perrin et al., 2013). *Six3Cre* mice express the Cre protein under the control of *six3* promoter, which allows the Cre protein expression only in the retina beginning at ~E9.5 (Chen et al., 2013; Furuta, Lagutin, Hogan, & Oliver, 2000). Electroretinography (ERG) responses of the β-actin CKO (flox/flox/Cre) mice showed that both scotopic and photopic amplitudes were reduced at 5 week of age, when compared with the control littermate (+/flox/Cre) (Figure 3.10). This indicates that there is both rod and cone dysfunction, a phenotype similar to *C8orf37*$^{del/del}$ mice. I next performed transmission electron microscopy on control littermate and β-actin CKO retinas. Unfortunately, the OS and the discs of β-actin CKO mice appeared normal when compared with the control littermates (Figure 3.11). This suggests that either β-actin is not essential for disc alignment or perhaps γ-actin compensates for β-actin loss. A double conditional knockout of β- and γ-actin would show if actin is dispensable for disc morphogenesis. Immunoblotting analysis showed that the

phenotype seen in *C8orf37* knockout mice begins at ~P5. Increase of β-actin occurs later at P18, suggesting that the increase of actin protein may be a secondary defect in *C8orf37* knockout mice.

3.3.2.1. Yeast two-hybrid screens

Yeast two-hybrid screens of the mouse brain and retinal cDNA libraries using C8ORF37 exon 6 as a bait were performed in order to identify further candidates. I cloned exon 6 (C-terminus) of C8ORF37 and fused it in-frame with the gal4 DNA-binding domain in the bait vector (C8ORF37-BD). Exon 6 fragment was chosen because it is highly conserved and the full-length C8ORF37 auto-activated the reporter genes in the assay. More than 2.5 million clones were screened. After several rounds of screening the expression of 4 different reporter genes on selective media, approximately 50 candidate genes were identified. Several candidates were selected based on their known functions: dynactin 6 (DCTN6), syntaxin 8 (STX8), S-arrestin, and retinol-binding protein 3 (RBP3/IRBP3). RBP3/IRBP3 is a retinol carrier protein located between the RPE cells and photoreceptors (den Hollander et al., 2009). Arrestin binds phosphorylated rhodopsin and quenches the phototransduction cascade (Nakazawa, Wada, & Tamai, 1998). DCTN6 is a subunit of the dynactin pointed-end complex, which is involved in binding cargo and thus associating vesicle cargos with the microtubule-based motor protein complex, dynein, during vesicle cargo transportation (Yeh, Quintyne, Scipioni, Eckley, & Schroer, 2012). STX8 belongs to the syntaxin protein family, which is known to function in membrane fusion as a component of the SNARE complex (Rizo & Südhof, 2012). CoIP studies using HEK293 showed that C8ORF37 interacted with DCTN6 and STX8, but not other proteins

(Figure 3.12**)**. However, the interactions of C8ORF37 with DCTN6 and STX8 were not confirmed by direct binding using their purified recombinant proteins. Future CoIP studies will need to be performed to confirm other potential C8ORF37-interacting candidates.

3.3.2.2. Immunoprecipitation from mouse retinal lysates

Affinity immunoprecipitation (IP) experiment from P30 *C8orf37*$^{+/del}$ and *C8orf37*$^{del/del}$ retinal lysates, followed by mass spectrometry, further identified C8ORF37-interacting candidates. Anti-C8ORF37 specific antibody and a negative control rabbit IgG were used for the IP pull-down. Four strong candidates were identified: RAB28, KTN1, UCHL1, and PSMD14. RAB28 may be implicated in transport and degradation (Lumb, Leung, Dubois, & Field, 2011; Roosing et al., 2013). RAB28 is a RAS-related small GTPase and may be involved in endocytosis, lysosomal sorting, and delivery of protein cargos (Lumb et al., 2011; Roosing, Collin, den Hollander, Cremers, & Siemiatkowska, 2014). Kinectin-1 (KTN1) is a ER resident protein involved in membrane protein synthesis (Ong, Lin, Zhang, Chia, & Yu, 2006). Ubiquitin carboxyl-terminal esterase L1 (UCHL1) and 26S proteasome non-ATPase regulatory subunit 14 (PSMD14) are involved in membrane protein degradation (Setsuie & Wada, 2007; Sorokin, Kim, & Ovchinnikov, 2009). Loss of C8ORF37 leads to the reduction of a group of OS membrane proteins. Several cellular pathways may be defective in *C8orf37*$^{del/del}$ retinas as follows: 1) the translation and folding of OS membrane proteins at the ER may be compromised 2) the OS membrane proteins may be transported less efficiently in *C8orf37*$^{del/del}$ photoreceptors and then rapidly degraded in the *C8orf37*$^{del/del}$ IS and; 3) C8ORF37 may function in inhibiting the protein degradation activity in the IS as OS membrane proteins are continuously

produced and transported.

The potential interaction of C8ORF37 with KTN1, an ER protein involved in membrane protein synthesis, suggests that C8ORF37 may function in the translation and folding of OS membrane proteins at the ER in photoreceptors. The potential interactions of C8ORF37 with PSMD14 and UCHL1, two proteins in ubiquitin metabolism would suggest a role of C8ORF37 in OS membrane protein degradation. In short, these results indicate that C8ORF37 may have a role in membrane protein homeostasis. Future studies will focus on these candidates.

3.3.2.3. Strengths and drawbacks of using the three biochemical approaches to identify C8-interacting proteins

Surprisingly, the three biochemical approaches (GST pull-down, yeast-two hybrid, and mouse IP studies) did not yield similar C8-interacting protein candidates. There are several possibilities as to why this may have occurred. The strengths of the GST pull-down assay from bovine retinal lysate is that bovine eyes are readily available and large quantities of proteins can be obtained from the bovine eyes in comparison to mouse eyes. The drawbacks, however, are optimizing the pull-down conditions (reducing/nonreducing agents, salt concentration) and the need for highly pure GST-C8ORF37 proteins. Purification of full-length C8ORF37 fused to GST from bacterial lysates is difficult because ~30% of the GST-C8ORF37 protein is soluble. After purification, there are several unknown factors that may be the reason why the GST pull-down experiment gave different results from mouse IP and yeast-two hybrid studies. First, it is difficult to know if the GST tag is blocking or altering the protein binding site of C8ORF37. Secondly, it is unknown if

GST-C8ORF37 adopts its native structure after purification. Thirdly, if GST-C8ORF37 does adopt its native structure, it is also unknown how C8ORF37 behaves throughout the pull-down process while using different buffers. In principle, the unknown behavior of GST-C8ORF37 is a limiting factor in determining real binding factors from artifacts.

Alternatively, yeast two-hybrid assay was used to screen millions of clones for potential interaction. The strength of this assay is that many candidates can be obtained. The drawback is that it is difficult to tell artifacts from real candidates from the many identified candidates. Unfortunately, yeast two-hybrid assays are known to give false positive candidates perhaps due to the leaky expression of the reported genes or auto-activation. In our yeast two-hybrid assay, I used the exon 6 fragment (RMP domain) because the full-length C8ORF37 auto-activated the reporter genes in the assay. Approximately 50 candidate genes were identified in our assay. The large number of potential interacting candidates is exciting but overwhelming because further studies are usually required to confirm the real binding candidates. As shown above, the four candidates of interest to us (DCTN6, STX8, S-arrestin, and IRBP3) and further followed by CoIP studies may not be real binding candidates.

After literature search and discussion with experts, we found that affinity immunoprecipitation from mouse retinal lysates may perhaps be ideal. This approach is great because purified proteins are not needed and we are able to overcome the cumbersome unknown factors of the GST tag and native structure of the C8ORF37 protein. This approach is also ideal because mice can easily be bred and retinas from both *C8orf37*$^{+/del}$ and *C8orf37*$^{del/del}$ lysates can be used. In our experiment, the biggest drawback, however, is the use of anti-C8ORF37 antibodies. Unfortunately, anti-C8ORF37 antibodies

are not specific in immunohistochemistry and show a similar pattern in both the control and knockout. It is possible that the lack of specificity of our antibody may be contributing to identifying nonspecific binding candidates. However, after stringent use of negative controls (*C8orf37*$^{del/del}$, rabbit IgGs, and unrelated proteins for comparisons), we are confident that some of the candidates that we identified may be real. Further studies will indeed determine if our predictions are accurate.

3.4 Materials and methods

3.4.1 Animals

The β-actin loxP-flanked mice were kindly provided by Dr. James M. Ervasti from the University of Minnesota, Minneapolis. The *Six3Cre* is the sine oculis-related homeobox 3 (*Six3*) mice were kindly provided by Dr. Monica Vetter from the University of Utah. Genotyping was done using the β-actin forward primer: 5' CAG CGC AGC GAT ATC GTC ATC CA 3' and reverse primer: 5' GGT CTG GCT TCC TGC CCT AGG TC 3'. The *Six3Cre* primers used are the forward primer: 5' TCG ATG CAA CGA GTG ATG AG 3' and reverse primer: 5' TTC GGC TAT ACG TAA CAG GG 3' in the Yang lab.

3.4.2 Antibodies

Full-length *C8orf37* cDNA and CRMP2 was cloned from mouse retinas by RT-PCR into the pET28 (EMD Millipore, Billerica, MA) vectors for fusion with His tag. These constructs were transformed into BL21-CodonPlus (DE3)-RIPL cells (Agilent Technologies, Santa Clara, CA) to generate recombinant proteins. His-tagged C8ORF37 and CRMP2 protein was purified from the inclusion body after IPTG induction using Ni-

NTA agarose (Qiagen, Valencia, CA) in the presence of 8 M guanidine. These proteins were used as antigens to immunize rabbits and chicken (Cocalico Biologicals, Stevens, PA). The GST-tagged C8ORF37 protein was purified from the soluble fraction of cell lysates using GST•Bind™ resin (EMD Millipore, Billerica, MA). This protein was immobilized to agarose beads using the AminoLink™ Plus Immobilization kit (Pierce Biotechnology, Rockford, IL) and used to affinity-purify the sera obtained from rabbits and chicken. The specificity of C8ORF37 antibodies was verified by immunoblotting analysis using *C8orf37* mutant retinas as a negative control.

3.4.3 Cell culture, transfection, immunostaining, and immunoblotting analyses

HEK293 cells were cultured according to the ATCC protocol and transfected by Lipofectamine® 2000 Transfection Reagent (Thermo Fisher Scientific, Waltham, MA). Immunostaining of cultured cells and mouse retinal sections were conducted as described previously (Wang, Zou, Shen, Song, & Yang, 2012).

3.4.4 Electroretinogram (ERG)

ERG tests were performed using a UTAS-E3000 instrument (LKC Technologies, Gaithersburg, MD) as previously described (Wang et al., 2012). Briefly, mice were dark-adapted overnight. After anesthesia with ketamine and xylazine (0.1 mg and 0.01 mg per g body weight) and pupil dilation with 1% tropicamide, the full-field scotopic retinal electrical responses of the mice were recorded in the dark upon a series of white light stimuli at different intensities. Subsequently, the full-field photopic retinal electrical

responses were recorded after light adaptation at 33.25 cd/m^2 for 10 min. The a-wave amplitude of scotopic ERGs was measured from the baseline to the peak of the cornea-negative wave, while the b-wave amplitude of photopic ERGs was measured from the peak of the cornea-negative wave to the peak of the major cornea-positive wave. OCT images were acquired using Spectralis® instrument (Heidelberg Engineering, Carlsbad, CA). Mice were first anesthetized as described above.

3.4.5 Histology and transmission electron microscopy

Eye cups were fixed overnight in buffered 2.5% glutaraldehyde, 1% formaldehyde and processed for resin embedding as previously described (Marc and Liu, 2000; Anderson et al., 2009). Retinal blocs were serially sectioned at 70 nm on a Leica UC6 ultramicrotome. Optical 70 nm sections were cut and processed for imaging as previously described (Anderson et al., 2009; Marc & Liu, 2000).

3.4.6 Yeast two-hybrid screen

Yeast AH109 competent cells were made and cotransformations were performed according to the Clontech Yeast Protocols Handbook (PT3024-1). Briefly, three yeast colonies with a diameter of 2–3 mm were picked and grown in 50 ml of YPDA broth at 30 °C with a shaking speed of 260 rpm for 16 hr. The resulting yeast broth with an A_{600} value greater than 1.5 was further transferred to 300 ml of YPDA broth and cultured for another 3 hr. After several washes, the competent cells were resuspended in 1× TE, 1× LiAc buffer. For cotransformation, 100 µl of the competent cells were mixed with 0.2 µg of bait and prey plasmid DNAs (0.1 µg each) and 100 µg of carrier DNA. After shaking at 30 °C for

30 min and heat shock at 42 °C for 15 min, the cells were spun down and resuspended in 100 µl of TE buffer. The transformed cells were spread on one DDO (SD/−Leu/−Trp) plate and grown at 30 °C. From the DDO plate, five grown colonies were picked and mixed well in 20 µl of DDO broth. Half of the mixed broth was streaked on a DDO plate, and the other half of the mixed broth was streaked on a QDO (SD/−Leu/−Trp/−Ade/−His) plate with X-α-Gal. Both plates were incubated at 30 °C for 5 days.

3.4.7 Inductively coupled plasma metal analysis

ICP-MS analyses were performed on retinal samples at a volume of 2 mL filtered (0.45 mm) and acidified (to yield 2.4% nitric acid) and heated (either 12 hr at 60° C in closed tube; or 1 hr at 95° C in an open tube). Instructions were followed as previously described (Huang et al., 2011).

3.4.8 GST pull-down and immunoprecipitation

GST- and His-tagged proteins were separately expressed in BL21-CodonPlus (DE3)-RIPL cells (Agilent Technologies, Santa Clara, CA) and lysed by sonication and lysozyme treatment in lysis buffer. Wild-type mouse retinas were homogenized in lysis buffer. The *Escherichia coli* cell lysates containing the GST- and His-tagged proteins and the retinal lysate were mixed and incubated with glutathione-Sepharose beads (GE Healthcare) for 2 hr. The Sepharose beads were spun down, washed with lysis buffer three times, and boiled in Laemmli sample buffer for 10 min. Lysate protein concentrations were determined in Coomassie Blue-stained SDS-polyacrylamide gels by densitometry using BSA (New England Biolabs, Ipswich, MA) as a standard. A GST-C8ORF37 full-length

and RMP fragment was incubated with the mouse retinal lysate and glutathione-Sepharose beads for 2 hr. The beads and their associated proteins were spun down, washed three times with lysis buffer, and incubated in lysis buffer. Then beads with associated proteins were spun down, and supernatants were mixed with Laemmli sample buffer and boiled for 10 min. The pellets were washed three times with lysis buffer and boiled in Laemmli sample buffer for 10 min.

3.4.9 FLAG pull-down assays

cDNA constructs of FLAG-tagged proteins and their putative associated proteins were cotransfected into HEK293 cells. After expression of these proteins, cells were homogenized in lysis buffer (50 mm Tris-HCl, pH 8.0, 150 mm NaCl, 0.5% (v/v) Triton X-100, 5 mm EDTA, 1× protease inhibitor, and 1 mm DTT). The cell lysates were then cleared by centrifugation at 21,000 × *g* for 10 min and incubated with anti-FLAG M2-agarose affinity gel (Sigma-Aldrich) for 2 hr or overnight with gentle agitation. Agarose beads and their binding proteins were subsequently spun down, washed four times with lysis buffer, and boiled in Laemmli sample buffer for 5 min.

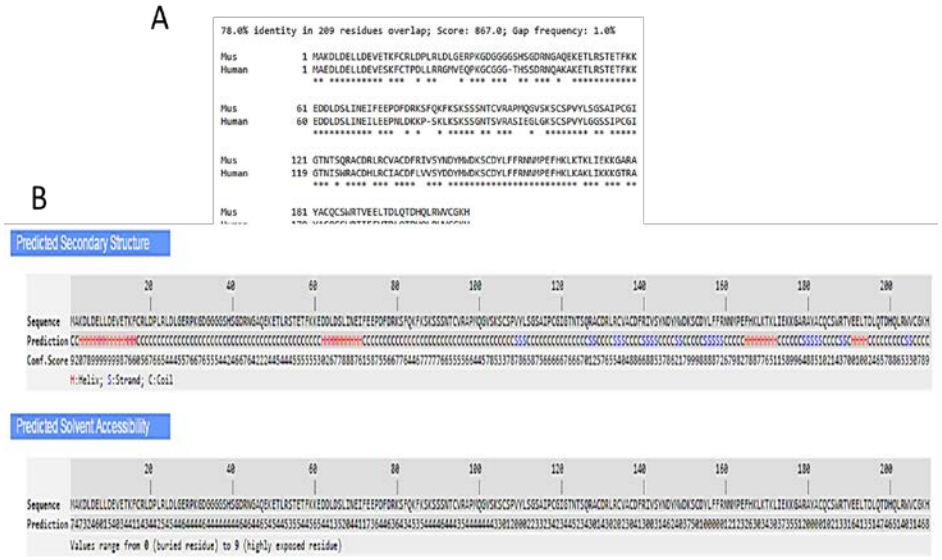

Figure 3.1: Amino acid sequence conservation of C8ORF37. (A) Amino acid sequence alignment of *Mus muscus* and human. Sequence identity of the residues is 78%. (B) Complete *Mus muscus* sequence with prediction of secondary structure. Confidence score from 0-9 (low-high) written under the sequence. Predicted solvent accessibility shown below. H-helix, C-coil, S-strand. Figure comparison was done using BLAST sequence alignment.

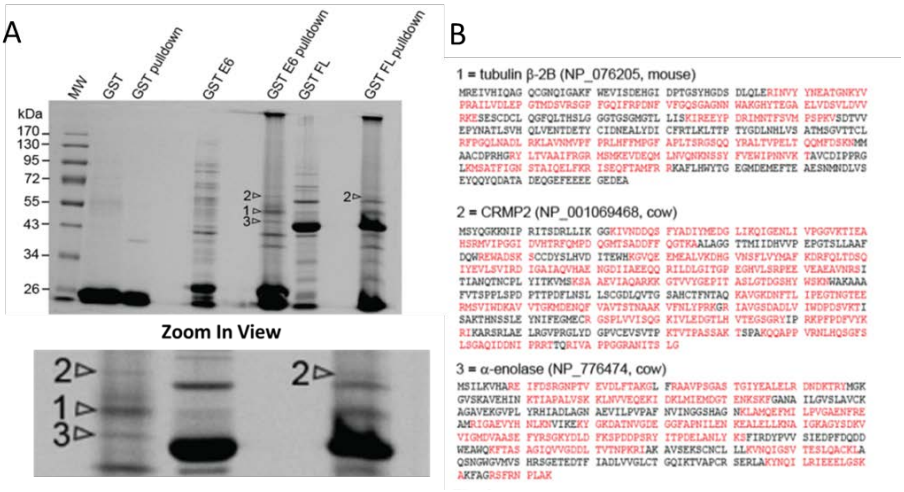

Figure 3.2: C8orf37-interacting candidates were identified**.** (A) Coomassie blue stained gel showing proteins pulled down by GST, GST-C8orf37 full length (FL), and GST-C8orf37 exon 6 (E6) proteins. GST protein was used as a negative control for the pull-down assay. Purified GST, GST-C8orf37 FL, and GST-C8orf37 E6 proteins are included as additional negative controls. Arrowheads point to the bands excised for mass spectrometry. (B) Results from mass spectrometry. The Arabic numerals correspond to image A. In the amino acid sequence, red colors denote sequences were identified by mass spectrometry.

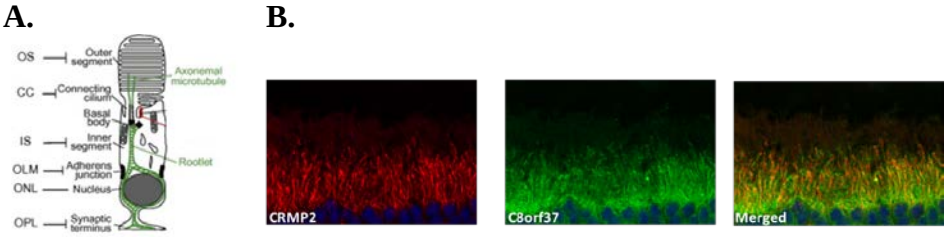

Figure 3.3: C8orf37 and CRMP2 colocalize in photoreceptors**.** (A) A schematic diagram of a rod photoreceptor. The outer segment, axonemal microtubule, basal bodies, and ciliary rootlet belong to the photoreceptor cilium. (B) C8orf37 (green) and CRMP2 (red) colocalize along the ciliary rootlet in photoreceptor inner segment (yellow in the merged view). Blue signal: photoreceptor nuclei from Hoechst 33342. Only photoreceptor outer segments, connecting cilia, inner segments, and a small number of nuclei are shown in these images.

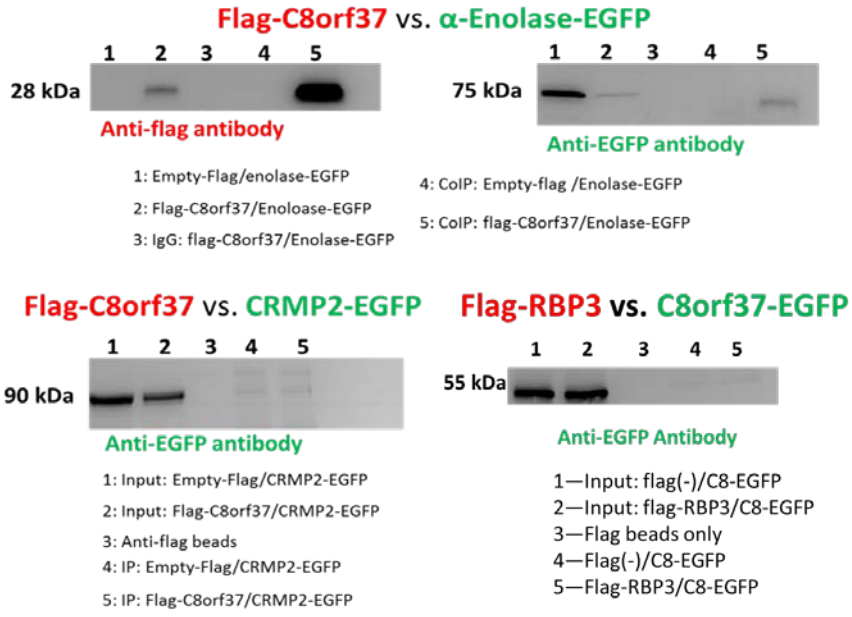

Figure 3.4: Protein Immunoprecipitation Assay. HEK293 cells were co-transfected as illustrated. Anti-EGFP antibody was used to see if there was a direct interaction. As illustrated, C8ORF37 interacts with enolase but not CRMP2 or RBP3.

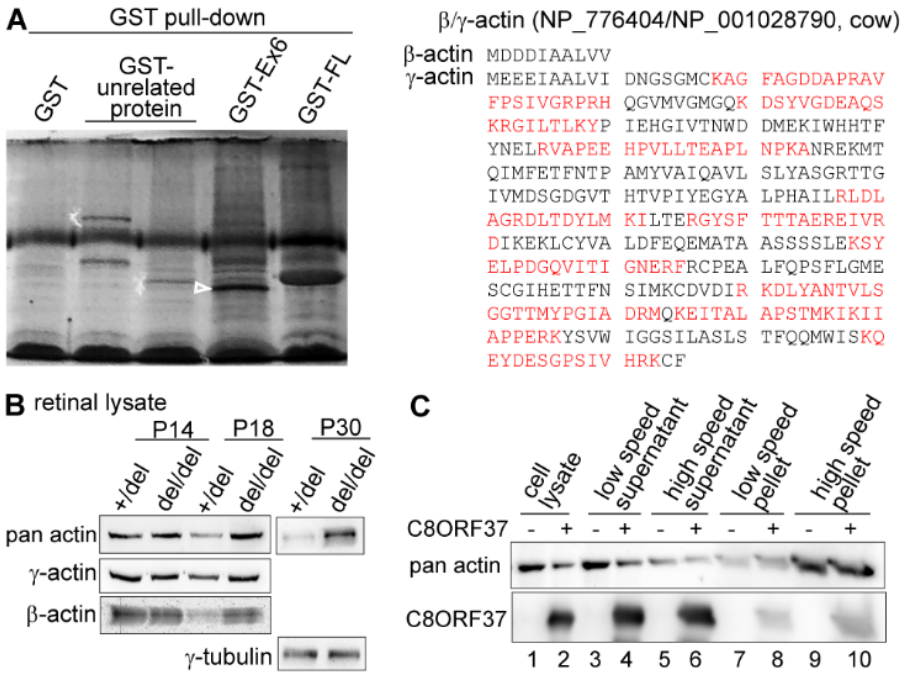

Figure 3.5: C8ORF37 interacts with actin and participates in actin polymerization. (A) β- and/or γ-actins were pulled down by GST-C8ORF37 exon 6 (Ex6) but not full-length (FL) fragment and identified by mass spectrometry. (B) β- and/or γ-actins were significantly increased in C8orf37del/del retinas at one month of age. γ-tubulin was used as a loading control. (C) Over-expression of C8ORF37 decreases the expression of β- and/or γ-actins in cultured cells (lanes 1 and 2). C8ORF37 was co-sedimented with F-actin (lane 10) and actin bundles (lane 8) at high and low speed centrifugations, respectively.

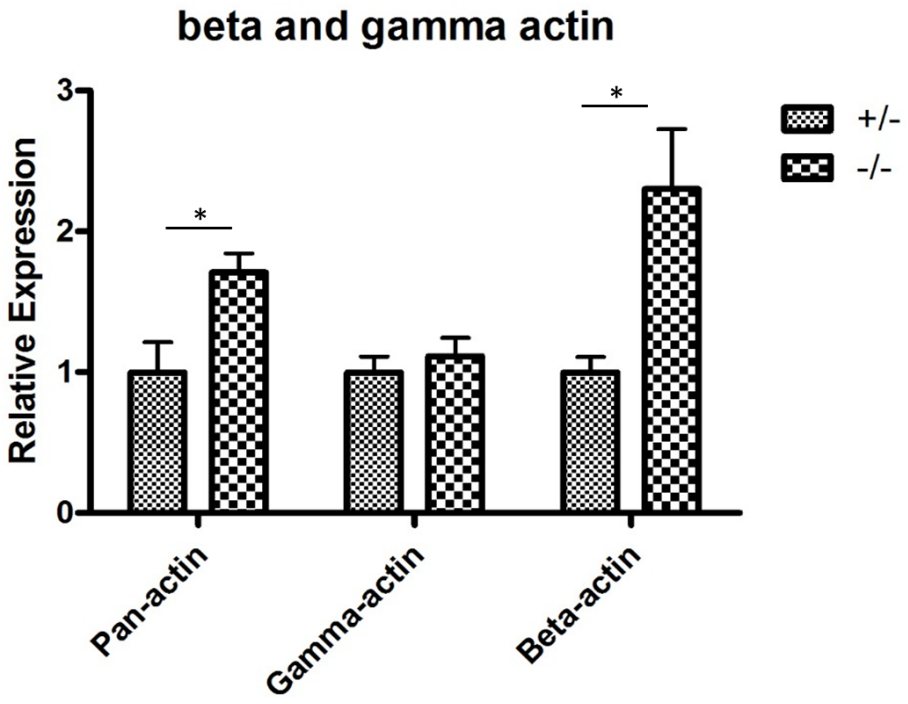

Figure 3.6: Actin is increased in *C8orf37* knockout mice. Quantification of actin from western blot of mouse retinal lysate reveled that pan-actin protein levels is significantly increased in the *C8orf37* knockout retina. Pan-actin antibody detects both gamma- and beta-actin proteins. Beta-actin specific antibodies revealed that beta-actin is doubled in *C8orf37* knockout mice when normalized to gamma-tubulin. $p<0.05$. $n=4$

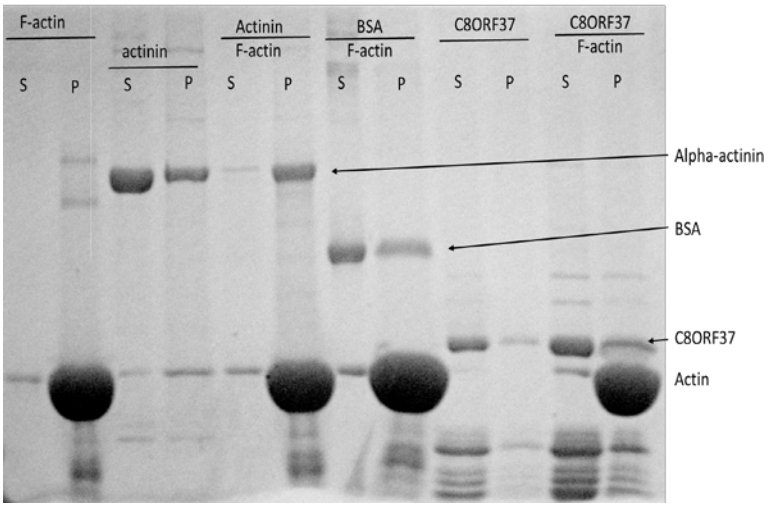

Figure 3.7: F-actin binding assay. Supernatant (S) and pellet (P) fractions were collected for each reaction and separated by a 15% gel and stained with Gelcode blue dye (Coomassie blue). From left to right: Reaction 1: F-actin alone. Reaction 2: alpha-actinin alone. Reaction 3: alpha-actinin and F-actin. Reaction 4: BSA and F-actin. Reaction 5: C8ORF37 alone. Reaction 6: C8ORF37 and F-actin. In reaction 7, increased C8ORF37 is found in the pellet.

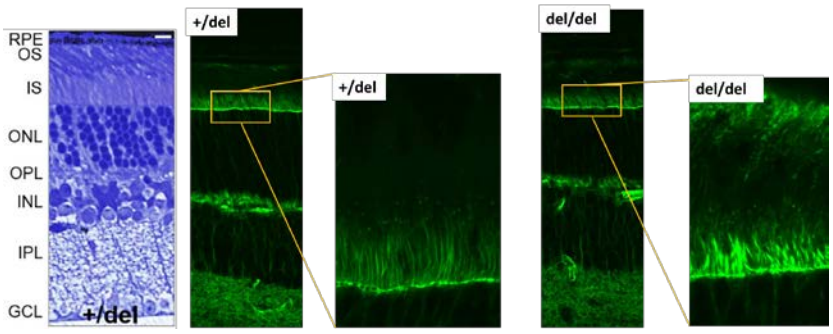

Figure 3.8: Abnormal actin cytoskeleton in *C8orf37* knockout retinas. Phalloidin staining shows difference of cytoskeleton between the control and the *C8orf37* knockout mice. In the *C8orf37*-null mice, the actin cytoskeleton appears wider and shorter.

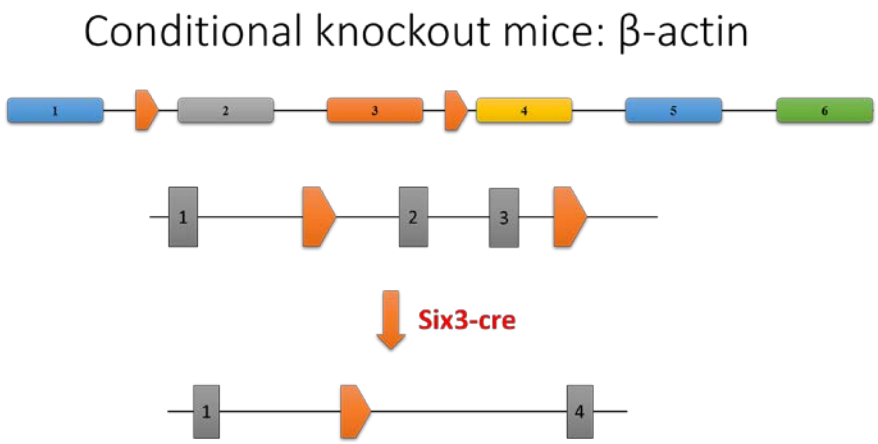

Figure 3.9: Generating beta-actin knockout mice. *Six3Cre* is the sine oculis-related homeobox 3 (Six3) promoter, a transcription factor that is required for the development of the retina. Beta-actin floxed mice were crossed with Six3Cre mice to generate retina specific knockout mice.

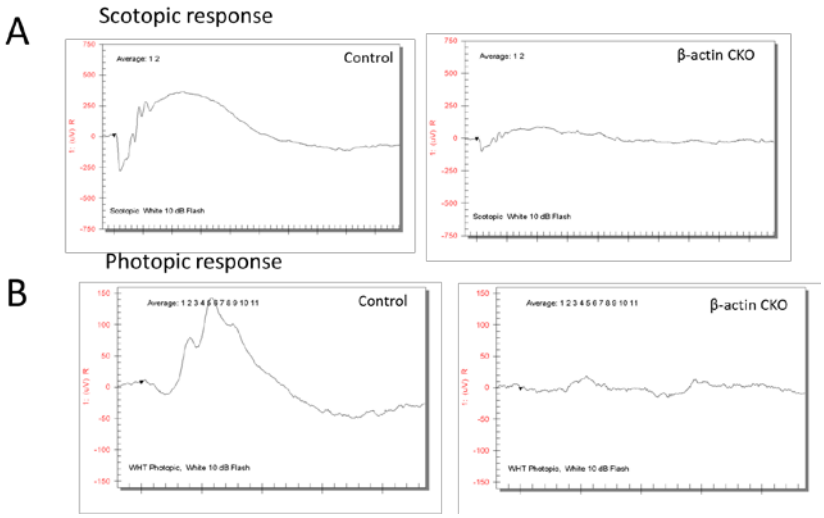

Figure 3.10: Electroretinography (ERG) responses from beta-actin conditional knockout mice. (A) Scotopic ERG responses show that the a-wave is severely reduced in the beta-actin CKO mice. (B) Photopic ERG shows that both a- and b-waves are severely reduced.

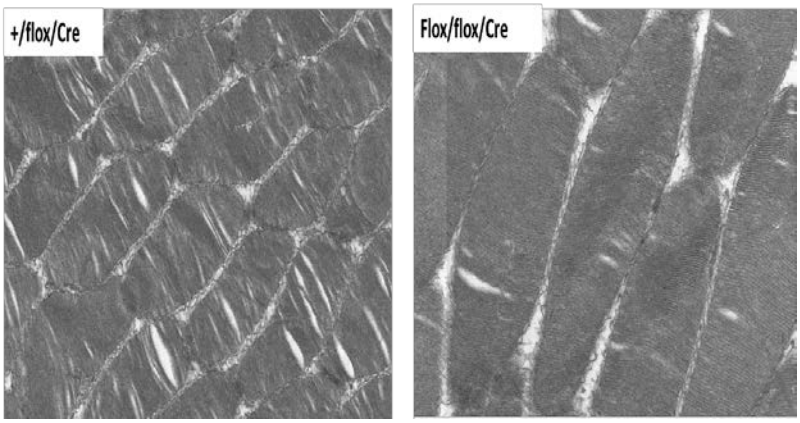

Figure 3.11: Transmission electron microscopy (TEM) of the photoreceptor outer segment (OS). Transmission electron microscopy shows that the OS of the beta-actin CKO mice (flox/flox/Cre) are normal. The discs and OS morphogenesis appears normal.

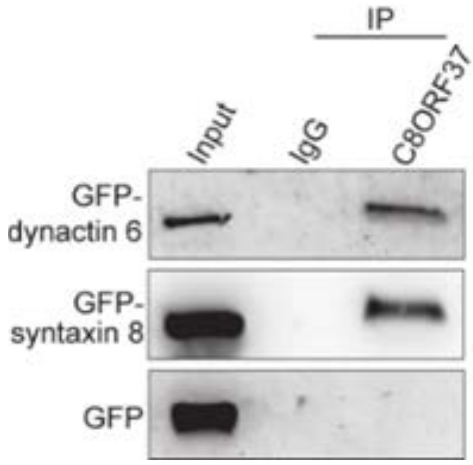

Figure 3.12: Coimmuno-precipitation of C8ORF37 with dynactin 6 and syntaxin 8 from their cotransfected culture cells. GFP was used as a negative control here.

3.5 References

Arimura, N., Hattori, A., Kimura, T., Nakamuta, S., Funahashi, Y., Hirotsune, S., Kaibuchi, K. (2009). CRMP-2 directly binds to cytoplasmic dynein and interferes with its activity. *Journal of Neurochemistry, 111*(2), 380-390. doi:10.1111/j.1471-4159.2009.06317.x

Chen, S., Li, H., Gaudenz, K., Paulson, A., Guo, F., Trimble, R., Xie, T. (2013). Defective FGF signaling causes coloboma formation and disrupts retinal neurogenesis. *Cell Research, 23*(2), 254-273. doi:10.1038/cr.2012.150

den Hollander, A. I., McGee, T. L., Ziviello, C., Banfi, S., Dryja, T. P., Gonzalez-Fernandez, F., Berson, E. L. (2009). A homozygous missense mutation in the IRBP gene (RBP3) associated with autosomal recessive retinitis pigmentosa. *Investigative Ophthalmology and Visual Science, 50*(4), 1864-1872. doi:10.1167/iovs.08-2497

Estrada-Cuzcano, A., Neveling, K., Kohl, S., Banin, E., Rotenstreich, Y., Sharon, D., Consortium, E. R. D. (2012). Mutations in C8orf37, encoding a ciliary protein, are associated with autosomal-recessive retinal dystrophies with early macular involvement. *American Journal of Human Genetics, 90*(1), 102-109. doi:10.1016/j.ajhg.2011.11.015

Fukata, Y., Itoh, T. J., Kimura, T., Ménager, C., Nishimura, T., Shiromizu, T., Kaibuchi, K. (2002). CRMP-2 binds to tubulin heterodimers to promote microtubule assembly. *Nature Cell Biology, 4*(8), 583-591. doi:10.1038/ncb825

Furuta, Y., Lagutin, O., Hogan, B. L., & Oliver, G. C. (2000). Retina- and ventral forebrain-specific Cre recombinase activity in transgenic mice. *Genesis, 26*(2), 130-132.

Gitlits, V. M., Toh, B. H., Loveland, K. L., & Sentry, J. W. (2000). The glycolytic enzyme enolase is present in sperm tail and displays nucleotide-dependent association with microtubules. *European Journal of Cell Biology, 79*(2), 104-111. doi:10.1078/S0171-9335(04)70012-6

Goldberg, A. F., Moritz, O. L., & Williams, D. S. (2016). Molecular basis for photoreceptor outer segment architecture. *Progress in Retinal and Eye Research*. doi:10.1016/j.preteyeres.2016.05.003

Heon, E., Kim, G., Qin, S., Garrison, J. E., Tavares, E., Vincent, A., Sheffield, V. C. (2016). Mutations in C8ORF37 cause Bardet Biedl syndrome (BBS21). *Human Molecular Genetics*. doi:10.1093/hmg/ddw096

Huang, W., Fernandez, D., Rudd, A., Johnson, W. P., Deubner, D., Sabey, P., Larsen, R. (2011). Dissolution and nanoparticle generation behavior of Be-associated materials in synthetic lung fluid using inductively coupled plasma mass

spectroscopy and flow field-flow fractionation. *Journal of Chromatography, 1218*(27), 4149-4159. doi:10.1016/j.chroma.2010.11.070

Keller, A., Peltzer, J., Carpentier, G., Horváth, I., Oláh, J., Duchesnay, A., Ovádi, J. (2007). Interactions of enolase isoforms with tubulin and microtubules during myogenesis. *Biochimica et Biophysica Acta, 1770*(6), 919-926. doi:10.1016/j.bbagen.2007.01.015

Kimura, T., Watanabe, H., Iwamatsu, A., & Kaibuchi, K. (2005). Tubulin and CRMP-2 complex is transported via Kinesin-1. *Journal of Neurochemistry, 93*(6), 1371-1382. doi:10.1111/j.1471-4159.2005.03063.x

Lin, P. C., Chan, P. M., Hall, C., & Manser, E. (2011). Collapsin response mediator proteins (CRMPs) are a new class of microtubule-associated protein (MAP) that selectively interacts with assembled microtubules via a taxol-sensitive binding interaction. *Journal of Biological Chemistry, 286*(48), 41466-41478. doi:10.1074/jbc.M111.283580

Liu, Q., Tan, G., Levenkova, N., Li, T., Pugh, E. N., Rux, J. J., Pierce, E. A. (2007). The proteome of the mouse photoreceptor sensory cilium complex. *Molecular & Cellular Proteomics, 6*(8), 1299-1317. doi:10.1074/mcp.M700054-MCP200

Lumb, J. H., Leung, K. F., Dubois, K. N., & Field, M. C. (2011). Rab28 function in trypanosomes: interactions with retromer and ESCRT pathways. *Journal of Cell Science, 124*(Pt 22), 3771-3783. doi:10.1242/jcs.079178

Nakazawa, M., Wada, Y., & Tamai, M. (1998). Arrestin gene mutations in autosomal recessive retinitis pigmentosa. *Archives of Ophthalmology, 116*(4), 498-501.

Ong, L. L., Lin, P. C., Zhang, X., Chia, S. M., & Yu, H. (2006). Kinectin-dependent assembly of translation elongation factor-1 complex on endoplasmic reticulum regulates protein synthesis. *Journal of Biological Chemistry, 281*(44), 33621-33634. doi:10.1074/jbc.M607555200

Perrin, B. J., Sonnemann, K. J., & Ervasti, J. M. (2010). β-actin and γ-actin are each dispensable for auditory hair cell development but required for Stereocilia maintenance. *PLoS Genetics, 6*(10), e1001158. doi:10.1371/journal.pgen.1001158

Perrin, B. J., Strandjord, D. M., Narayanan, P., Henderson, D. M., Johnson, K. R., & Ervasti, J. M. (2013). β-Actin and fascin-2 cooperate to maintain stereocilia length. *Journal of Neuroscience, 33*(19), 8114-8121. doi:10.1523/JNEUROSCI.0238-13.2013

Rizo, J., & Südhof, T. C. (2012). The membrane fusion enigma: SNAREs, Sec1/Munc18 proteins, and their accomplices--guilty as charged? *Annual Review of Cell and*

Developmental Biology, 28, 279-308. doi:10.1146/annurev-cellbio-101011-155818

Roosing, S., Collin, R. W., den Hollander, A. I., Cremers, F. P., & Siemiatkowska, A. M. (2014). Prenylation defects in inherited retinal diseases. *Journal of Medical Genetics, 51*(3), 143-151. doi:10.1136/jmedgenet-2013-102138

Roosing, S., Rohrschneider, K., Beryozkin, A., Sharon, D., Weisschuh, N., Staller, J., Consortium, E. R. D. (2013). Mutations in RAB28, encoding a farnesylated small GTPase, are associated with autosomal-recessive cone-rod dystrophy. *American Journal of Human Genetics, 93*(1), 110-117. doi:10.1016/j.ajhg.2013.05.005

Setsuie, R., & Wada, K. (2007). The functions of UCH-L1 and its relation to neurodegenerative diseases. *Neurochemistry International, 51*(2-4), 105-111. doi:10.1016/j.neuint.2007.05.007

Sorokin, A. V., Kim, E. R., & Ovchinnikov, L. P. (2009). Proteasome system of protein degradation and processing. *Biochemistry (Moscow), 74*(13), 1411-1442.

Vaughan, D. K., & Fisher, S. K. (1989). Cytochalasin D disrupts outer segment disc morphogenesis in situ in rabbit retina. *Investigative Ophthalmology and Visual Science, 30*(2), 339-342.

Wang, L., Zou, J., Shen, Z., Song, E., & Yang, J. (2012). Whirlin interacts with espin and modulates its actin-regulatory function: an insight into the mechanism of Usher syndrome type II. *Human Molecular Genetics, 21*(3), 692-710. doi:ddr503 [pii] 10.1093/hmg/ddr503

Williams, D. S., Linberg, K. A., Vaughan, D. K., Fariss, R. N., & Fisher, S. K. (1988). Disruption of microfilament organization and deregulation of disk membrane morphogenesis by cytochalasin D in rod and cone photoreceptors. *Journal of Comparative Neurology, 272*(2), 161-176. doi:10.1002/cne.902720202

Yang, Z., Chen, Y., Lillo, C., Chien, J., Yu, Z., Michaelides, M., Zhang, K. (2008). Mutant prominin 1 found in patients with macular degeneration disrupts photoreceptor disk morphogenesis in mice. *Journal of Clinical Investigation, 118*(8), 2908-2916. doi:10.1172/JCI35891

Yeh, T. Y., Quintyne, N. J., Scipioni, B. R., Eckley, D. M., & Schroer, T. A. (2012). Dynactin's pointed-end complex is a cargo-targeting module. *Molecular Biology of the Cell, 23*(19), 3827-3837. doi:10.1091/mbc.E12-07-0496

CHAPTER 4

SUMMARY AND FUTURE DIRECTIONS

Inherited retinal degenerations (IRDs) are a group of incurable and heterogeneous genetic disorders (Sahel, Marazova, & Audo, 2015). Retinitis pigmentosa (RP) is the most common form of IRD and affects 1 in 4000 people worldwide (Hartong, Berson, & Dryja, 2006). RP patients present the primary loss of rod photoreceptors and then followed by cone photoreceptor loss (Hartong et al., 2006). Cone-rod dystrophy (CRD) is another form of IRD characterized by the predominant loss of cone photoreceptors (Roosing et al., 2014). Cone photoreceptor loss precedes rod degeneration in CRD; however, in some cases, both the cones and rods can simultaneously degenerate (Thiadens et al., 2012). CRD patients exhibit loss of visual acuity, increased sensitivity to bright lights (photophobia), poor color vision, and eventually blindness (Thiadens et al., 2012). Bardet-Biedl (BBS) syndrome is a syndromic form RP. BBS is characterized by polydactyly, obesity, mental retardation, renal dysfunction, and retinal degeneration (Suspitsin & Imyanitov, 2016). To date, there are more than 200 genes identified to cause IRDs (Siemiatkowska, Collin, den Hollander, & Cremers, 2014). The function of many of these genes remains unclear. Mutations in the *C8ORF37* gene were identified in patients with autosomal recessive RP, CRD, and BBS (Estrada-Cuzcano et al., 2012; Heon et al., 2016).

C8ORF37 was initially identified by homozygosity mapping and next-generation sequencing from four consanguineous families carrying mutations in the *C8ORF37* gene (Estrada-Cuzcano et al., 2012). In humans, *C8ORF37* is located at region 22.1 on the long arm of chromosome 8. Several types of mutations have been identified in patients: missense, nonsense, splice-site, and frame-shift mutations. The *C8ORF37* gene consists of six exons (Estrada-Cuzcano et al., 2012). The C8ORF37 protein is 207 amino acids long and has no known homologs in the mammalian genome. C8ORF37 mRNA is expressed in

multiple tissues including the retina, brain, and testis (Estrada-Cuzcano et al., 2012). Its C-terminal Retinal Maintenance Protein (RMP) domain is highly conserved from lower eukaryotes to humans, and is enriched with human missense mutations, indicating the importance of this domain. However, no studies have been reported to reveal the functions of C8ORF37. Our research is a pioneering study of the function of C8ORF37 *in vivo*.

To determine the *in vivo* role of C8ORF37 and to study the consequence of C8ORF37 disruption in the retina, I generated three lines of *C8orf37* mutant mice: *C8orf37*$^{ex1/ex1}$, *C8orf37*$^{ex5/ex5}$, and *C8orf37*$^{del/del}$ using the CRISPR/Cas9 technology. The generated mutant mice were all *C8orf37*-null mice and the absence of off-target mutations were confirmed by analyzing three lines of mice. Our data show that *C8orf37*-null mice exhibit photoreceptor dysfunction as early as P21. With increase in age, there is progressive retinal dysfunction in *C8orf37* knockout mice. Optical coherence tomography displayed missing OS/IS junction at 2 months and reduction of ONL thickness at 6 months. Additionally, histology revealed severe retinal degeneration in *C8orf37* knockout mice as indicated by the reduction of OS and ONL thickness. *C8orf37* knockout mice have normal body weight and absence of polydactyly. These findings indicate a significant role for C8ORF37 in the retina.

To understand why photoreceptor function and survival are compromised in *C8orf37* knockout mice, ultrastructural studies of the photoreceptors was performed. Scanning electron microscopy (SEM) reveals that the OS morphology of *C8orf37* knockout mice is abnormal. In comparison to the controls, the OS in *C8orf37* knockout mice at P30 is wider, less dense, and nonuniform. The phenotype seen in the SEM began as early as P10, a time point when OS extends in rodents. To determine why the OS

morphology is altered, transmission electron microscopy (TEM) reveals that C8ORF37 loss affects discs morphogenesis and alignment. A significant number of *C8orf37* knockout OS discs were vertically aligned and parallel with the long axis of the OS. Notably, the discs outgrow at the OS periphery explaining why the OS is wide and nonuniform. In general, TEM showed that the photoreceptor OS of *C8orf37* knockouts were severely disorganized throughout the entire plane of retinal section. This suggests that C8ORF37 has a crucial role in OS morphogenesis and disc alignment.

For more than three decades, the molecular mechanism regulating disc morphogenesis in photoreceptors has been unknown (Steinberg, Fisher, & Anderson, 1980). The OS is dynamic and many proteins are trafficked across the CC to the OS (Pearring et al., 2013). Protein synthesis and modifications occur in the ER and Golgi, respectively, in the IS. Interestingly, *C8orf37*-null retinas showed reduction of several OS membrane proteins at P30 in comparison to controls. GARP2 and rhodopsin were reduced as early as P5 in *C8orf37*-null retinas. Previous studies have shown that knockout of GARPs and CNGB1 disrupts disc morphogenesis and rod outer segment structural integrity (Zhang et al., 2009). Therefore, the reduction of OS membrane proteins in *C8orf37* knockout retinas may be the reason for the disorganization of the OS membrane discs.

To gain insights into the function of C8ORF37, I characterized the C8ORF37 protein. *In silico* prediction of C8ORF37 structure gave poor confidence levels. However, C8ORF37 is highly conserved evolutionarily at its C-terminal half, which has been named the retinal maintenance protein (RMP) domain. Inductively coupled plasma (ICP) analysis determined that this domain of C8ORF37 binds Zinc at a ratio of one C8ORF37 protein to

two Zn^{2+} ions. Zinc deficiency and zinc toxicity were not found in *C8orf37*-null retinas when compared with controls. Crystallography studies of full-length C8ORF37 and the RMP domain were attempted however, C8ORF37 was found to be unstable to obtain crystals. Identifying C8ORF37-interacting candidates would potentially facilitate crystal formation of C8ORF37 complexes.

Therefore, the molecular function of C8ORF37 was analyzed by dissecting the protein-interacting network of C8ORF37. GST pull-down experiments, yeast two hybrid, and mouse CoIP were performed in order to identify C8ORF37-interacting candidates. We have found that C8ORF37 interacts with α-enolase and potentially RAB28 and several proteins involved in protein synthesis and degradation including KTN1, UCHL1, and PSMD14. Our data, therefore, suggested that C8ORF37 may function in OS membrane proteins homeostasis in the inner segment.

Unexpectedly, I found that C8ORF37 weakly interacted with F-actin. Interestingly, the protein level of actin was doubled in the *C8orf37* knockout retinas, specifically β-actin. I generated β-actin conditional knockout mice, which did not express β-actin in the retina. ERG analysis showed both rod and cone dysfunction when compared to their littermate controls. However, the photoreceptor OS discs morphogenesis was normal in these mice. There are two types of actin in nonmuscle tissues, β- and γ-actin. The difference between β- and γ-actin is four residues at the protein N-terminus. It is possible that γ-actin may compensate for β-actin loss in the β-actin conditional knockout retinas.

In short, defects in photoreceptor OS morphogenesis and disc alignment have been clearly shown to be involved in several types of retinal degenerations. Based on our studies in mice, we propose the etiology of RP and CRD in *C8ORF37* patients as abnormal disc

morphogenesis and reduced OS membrane proteins. Furthermore, our mutant mice provide a great model to examine OS morphogenesis, disc alignment, and protein homeostasis in the photoreceptors. These mouse models will also be used for the development of novel therapeutics.

In the future, our lab aims to develop effective treatments for patients carrying *C8ORF37* mutations. We aim to deliver full-length *C8orf37* into *C8orf37*$^{-/-}$ retinas by subretinal injection of adeno-associated viral vectors. Subretinal injections provide the advantage of minimal immune response, good gene delivery efficiency, and direct targeting of photoreceptors. The rescue of retinal phenotypes will be evaluated and monitored by ERG and histology. These results will be a proof of concept for future treatment development for patients with *C8ORF37* mutations. We also hope to verify the C8ORF37-interacting candidates identified from our protein-protein interaction assays and to decipher the exact molecular mechanism C8ORF37 plays in the photoreceptors.

4.1 References

Anderson, J. R., Grimm, B., Mohammed, S., Jones, B. W., Spaltenstein, J., Koshevoy, P., et al. (2011a). The Viking viewer: scalable multiuser annotation and summarization of large connectomics datasets. *Journal of Microscopy, 241*, 13–28. doi: 10.1111/j.1365-2818.2010.03402.x

Ding, W. X., & Yin, X. M. (2008). Sorting, recognition and activation of the misfolded protein degradation pathways through macroautophagy and the proteasome. *Autophagy*, *4*(2), 141-150.

Duricka, D. L., Brown, R. L., & Varnum, M. D. (2012). Defective trafficking of cone photoreceptor CNG channels induces the unfolded protein response and ER-stress-associated cell death. *Biochemical Journal*, *441*(2), 685-696. doi:10.1042/BJ20111004

Estrada-Cuzcano, A., Neveling, K., Kohl, S., Banin, E., Rotenstreich, Y., Sharon, D., Consortium, E. R. D. (2012). Mutations in C8orf37, encoding a ciliary protein, are

associated with autosomal-recessive retinal dystrophies with early macular involvement. *American Journal of Human Genetics, 90*(1), 102-109. doi:10.1016/j.ajhg.2011.11.015

Hartong, D. T., Berson, E. L., & Dryja, T. P. (2006). Retinitis pigmentosa. *Lancet, 368*(9549), 1795-1809. doi:10.1016/S0140-6736(06)69740-7

Heon, E., Kim, G., Qin, S., Garrison, J. E., Tavares, E., Vincent, A., Sheffield, V. C. (2016). Mutations in C8ORF37 cause Bardet Biedl syndrome (BBS21). *Human Molecular Genetics*. doi:10.1093/hmg/ddw096

Marc, R. E., and Liu, W. (2000). Fundamental GABAergic amacrine cell circuitries in the retina: nested feedback, concatenated inhibition, and axosomatic synapses. *Journal of Comparative Neurology*. *425*, 560–582. doi: 10.1002/1096-9861(20001002) 425:43.0.CO;2-D

Pearring, J. N., Salinas, R. Y., Baker, S. A., & Arshavsky, V. Y. (2013). Protein sorting, targeting and trafficking in photoreceptor cells. *Progress in Retinal and Eye Research, 36*, 24-51. doi:10.1016/j.preteyeres.2013.03.002

Roosing, S., Thiadens, A. A., Hoyng, C. B., Klaver, C. C., den Hollander, A. I., & Cremers, F. P. (2014). Causes and consequences of inherited cone disorders. *Progress in Retinal and Eye Research, 42*, 1-26. doi:10.1016/j.preteyeres.2014.05.001

Sahel, J. A., Marazova, K., & Audo, I. (2015). Clinical characteristics and current therapies for inherited retinal degenerations. *Cold Spring Harbor Perspectives in Medicine, 5*(2), a017111. doi:10.1101/cshperspect.a017111

Siemiatkowska, A. M., Collin, R. W., den Hollander, A. I., & Cremers, F. P. (2014). Genomic approaches for the discovery of genes mutated in inherited retinal degeneration. *Cold Spring Harbor Perspectives in Medicine, 4*(8). doi:10.1101/cshperspect.a017137

Steinberg, R. H., Fisher, S. K., & Anderson, D. H. (1980). Disc morphogenesis in vertebrate photoreceptors. *Journal of Comparative Neurology, 190*(3), 501-508. doi:10.1002/cne.901900307

Suspitsin, E. N., & Imyanitov, E. N. (2016). Bardet-Biedl Syndrome. *Molecular Syndromology, 7*(2), 62-71. doi:10.1159/000445491

Thiadens, A. A., Phan, T. M., Zekveld-Vroon, R. C., Leroy, B. P., van den Born, L. I., Hoyng, C. B., . . . Consortium, W. C. f. t. C. D. S. G. (2012). Clinical course, genetic etiology, and visual outcome in cone and cone-rod dystrophy. *Ophthalmology, 119*(4), 819-826. doi:10.1016/j.ophtha.2011.10.011

Volland, S., Hughes, L. C., Kong, C., Burgess, B. L., Linberg, K. A., Luna, G., Williams, D. S. (2015). Three-dimensional organization of nascent rod outer segment disk membranes. *Proceedings of the National Academy of Sciences USA, 112*(48), 14870-14875. doi:10.1073/pnas.1516309112

Zhang, Y., Molday, L. L., Molday, R. S., Sarfare, S. S., Woodruff, M. L., Fain, G. L., Pittler, S. J. (2009). Knockout of GARPs and the β-subunit of the rod cGMP-gated channel disrupts disk morphogenesis and rod outer segment structural integrity. *Journal of Cell Science, 122*(Pt 8), 1192-1200. doi:10.1242/jcs.042531